*Author:*
**Bykowska, Ola**

*Title:*
**Excitatory and Inhibitory Transmission in Prefrontal Cortex**

# Excitatory and Inhibitory Transmission in Prefrontal Cortex

Aleksandra Bykowska

February 2019

A dissertation submitted to the University of Bristol in accordance with the requirements of the degree of Doctor of Philosophy by advanced study in the Faculty of Life Sciences


Word Count: 31,632

# Abstract

Cholinergic modulation of the medial prefrontal cortex (mPFC) is important in attentional and mnemonic processes. These functions are mediated by excitatory pyramidal neurons and inhibitory interneurons within the mPFC. The largest class of neocortical interneurons, parvalbumin-expressing interneurons (PV+), create recurrent connections with excitatory pyramidal neurons within the mPFC. Little is known about how the strength of the connection between PV+ and pyramidal neurons within the deeper layers of the mPFC is modulated during sustained activity or how this activity is influenced by the neurotransmitter acetylcholine.

Using whole-cell paired recordings between PV+ interneurons and pyramidal neurons within layer 5/6 of the mPFC, the short-term dynamics of these connections were investigated over a wide range of frequencies (5 – 200Hz). Model selection identified the most parsimonious short-term plasticity models to capture the dynamics between these cells. While the excitatory synapse is best described with a simple short-term depression model, the inhibitory synapse is best explained by a model which includes heterogeneous vesicle pools with different release probabilities.

Activation of acetylcholine receptors with carbachol reduced the strength of the connection between pyramidal and PV+ neurons. Furthermore, carbachol reduced the short-term depression of inhibitory transmission at frequencies above 20Hz. The mechanisms underlying this shift in short-term plasticity were investigated using short-term plasticity models. Computational modelling indicated that the change in short-term depression is mediated by reduction in release probability and slower vesicle replenishment.

These findings show that the underlying mechanisms of short-term plasticity in excitatory and inhibitory transmission are mediated by different processes and that the connection between PV+ and pyramidal neurons is subject to cholinergic modulation.

# Acknowledgements

First and foremost, I would like to thank my supervisors, Professor Zafar Bashir and Dr Conor Houghton, for their guidance and support during my PhD.

I would also like to thank all the past/present members of the Bashir/Warburton group. It's been a pleasure working with all of you. Special thanks go to Ellen and Jasmine for always patiently answering all my questions, and to Kat and Mahsa for the unbelievable amount of support.

A huge thank you goes to my family who have been a source of inspiration throughout my life and have always supported me.

And finally, to Stephen, thank you for always being there for me and always believing in me.

# Author's declaration

I declare that the work in this dissertation was carried out in accordance with the requirements of the University's Regulations and Code of Practice for Taught Postgraduate Programmes and that it has not been submitted for any other academic award. Except where indicated by specific reference in the text, this work is my own work. Work done in collaboration with, or with the assistance of others, is indicated as such. I have identified all material in this dissertation which is not my own work through appropriate referencing and acknowledgement. Where I have quoted from the work of others, I have included the source in the references/bibliography. Any views expressed in the dissertation are those of the author.

SIGNED:..... DATE: .....

# Table of Contents

# List of Figures

# List of Tables

# List of Abbreviations

| | |
|---|---|
| aCSF | Artificial cerebrospinal fluid |
| AHP | Afterhyperpolarising potentials |
| AMPA | α-amino-3-hydroxy-5-methyl-4-isoxazolepropionic acid |
| ANOVA | Analysis of variance |
| AP | Action potential |
| EGTA | Ethylene glycol tetraacetic acid |
| EPSC | Excitatory postsynaptic current |
| EPSP | Excitatory postsynaptic potential |
| GABA | γ-Aminobutyric acid |
| G-protein | Guanosine nucleotide-binding protein |
| IPSC | Inhibitory postsynaptic current |
| IPSP | Inhibitory postsynaptic potential |
| mPFC | Medial prefrontal cortex |
| NMDA | N-methyl-D-aspartate |
| PSP | Postsynaptic potential |
| PV | Parvalbumin |
| Pyr | Pyramidal neuron |
| STP | Short-term plasticity |
| TM | Tsodyks-Markram |
| 5HT3a | 5-hydroxytryptamine 3a |

# Chapter 1. General Introduction

## 1.1 Medial prefrontal cortex

The medial prefrontal cortex (mPFC) in rodents is regarded as homologous to the prefrontal cortex of primates (Uylings et al., 2003). The mPFC includes three areas: prelimbic, infralimbic and anterior cingulate area that are reciprocally connected with other brain regions including the mediodorsal thalamus, hippocampus and amygdala (Heidbreder and Groenewegen, 2003; Hoover and Vertes, 2007). These regions are divided into five cortical layers, layer 1-3 and layer 5 and 6; in contrast to primates, the rodent mPFC has no distinguishable granular layer 4 (van Eden and Uylings, 1985).

## 1.2 Inhibitory cells of the mPFC

Inhibitory interneurons represent around 10-20% of neurons in the mPFC and mediate the feedforward and feedback inhibition within the cortex (Riga et al., 2014). Interneurons are a diverse group and are classified based on their morphological, electrophysiological, and molecular properties (Ascoli et al., 2008). Approximately 80% of cortical interneurons express calcium binding protein parvalbumin (PV) or neuropeptide somatostatin (Rudy et al., 2010). The remaining 20% of interneurons express the serotonergic 5HT3a receptor (Rudy et al., 2010). For the purpose of this thesis, PV-expressing interneurons (PV+) will be focused on. Fast-spiking PV+ interneurons are important in the generation of cortical activity at gamma frequencies (30-80Hz) (Cardin et al., 2009; Sohal et al., 2009). This frequency range has been found to be associated with both cognitive and sensory functions (Jia and Kohn, 2011). Indeed, disturbances in the signalling of cortical GABAergic interneurons, especially PV+ interneurons, have been implicated in the pathogenesis of affective disorders, autism and schizophrenia (Marín, 2012). For example, reduced levels of GABA synthesising enzyme, GABA membrane transporter and parvalbumin have been consistently reported in schizophrenia (Gonzalez-Burgos, 2005).

PV+ interneurons within the mPFC can be further subdivided into two types. The first type, basket cells, innervate the soma and proximal dendrites of pyramidal cells. The second type, chandelier cells, also referred to as axo-axonic cells, target the axon initial segment of pyramidal cells (Kawaguchi and Kubota, 1997). Pyramidal neurons in the deeper output layers 5 and 6 of the mPFC are broadly divided based on their projection targets. Thick

tufted neurons that target subcortical regions are referred to as 'type A' neurons, and thin tufted neurons that project to contralateral cortex and striatum are referred to as 'type B' neurons (Dembrow and Johnston, 2014; Lee et al., 2014). It has been found that within layer 5 of the mPFC, which is of interest to this thesis, PV+ interneurons preferentially synapse onto subcortically projecting, type A, pyramidal neurons (Lee et al., 2014).

## 1.3 The functional role of PV+ interneurons in the mPFC

PV+ interneurons modulate the activity of pyramidal neurons within the mPFC via recurrent cortical activity and via feedforward inhibition mediated by inputs from other brain regions such as the thalamus and hippocampus (Gabbott et al., 2002; Rotaru et al., 2005; Delevich et al., 2015). Hippocampal and thalamic activation of PV+ interneurons within the mPFC mediates feedforward inhibition onto pyramidal neurons, this feedforward inhibition controls the time window in which pyramidal cells can integrate incoming inputs (Tierney et al., 2004; Delevich et al., 2015).

The functional role of this inhibition has received a lot of attention (Ferguson and Gao, 2018). PV+ interneurons within the mPFC support cognitive flexibility and working memory, contribute to fear expression, and unsurprisingly given the undisputed role of the mPFC in attention, the activity of prefrontal PV+ cells has been shown to be important in attentional tasks (Sparta et al., 2014; D. Kim et al., 2016; H. Kim et al., 2016). An investigation into the roles of PV+ interneurons *in vivo* has been accelerated by the development of optogenetic tools that allow the activation and perturbation of specific cell subtypes during behaviour. Additionally, optical tools such as calcium imaging at the level of single cell resolution have improved our understanding of the patterns of activity of the different cell subtypes during behaviour.

A recent study has utilised these tools to characterise the activity of the major interneuron subtypes within the mPFC, including PV+ interneurons, during a simple auditory discrimination task (Pinto and Dan, 2015). During the task, each trial started with a flash of light which serves a signal to the animal to allocate attention. The animal is presented with one of two tones at frequencies discernible to mice. The animal is trained to react with licking to one of the tones; if the animal successfully licks in response to this tone it is rewarded with water, however, if the animal reacts with licking to the other tone, it is punished. The study used calcium imaging to monitor the activity of interneurons and pyramidal neurons during this simple, goal-directed behaviour task. The study showed that

pyramidal cells exhibit heterogeneous activity that, to an extent, can be accounted for by their laminar location. In contrast to the pyramidal cells, all the investigated interneuron subtypes show highly correlated and homogeneous activity during specific parts of the task. It was identified that the activity of majority of recorded PV+ interneurons was significantly elevated in response to all events during the task, including the initial flash of light, onset of auditory stimuli and onset of reward or punishment. This study provided convincing evidence of subtypes of neurons, including PV+ interneurons, serving multiple functions by encoding different events within the mPFC during goal-directed behaviour.

The recruitment of PV+ interneurons within the mPFC has also been shown to be important in successful allocation of attention. This was demonstrated in a study where patterns in activity of fast-spiking interneurons within the mPFC were investigated during an attentional task (H. Kim et al., 2016). During the task, the start of the trial was indicated by a light flash which was followed by a short delay. After the short delay, a visual cue was presented in a specific location. The animal had to respond to a visual cue by indicating with a nose-poke where the cue was presented. The animal learnt that when it performed a nose-poke which correctly identified the location of the cue, it received a reward. The delay period between the light flash and the onset of the cue is regarded as the time when the animal is allocating its attention to the cue presentation area. Independent of behavioural performance, the activity of the fast-spiking cells was reported to be significantly elevated during this delay period. Importantly, in correct trials, the activity of fast-spiking cells was significantly higher compared to incorrect trials. This elevation in activity was so prominent that the authors noted that it was possible to predict the success of the trial based on the levels of activity of the fast-spiking neurons. In contrast to the homogeneous activity of PV+ cells, pyramidal neurons showed heterogeneous changes in activity; heterogeneity of pyramidal cell activity was also reported in the study discussed above by Pinto and Dan (2015). In correct trials, around half of the excitatory neurons showed activity that was significantly decreased during the delay while the activity of the other half was significantly increased. Examining the cross-correlograms for pairs of PV+ and pyramidal neurons revealed putative monosynaptic connections between the fast-spiking interneurons and the pyramidal neurons that showed decreased activity during the delay. Therefore, these results suggest the decreased activity of half of the pyramidal cells is mediated by elevated firing of fast-spiking cells. Perturbing the activity of PV+ interneurons during the delay period, where the PV+ cells showed increased activity in correct trials, by either driving the cells optogenetically at 10Hz or silencing the cells more than doubled the number of errors. Therefore, the appropriate recruitment of PV+ cells within the mPFC is important in attentional processes.

Prefrontal PV+ interneurons have been also found to play a role in fear expression (Courtin et al., 2014). In this study, the animals were submitted to an auditory fear conditioning task where a foot shock was paired with a non-aversive auditory tone. After the animals learnt to associate these two stimuli, when an animal is exposed to only the non-aversive stimulus, it still responds by freezing. With repetitive re-exposure to only the non-aversive stimulus, the animals eventually disassociate the two stimulus and do not respond by freezing. The part of the task where the animal learns to disassociate the stimuli is referred to as fear extinction. Courtin et al. (2014), recorded the single-unit activity of neurons within the mPFC during delivering a foot shock to the animals. The recordings showed the firing of pyramidal cells significantly increased and the activity of PV+ interneurons was strongly reduced during freezing. This suggested that the increase in pyramidal cell firing is due to disinhibition from PV+ interneurons and this phasic disinhibition drives fear expression response in the animal such as freezing. This hypothesis was tested by optogenetically silencing PV+ interneurons within the mPFC. It was reported that silencing PV+ interneurons even before fear conditioning caused freezing in the animals. Additionally, after fear extinction, silencing PV+ cells while exposing the animal to the conditioned stimulus reinstated the freezing fear response in the animals. Therefore, this study provided evidence that PV+ interneurons within the mPFC are involved in fear expression.

Additionally, prefrontal PV+ interneurons have been demonstrated to contribute to cognitive flexibility (Sparta et al., 2014). In this study, the animals were trained in a simple Pavlovian task during which an animal forms an association between a cue and a food reward. The study examined the extinction of this association which can be quantified by the number of licks during cue presentation. It was demonstrated that optogenetically activating PV+ cells within the prelimbic and infralimbic areas of the mPFC during presentation of a cue accelerates the extinction of a trained reward seeking behaviour in mice. Therefore, these data suggested a role for prefrontal PV+ interneurons in transition to a behaviourally flexible state (Sparta et al., 2014).

Specific optogenetic activation of PV+ interneurons within the mPFC has also been demonstrated to mediate pro-cognitive effects (Cho et al., 2015; H. Kim et al., 2016). For example, specific recruitment of PV+ interneurons within the mPFC were examined in a mouse model (*Dlx5/6*$^{+/-}$) that shows aberrant development of the intrinsic and synaptic properties of PV+ interneurons (Cho et al., 2015). In this study, animals were presented with two possible locations of a reward. The task required the animals to learn the association between a reward location and a factor that predicts where the rewards is, for

example an odour. Once the animal forms this association the rule changes and the reward is associated to a different factor. Therefore, the animal has to detect this rule shift. The mouse model used in the study by Cho et al. (2015) could learn the initial association, however, the animals performed poorly on learning the rule-shift. This deficit in cognitive flexibility was ameliorated by optogenetically activating PV+ interneurons within the mPFC at frequencies of 40 or 60Hz. The pro-cognitive effect was frequency-dependent as activation at any other frequencies did not induce the same level of improvement in behavioural performance. This study was the first direct report of pro-cognitive effects induced by selectively activating PV+ interneurons within the mPFC. Given the evidence that optogenetically activating PV+ interneurons at gamma frequencies induces gamma oscillations (Cardin et al., 2009; Sohal et al., 2009), the authors suggest that the pro-cognitive effects observed are mediated by PV+ facilitated gamma oscillations. Pro-cognitive effects have also been reported in a study that linked prefrontal PV+ interneurons to attentional processes (H. Kim et al., 2016). In this study, optogenetically activating PV+ interneurons at gamma frequencies deceased the number of errors.

Therefore, the studies discussed above have shown that PV+ interneurons serve an important role supporting the prefrontal circuits during behavioural functions such as attention, fear and cognition.

## 1.4 Acetylcholine and the mPFC

The mPFC is innervated by cholinergic projections emerging from the basal forebrain (Mesulam et al., 1983; Zhang, 2010). The cholinergic innervation of the mPFC is well characterised and shows a topographical organisation (Bloem et al., 2014). While all the layers of the mPFC receive projections from the more rostral nuclei of the basal forebrain, the deeper layers of the mPFC are additionally innervated by the more caudal nuclei.

Acetylcholine acts on muscarinic and nicotinic receptors. Muscarinic receptors are metabotropic and act via intracellular interaction with G proteins. Nicotinic receptors are ligand-gated ion channels thus upon activation allow direct influx of $Na^+$, $K^+$ and $Ca^{2+}$ ions (Kabbani et al., 2013). There are five muscarinic receptor types, M1-5, and these are further subdivided into subtypes based on their intracellular mechanisms of action. M1-type muscarinic receptors comprise of M1, M3 and M5 receptors and interact with Gq-type G proteins. M2-type muscarinic receptors comprise of M2 and M4 receptors and interact with Gi/Go-type G proteins (Thiele, 2013).

Earlier studies into the functional role of acetylcholine reported elevated levels of acetylcholine during behaviours such as attention (Dalley et al., 2001), sleep (Marrosu et al., 1995) and working memory (Hironaka et al., 2001). However, the time resolution of these measurements was limited to monitoring changes over minutes (Nandi and Lunte, 2009). Technological advances such as development of amperometric biosensors have allowed the recording of real-time acetylcholine levels (Sarter and Kim, 2015). This showed that in the mPFC acetylcholine acts on both longer, tonic timescales and shorter, phasic timescales. These two forms of acetylcholine release have been proposed to be supported by two subtypes of cholinergic neurons in the basal forebrain; these are early-firing and late-firing neurons respectively (Unal et al., 2012). The early-firing neurons that show high spike adaptation are proposed to support transient acetylcholine signalling while the late-firing neurons show less spike adaptation and exhibit sustained firing are proposed to support tonic acetylcholine signalling (Unal et al., 2012).

As stated above, the methods employed in the earlier studies of cholinergic modulation were temporally limited and acetylcholine levels were shown to be elevated on tonic timescales. Additionally, cholinergic receptors have been shown to be expressed extra synaptically (Mrzljak, 1993). This led to a belief that acetylcholine acts as a neuromodulator through diffuse, volume transmission (Descarries et al., 1997). However, the discovery of behaviourally relevant acetylcholine activity on shorter timescales challenged the canonical view of acetylcholine as a neuromodulator and provided evidence that acetylcholine not only modulates, but also mediates activity within the mPFC (Ballinger et al., 2016). Current evidence suggests that both modes of acetylcholine release are present in the mPFC (Bloem et al., 2014). Phasic acetylcholine release, however, is not a feature limited just to the mPFC as phasic signals have also been recorded in the hippocampus (Teles-Grilo Ruivo et al., 2017). Additionally, both modes of release have been previously reported to be coordinated between brain structures. For example, both tonic and phasic acetylcholine release are coordinated between the hippocampus and the mPFC (Teles-Grilo Ruivo et al., 2017).

### 1.4.1 Effects of acetylcholine on PV+ and pyramidal neurons

In *in vitro* slice preparations, cholinergic innervation of the mPFC has been shown to modulate the synaptic transmission of the connections between PV+ and pyramidal cells (Pafundo et al., 2013). Multiple studies have consistently shown that GABA and glutamate

release are reduced by the activation of the presynaptic muscarinic receptors, this reduction in release has been reported in the mPFC, CA1, CA3, dentate gyrus, piriform cortex and somatosensory cortex (Hasselmo and Bower, 1992; Kruglikov and Rudy, 2008; Levy et al., 2008; Chiang et al., 2010; Szabó et al., 2010; Pafundo et al., 2013; Lawrence et al., 2015). Interestingly, some reports show that the effects of acetylcholine on synaptic transmission are region-dependent. For instance, while multiple reports have indicated activating muscarinic receptors reduces GABA release from the presynaptic interneurons, in dentate gyrus GABA release mediated by basket cells onto granule cells is elevated by activating cholinergic receptors (Chiang et al., 2010).

The effect of acetylcholine on intrinsic properties of interneurons and pyramidal cells is somewhat more complicated. However, a general principle emerges where acetylcholine enhances the excitability of pyramidal neurons but, in contrast to other interneurons, has limited effects on the excitability of neocortical PV+ interneurons (Kawaguchi and Kubota, 1997; Gulledge et al., 2007; Kruglikov and Rudy, 2008).

Studies of PV+ interneurons within the neocortex, including the mPFC, have reported lack of effect of acetylcholine on excitability of PV+ cells. For example, tonic activation of nicotinic or muscarinic receptors showed no effects on the excitability of PV+ interneurons in the somatosensory cortex and the mPFC (Kawaguchi and Kubota, 1997; Kruglikov and Rudy, 2008). Additionally, it has been also reported that within the mPFC, focal application of acetylcholine has no effects on PV+ interneurons (Gulledge et al., 2007). Interestingly, studies suggest that the lack of effects of acetylcholine on excitability of PV+ interneurons is region specific and the excitability of PV+ cells in other regions such as hippocampus is modulated by acetylcholine. For example, recordings from layer 2/3 PV+ interneurons within the mPFC showed that acetylcholine had no effect on after-hyperpolarising currents, this was in contrast to PV+ neurons within the hippocampus where it converted these currents to afterdepolarising currents (Yi et al., 2014). Furthermore, no changes were observed in the holding current of prefrontal PV+ neurons, suggesting there were no changes in the resting membrane potential. This was in contrast to hippocampal PV+ neurons where their holding current increased, suggesting depolarisation (Yi et al., 2014). These region-specific differences are further highlighted by an electrophysiological study in the dentate gyrus, where muscarine has a powerful depolarising effect on PV+ basket cell while as mentioned before such effects are not observed in the cortex (Chiang et al., 2010). Therefore, while acetylcholine has limited or no effects on excitability of PV+ interneurons within the cortex, including the mPFC, it has been shown to affect PV+ interneurons in other brain regions.

As mentioned before, acetylcholine increases excitability of pyramidal neurons. It has been demonstrated that tonic activation of cholinergic receptors within the mPFC increases the firing of pyramidal neurons in the mPFC (Pafundo et al., 2013; Tikhonova et al., 2018). The effects of acetylcholine on pyramidal cells have been shown to depend on the subtype of the pyramidal cell and also on its laminar location. This was demonstrated in a study that showed that the activation of cholinergic receptors enhanced persistent firing in subcortically-projecting pyramidal neurons but not contralaterally-projecting pyramidal neurons within the mPFC (Dembrow et al., 2010). The layer-dependece of cholinergic modulation was demonstrated in a study that showed that short, focal application of acetylcholine mediated stronger and more reliable inhibition in layer 5 pyramidal neurons compared to layers 2/3 (Gulledge et al., 2007).

The studies described above utilize bath or puff application of pharmacological agents which might activate extrasynaptic cholinergic receptors, and also lead to desensitization of receptors. More recent studies have used optogenetics to selectively activate cholinergic neurons and the direct responses to endogenous release of acetylcholine were investigated in *in vitro* neocortical slices. These studies revealed that selective activation of cholinergic neurons in the basal forebrain mediates direct synaptic transmission in pyramidal neurons in deeper layers but not superficial layers of the neocortex (Arroyo et al., 2012; Hedrick and Waters, 2015; Hay et al., 2016; Verhoog et al., 2016).

Additionally, in superficial layers of neocortex (L1, L2/3), optogenetic activation of cholinergic neurons elicits excitatory responses mediated by nicotinic receptors in non-fast-spiking interneurons (Arroyo et al., 2012; Bennett et al., 2012). This excitation in turn causes feedforward inhibitory responses in pyramidal and fast-spiking neurons within these layers,

The described studies therefore collectively demonstrate the cell-, layer- and regional-dependent influences of acetylcholine in neurotransmission. Furthermore, recent optogenetic studies *in vitro* confirmed that endogenous acetylcholine release mediates fast, point-to-point synaptic transmission within the neocortex that is also layer-dependent.

### 1.4.2 The role of acetylcholine in memory and attention

Acetylcholine has been proposed to support memory and attention by mediating selective suppression of the feedback connections within the hippocampal and cortical structures thus enhancing the incoming sensory inputs (Hasselmo and McGaughy, 2004). This theory is supported by network modelling studies (Hasselmo and Bower, 1992), and by electrophysiological evidence from different brain regions including the piriform cortex, hippocampus, somatosensory cortex and mPFC (Hasselmo and Schnell, 1994; Hasselmo and Cekic, 1996; Gil et al., 1997; Gioanni et al., 1999; Lambe et al., 2003; Kruglikov and Rudy, 2004; Carr and Surmeier, 2007; Caruana et al., 2011).

The theory of the role of acetylcholine in memory and attention was developed in the early 1990s by Hasselmo and colleagues based on their work in the piriform cortex. The anatomical separation of intracortical and afferent fibres in the piriform cortex facilitated the investigation of cholinergic modulation of separate projections into this area (Hasselmo and Bower, 1992). The strength of the excitatory afferent drive into the piriform cortex is only mildly reduced by application of an acetylcholine agonist carbachol. This is in contrast to large reductions observed in the intracortical excitatory connections. The differences detected were staggering with a ~10% reduction of the strength of the afferent inputs compared to ~70% reduction of the intracortical inputs. Based on these observations, it was proposed that acetylcholine increases the net impact of afferent inputs on the activity within the piriform cortex by preferential reduction of the strength of intracortical connections.

This work was further extended into the hippocampal regions showing that the perforant pathway, the afferent pathway from the entorhinal cortex into the hippocampus, is suppressed less by cholinergic receptor activation compared to the Schaffer collateral inputs onto the CA1 pyramidal neurons (Hasselmo and Schnell, 1994). This finding suggests that during learning the entorhinal inputs into CA1 are stronger relative to the intrinsic connections within CA1. Similar patterns of selective suppression of afferent thalamic fibres have also been observed in the somatosensory cortex (Hasselmo and Cekic, 1996; Gil et al., 1997; Kruglikov and Rudy, 2008).

The cholinergic modulation of afferent inputs to the mPFC has not been investigated in as much detail as in other cortical areas such as somatosensory cortex. However, there is evidence that shows that excitatory transmission mediated by thalamic inputs onto pyramidal neurons in layer 2-3 and 5 within the mPFC are facilitated by the activation of

nicotinic receptors (Gioanni et al., 1999; Lambe et al., 2003). Moreover, a number of studies have shown that the evoked intracortical transmission within the mPFC is suppressed by acetylcholine (Carr and Surmeier, 2007; Caruana et al., 2011; Martin et al., 2015). These studies demonstrated that the intracortical excitatory transmission mediated by superficial layers onto layer 5/6 pyramidal neurons in the prelimbic region is suppressed by acetylcholine agonist carbachol (Carr and Surmeier, 2007; Caruana et al., 2011). Cholinergic activity also reduces the strength of the excitatory connections emerging from within layer 5 onto layer 5 pyramidal neuron in the mPFC (Martin et al., 2015). Therefore, evidence suggests that cholinergic modulation potentiates afferent thalamic inputs into the mPFC while suppressing intracortical excitatory drive onto pyramidal neurons. In the light of the theory discussed above, this suggests that during memory and attentional processes, cholinergic modulation might be mediating selective suppression of recurrent intracortical connections while enhancing the incoming sensory inputs.

### 1.4.3 The role of acetylcholine release in the mPFC

The activity of the cholinergic system within the mPFC has been shown to be important in attentional processing (Parikh et al., 2007; Howe et al., 2017). Both tonic, task-related elevation and brief, phasic release of acetylcholine within the mPFC have been proposed to contribute to attentional processing (Hasselmo and Sarter, 2010). Phasic increases in acetylcholine levels in the mPFC have been shown to mediate successful cue detection in tasks that demand successful shifts in attention. Recordings of acetylcholine levels during the cue detection identified that detection of a cue was followed by acetylcholine transients in the mPFC (Parikh et al., 2007). This led to a hypothesis that cholinergic transients within the mPFC mediate cue detection.

Current optogenetic studies suggest that fast cholinergic signalling in neocortex is important in stimuli detection. Hangya et al. (2015) conducted extracellular single-unit recordings of cholinergic neurons within the basal forebrain in awake mice during an auditory task (Hangya et al., 2015). Optogenetics allowed identification of cholinergic neurons by selecting neurons that responded with short-latency to light pulses. Cholinergic neurons that project to the PFC and the auditory cortex showed subsecond, short-latency, precise firing in response to both reward and punishment stimuli. Therefore, this study supports the idea that cholinergic neurons in basal forebrain support cholinergic transmission time-locked to salient events. Additionally, it has been demonstrated that optogenetically induced acetylcholine transients within the mPFC increased the successful detection of cues (Gritton et al., 2016) and brief optogenetic activation of cholinergic

neurons within the basal forebrain improved visual coding in awake behaving mice (Pinto et al., 2013). Therefore, the specific, time-locked activation of cholinergic neurons suggests phasic cholinergic activity might send a reinforcement signal to cortical structures which serves a function of enhancing the cortical coding of salient events.

It is not clear how cholinergic transients within the mPFC mediate cue detection. It has been proposed that the transients increase the gamma power within the mPFC which supports the processing of the cues (Sarter et al., 2014). This proposal is supported by the fact that the power of prefrontal gamma oscillations is enhanced during cue detection (Howe et al., 2017). Furthermore, it has also been shown that application of muscarinic and nicotinic antagonists reduced gamma power within the mPFC and as a consequence impaired cue detection during the task (Howe et al., 2017). As the focus of this thesis are PV+ interneurons within the mPFC, it is interesting to note that the role of prefrontal PV+ interneurons in attention has been previously reported (see section 1.3 for a detailed description of the study) (H. Kim et al., 2016). In the study by Kim et al. (2016), driving prefrontal PV+ interneurons at gamma frequencies increased the recorded gamma power and decreased failures in cue detection in attentional tasks. Therefore, these observations corroborate the results reported by Howe et al. (2017) that gamma oscillations are important in cue detection. Additionally, in a previously discussed study that recorded the activity of different interneuron subtypes during a goal-directed behaviour (see section 1.3 for a detailed description of the study) (Pinto and Dan, 2015), PV+ interneurons within the mPFC show an elevated activity after the onset of a cue, a feature not observed in pyramidal neurons or other interneuron types. As described above (see section 1.4.1), the direct effects of acetylcholine on the excitability of prefrontal PV+ interneurons are limited. Nevertheless, it is possible that acetylcholine transients indirectly modulate the PV+ interneurons activity by disinhibition, however, this has not been investigated.

While transient increases of acetylcholine are linked to cue detection, the elevated tonic levels of acetylcholine are proposed to prepare the mPFC for processing of incoming sensory information (Sarter et al., 2014). The levels of tonic acetylcholine release have been positively correlated to attentional effort rather than task performance. It was demonstrated that attentional effort increases in response to increased incentives or increased distractions (Sarter et al., 2006). Hence, it has been proposed that tonic task-related levels of acetylcholine, reduce the probability of halting current actions by reducing the opportunity cost of switching to alternative tasks (Sarter et al., 2014). The influence of tonic levels on the modulation of the opportunity cost has been demonstrated by comparing task-related levels of acetylcholine in rats with varying performance on sustained attention

tasks (Paolone et al., 2013). While the basal acetylcholine levels were the same in both groups, the animals with poor attentional control show reduced levels of acetylcholine during attentional tasks (Paolone et al., 2013). Therefore, this suggests that elevated tonic levels of acetylcholine support attentional control.

## 1.5 Short-term plasticity

The excitatory and inhibitory synapses formed by PV+ interneurons and pyramidal neurons within the mPFC show short-term synaptic plasticity (STP). STP refers to changes in the efficacy of synaptic transmission, on a scale of tens to hundreds of milliseconds, that are dependent on the previous activity of the synapse (Zucker, 2002). Synapses that show short-term depression become weaker with repetitive stimulation; these synapses function as low-pass filters of synaptic activity. Synapses that show short-term facilitation however, become stronger with repetitive stimulation and function as high-pass synaptic filters. A combination of short-term depression and facilitation allows the synapses to become tuned to a particular range of frequencies and thus act as band-pass filters (Anwar et al., 2017).

A general rule is that short-term dynamics of the inhibitory synapse between interneurons and pyramidal cells are dependent on the presynaptic subtype of the interneuron. In contrast, the short-term dynamics of the excitatory synapse between these cells is a function of the postsynaptic target (Markram et al., 1998; Ma et al., 2012). The excitatory synapse formed by pyramidal onto PV+ cells has been shown to exhibit both short-term depression and facilitation, while the inhibitory synapse between PV+ and pyramidal neurons shows only short-term depression.

There has been considerable attention given to the short-term plasticity between PV+ and pyramidal neurons across different cortical brain regions. In addition to the mPFC, studies from other cortical areas are discussed below as the general rules of short-term dynamics are highly conserved across cortical regions.

### 1.5.1 Short-term plasticity of the excitatory synapse onto PV+ interneurons

Excitatory transmission between pyramidal and PV+ interneurons shows variability in its short-term dynamics that has been attributed to development, postsynaptic AMPA receptor subunit composition and laminar location.

In terms of development, short-term depression between pyramidal and fast-spiking cells within layer 5 of the motor cortex shows age-dependence. Younger animals (postnatal day 14-20) show paired-pulse depression while older animals show either paired-pulse depression or facilitation (postnatal day 27-36) (Angulo et al., 1999).

The developmental patterns of reduction in short-term depression of the excitatory between pyramidal and PV+ cells were also observed in layer 2/3 of the auditory cortex (Oswald and Reyes, 2010) and in layer 5 of the somatosensory cortex (Voinova et al., 2016). In the study by Voinova et al. (2016), however, no developmental differences in short-term dynamics were observed in layer 2/3, suggesting the developmental switch might be dependent on the laminar and/or regional location of the cells.

The heterogeneity in short-term dynamics of excitatory synapse onto PV+ interneurons has also been linked to the subtype composition of the AMPA receptors expressed by PV+ cells. PV+ interneurons express calcium-permeable AMPA receptors that lack GluA2 subunit and show rectification in the current-voltage relationship (Isaac et al., 2007). The correlation between these receptors and short-term depression has been examined in the mPFC (Wang and Gao, 2010). The differences in short-term plasticity were correlated with the expression of low or high rectification levels of AMPA receptors. The majority, ~80%, of the fast-spiking cells showed a low rectification index, suggesting that their AMPA receptors are permeable to calcium. Most of the fast-spiking cells with calcium-permeable AMPA receptors showed paired-pulse facilitation, while the fast-spiking cells with calcium-impermeable AMPA receptors showed paired-pulse depression.

### 1.5.2 Short-term plasticity of the inhibitory synapse between PV+ interneurons and pyramidal neurons

The short-term dynamics of inhibitory synapses formed by interneurons onto any neuron subtype are largely homogeneous and are dependent on the presynaptic neuron subtype (Gupta, 2000). Accordingly, the synapses formed by PV+ interneurons onto pyramidal cells show marked short-term depression. The inhibitory inputs onto excitatory cells have been shown to be depressing in the mPFC (Pafundo et al., 2013), somatosensory cortex (Reyes et al., 1998; Beierlein, 2003; Ma et al., 2012), dentate gyrus (Kraushaar et al., 2000), and CA1 (Maccaferri et al., 2000). Unlike the excitatory synapse between pyramidal and PV+ neurons, the magnitude of short-term depression at the inhibitory synapse formed by these neurons is stable throughout development (Oswald and Reyes, 2010).

The simplest form of short-term depression is mediated by the balance of depletion and vesicle replenishment that have homogeneous release probabilities (Zucker, 2002). However, a number of reports suggests that such a simple model is insufficient to explain the short-term depression of the inhibitory connection between PV+ and pyramidal neurons (Galarreta and Hestrin, 1998; Kraushaar et al., 2000; Gittis et al., 2010; Lawrence et al., 2015). A study that examined the short-term depression between fast-spiking interneurons and granule cells in dentate gyrus showed that there was no correlation between the amplitude of the first and the second peak during trains of stimulation (Kraushaar et al., 2000). This suggested that the paired-pulse depression at this synapse is independent of the previous release and hence is unlikely to be solely mediated by vesicle depletion. The study used computational STP models to investigate the mechanisms of these observations by comparing the predictions of a simple model with a constant rate of depletion and recovery of vesicles, against two models with an activity-dependent component. In one of the alternative models, the rate of the replenishment of the vesicles was increased at spike time, whereas in the other model, release probability was reduced at spike time. STP model simulations identified that the model with an activity-dependent decrease in release probability was most consistent with features observed in the experimental data. The authors therefore suggested that the release-independent depression at this synapse is able to gate the release of vesicles and thus, minimise the depletion of synaptic resources. This study uncovered features of inhibitory transmission that were inconsistent with the theory that short-term depression is solely mediated by the depletion of vesicles. These observations were further corroborated by studies examining the inhibitory connection between PV+ and pyramidal neurons within hippocampus and striatum (Gittis et al., 2010; Stone et al., 2014; Lawrence et al., 2015). To reproduce the short-term dynamics at the hippocampal synapses, the STP models had to include a frequency-dependent recovery (Stone et al., 2014; Lawrence et al., 2015). In striatum the steady-state transmission between PV+ and excitatory cells has been shown to be minimally regulated by the presynaptic firing frequencies which can not be explained with a simple short-term depression model that has constant rates of vesicle depletion and replenishment (Gittis et al., 2010).

### 1.5.3 Mechanisms of short-term plasticity

Synaptic transmission is mediated by a release of neurotransmitter from the presynaptic terminal that then binds to the postsynaptic receptors. The neurotransmitter is released from vesicles that are docked at the presynaptic terminal where they are primed for release; the

priming refers to molecular modification of vesicles that allow the vesicles to readily fuse with the presynaptic membrane upon the arrival of a spike (Sudhof, 2004). When an action potential arrives at the presynaptic terminal, it triggers an opening of voltage-gated calcium channels, calcium ions enter the presynaptic compartment causing fusion of the primed, docked vesicles leading to the release of the neurotransmitter into the synaptic cleft (Sudhof, 2004).

Short-term depression can be mediated pre and post-synaptically. Postsynaptically postsynaptic receptor desensitisation and saturation contribute to short-term depression (Wadiche et al., 2001; Koike-tani et al., 2008). Presynaptically, vesicle depletion is thought of as a main contributor to short-term depression of neurotransmission. The number of vesicle docking sites and vesicles in the presynaptic terminal are finite which means that the rate of replenishment of vesicles imparts a limiting factor on synaptic transmission. It is unknown what mechanisms mediate short-term facilitation. The most widely accepted theory is that the increases of residual calcium with repetitive activity at the presynaptic terminal elevate the release probability of the vesicles, which leads to facilitation. However, the downstream mechanisms of how elevated calcium increases in the release probability are yet to be elucidated (Jackman et al., 2016).

The notion that short-term plasticity is a result of the balance between vesicle depletion, replenishment and the build-up of residual calcium led to the development of simple deterministic short-term plasticity models (Hennig, 2013). The most widely adopted model, Tsodyks-Markram model, translated these concepts into two differential equations governed by two to four parameters (Tsodyks and Markram, 1997; Tsodyks and Markram, 1998). The parameters of these models include release probability which controls the probability of release of docked and primed vesicles at their active zones. After release, the empty docking sites are replenished from a pool of vesicles, which for the model is treated as infinite, and the rate of recovery is controlled by a single recovery time constant. To account for facilitation, the model can be extended with a facilitation rate parameter that controls the proportion of increase in the release probability following a spike. Between spikes, the release probability decays back to its original value controlled by a facilitation time constant parameter. The simplicity of these models and the physiologically relevant parameters meant that these models were adopted to capture the synaptic properties of a variety of synapses across different regions of the brain (Hennig, 2013).

Despite the success of the Tsodyks-Markram models, evidence gathered over the past two decades suggests that these models are too simplistic to describe some synapses, including

the inhibitory synapse formed by PV+ interneurons onto pyramidal neurons as described above (see section 1.5.2). Short-term plasticity dynamics that can not be accounted for by models with homogeneous release probability, have been described at cortical, hippocampal, cerebellar and calyceal synapses (Kraushaar et al., 2000; Fuhrmann et al., 2002; Hallermann et al., 2010; Taschenberger et al., 2016). Below, ideas about the mechanisms of short-term plasticity that have emerged from these studies are discussed. Growing evidence suggests that synaptic transmission is mediated by vesicles with heterogeneous release probabilities, however, the mechanisms of how heterogeneous release probabilities arise are currently not clear.

### 1.5.4 Heterogeneous release probability

The earliest reports of non-uniform release sites came from work in hippocampus. One study used a NMDA receptor channel blocker, MK-801, to examine release probability across different release sites in autaptic connections in cultured hippocampal neurons (Rosenmund et al., 1993). MK-801 blocks NMDA receptor channels in a use-dependent manner, hence the differences in the recorded postsynaptic peaks during trains of stimuli are indicative of release probability. The study recorded NMDA currents in response to repetitive stimulation. The assumption was that if the release probability remains constant throughout the stimulation, the block mediated by MK-801 will follow the dynamics of a single exponential model. This, however, was not observed and the block followed a biexponential trend, suggesting that the transmission was mediated by release sites with non-uniform release probabilities. Using the same method, these results were corroborated in hippocampal slices where six-fold differences in release probabilities were reported (Hessler et al., 1993). The non-uniform release probabilities in hippocampal synapses were also confirmed using other methods such as styryl dye measurements (Murthy et al., 1997). The heterogeneous release probability has also been reported at other synapses. At the Calyx of Held, it was observed that the release probability of vesicles during steady-state transmission is lower than the release probability at the start of the transmission (Wu and Borst, 1999; Mahfooz et al., 2016). The newly recruited vesicles had a seven to eight-fold lower release probability compared to higher release vesicles (Wu and Borst, 1999).

The mechanisms underlying the non-uniformity in release probability have been extensively investigated. They have been proposed to arise due to heterogeneous release sites, which in this thesis will be referred to as two-pool models. Another widely explored

hypothesis postulates that the release probability at rest is uniform, however, with repetitive activity it decreases due to reduction in calcium influx.

### 1.5.5 Two-pool short-term plasticity models

Experimental and modelling evidence suggests that the synaptic transmission at the Calyx of Held and some cerebellar synapses is best explained by models with two pools of vesicles that differ in their release probability and recovery kinetics. The first pool has a lower release probability and is rapidly replenished. The second pool has a higher release probability and its replenishment is slower relative to the first pool (Trommershäuser et al., 2003; Hallermann et al., 2010; Taschenberger et al., 2016; Turecek et al., 2016).

Studies from large excitatory synapses, such as cerebellar mossy fibre synapse to granule cell synapse, show that the transmission at that synapse can be described with a two-pool model with different recovery kinetics (Hallermann et al., 2010). Similar observations have been reported in studies examining the transmission at the Calyx of Held. It was shown that at the Calyx of Held, the steady-state transmission at higher frequencies converges onto the same strength of transmission (Taschenberger et al., 2016). This feature was not reproduced with a one-pool STP model and the models performance is not improved by the addition of facilitation, calcium dependent vesicle recruitment, or both (Trommershäuser et al., 2003). However, models with two heterogeneous release sites with their own release probability that are refilled in parallel, reproduce the experimental observations. The lower release probability vesicles are replenished rapidly while the higher release probability vesicles are replenished more slowly (Trommershäuser et al., 2003; Taschenberger et al., 2016). Model simulations showed that the steady-state transmission is mediated by lower release probability vesicles, while the initial transmission is mediated by vesicles with a release probability five-fold higher than the probability of the low release probability vesicles.

These observations are not limited to glutamatergic synapses. At the inhibitory synapse formed by Purkinje neurons to deep cerebellar nuclei the steady-state transmission is largely frequency-independent (Jackman et al., 2016). Stimulation of the synapse using Purkinje cell firing patterns *in vivo* shows that the inhibitory currents recorded in deep cerebellar nuclei show very little variation – with Purkinje cells exerting constant, stable inhibition, regardless of the stimulation frequency. As in the study described above, a simple depletion model with homogeneous release probability does not replicate such

features. However, the data were well described with a model that assumes two heterogeneous release probabilities with the lower release probability pool being replenished quicker than higher release probability pool. Based on simulations, similar observations were made as to the reports at the Calyx of Held, where the model predicts that lower release probability vesicles maintain steady state transmission while high release probability vesicles contribute to the initial transmission.

There is currently no agreement as to whether the heterogeneous pools are refilled independently or sequentially. In a sequential model, once docked, the lower release probability vesicles can transition into a higher release state. In the parallel model, the two pools arise independently. Due to the experimental challenge in proving the exact mechanism, it is currently not clear which model is correct.

Both sequential and parallel two-pool models postulate a difference in release probability arising from either a molecular or positional modification, sometimes referred to as 'superpriming' (Taschenberger et al., 2016). In the sequential model, this modification has been proposed to be either a molecular step that increases the sensitivity of vesicles to calcium, or a positional step that brings the docked vesicle closer to calcium channels. In the parallel two-pool model, according to the positional hypothesis, docking sites are heterogeneous, mostly attributed to the differential distribution of calcium channels, and the release probability of the vesicle is dictated by its docking location (Wadel et al., 2007; Wolfel et al., 2007; Lee et al., 2013; Taschenberger et al., 2016). The molecular hypothesis, in the light of the parallel model, suggests that once vesicles are docked, a proportion of the vesicles will be primed, but some vesicles are 'superprimed'. Studies exist that support the positional hypothesis (Wadel et al., 2007) and also that support the molecular hypothesis (Wolfel et al., 2007).

### 1.5.6 A posteriori reduction in release probability

As stated in section 1.5.4, short-term depression has also been shown to be mediated by decreases in release probability at spike arrival. This depression is independent of vesicle release which means even when no vesicles are released the next postsynaptic response will be reduced. Release-independent depression was first reported at hippocampal synapses (Dobrunz and Stevens, 1997). One of the ways in which this type of plasticity has been investigated is by examining the correlations between the first and second peak amplitude in a train of stimulations. The lack of correlation between the two peaks is

indicative of release-independent depression. Such patterns have been reported at excitatory synapses in the neocortex and hippocampus (Thomson and Bannister, 1999; Fuhrmann et al., 2004) and as described previously (see section 1.5.2) these patterns were also observed at the basket interneuron connection onto granule cells in dentate gyrus.

This type of short-term depression has been attributed to the reductions in calcium influx due to inactivating calcium channels during action potentials trains (Patil et al., 1998), and/or changes in action potential waveform (Kawaguchi and Sakaba, 2015). The reduction in calcium current due to repetitive stimulation has been reported at a variety of synapses. One study stimulated single GABAergic synaptic boutons in cell cultures of the superior colliculi while imaging the calcium currents (Kirischuk et al., 2002). It was shown that calcium influx into the presynaptic terminals is reduced with repetitive stimuli. This reduction was alleviated by including a calcium buffer, EGTA, in the presynaptic cell, hence it was suggested that the reduction in calcium influx is caused by residual calcium. Additionally, at the calyx of Held synapse, recordings from the presynaptic terminal showed that P-type calcium currents decrease with repetitive stimulations (Forsythe et al., 1998). At the calyx of Held, these reductions in calcium currents were suggested to be the main mechanism mediating the short-term depression at stimulation frequencies below 100Hz (Xu and Wu, 2005).

Action potential waveform has also been reported to control the short-term plasticity by reducing or increasing calcium influx into the presynaptic terminal (Geiger et al., 2000; Kawaguchi and Sakaba, 2015). Recordings from presynaptic terminals in cultures of Purkinje cells have shown that action potential amplitude decreases with repetitive stimulation which in turn reduces calcium influx and release probability (Kawaguchi and Sakaba, 2015). Interestingly, action potential waveform changes can also mediate facilitation. Broadening of action potentials, as recorded in the presynaptic terminal of mossy fibre synapses onto CA3 pyramidal neurons, allows a higher influx of calcium ions which mediates facilitation at this synapse (Geiger et al., 2000).

## 1.6 The current study

### 1.6.1 Aims and objectives

The aim of this thesis was to characterise the short-term plasticity of excitatory and inhibitory synapses formed by PV+ and pyramidal neurons within the mPFC and to investigate the cholinergic modulation of these synapses.

The specific objectives were:

1. Use short-term plasticity models to characterise the short-term dynamics of excitatory and inhibitory synapse between pairs of connected pyramidal and PV+ interneurons within the mPFC.
2. Investigate the cholinergic modulation of baseline transmission between PV+ and pyramidal neurons.
3. Examine the cholinergic modulation of short-term plasticity between PV+ and pyramidal neurons.
4. Use a short-term plasticity models identified in (1) to understand the mechanisms of cholinergic modulation.

### 1.6.2 Organisation of thesis

The results of this thesis are presented in two chapters. The results of computational modelling are described in Chapter 3: Modelling short-term plasticity of inhibitory and excitatory transmission. The chapter describes fitting short-term plasticity models to excitatory and inhibitory data collected by conducting *in vitro* paired-recordings. First, simple short-term plasticity models are used. This is followed by fitting extended plasticity models to examine if these provide better fits to the data.

Chapter 4: Cholinergic modulation of excitatory and inhibitory transmission, investigates the cholinergic modulation of synapses formed by pairs of PV+ and pyramidal neurons. Initially, the chapter describes *in vitro* experiments conducted to assess cholinergic modulation of baseline and short-term plasticity between these cells. The short-term plasticity data under cholinergic modulation are then used to infer synaptic changes that underlie the observed experimental results.

# Chapter 2. Materials and Methods

## 2.1 Animals

PV-Cre/tdTomato mice were created by crossing of homozygous tdTomato and homozygous PV-Cre mice. All mice were on a C57BL/6 background. *In vitro* slice electrophysiology experiments were conducted using female and male PV-Cre/tdTomato mice aged postnatal day 25-47 obtained from a breeding colony of the University of Bristol. Animals were housed under 12 hour light/dark cycle (lights on 0700-1900), food and water were available *ad libitum*. All animal procedures were in accordance with the UK Animals (Scientific Procedures) Act of 1986.

## 2.2 Brain slice preparation

Mice were sacrificed by cervical dislocation and decapitated. Brains were removed and placed in ice-cold sucrose cutting solution. Coronal slices (300μm) of PFC were sectioned using a vibratome (7000smz, Campden instruments, Loughborough). Following the sectioning, slices were placed in artificial cerebrospinal fluid (aCSF). Slices were incubated at 35°C for 30 minutes and then kept at room temperature.

## 2.3 Solutions

Coronal slices of the mPFC were sectioned in cold (~4°C) sucrose cutting solution containing in mM: 189 sucrose, 10 D-glucose, 26 $NaHCO_3$, 3 KCl, 5 $MgSO_4$, 0.1 $CaCl_2$, 1.25 $NaH_2PO_4$. Post-sectioning slices were kept in aCSF, in mM: 124 NaCl, 3 KCl, 26 $NaHCO_3$, 1.25 $NaH_2PO_4$, 1 $MgSO_4$, 10 D-glucose, 2 $CaCl_2$. Both sucrose solution and aCSF were saturated with carbogen (95% $O_2$, 5% $CO_2$). For whole-cell recordings, pipettes were filled with a potassium-based intracellular solution. The intracellular solution used for recording from PV+ interneurons contained, in mM: 130 K-gluconate, 10 HEPES, 0.5 EGTA, 4 Mg-ATP, 0.3 Na-GTP, 9 KCl. To increase the signal to noise ratio of inhibitory transmission, pyramidal neurons were filled with a high-chloride intracellular solution, in mM: 65 K-gluconate, 10 HEPES, 0.5 EGTA, 4 Mg-ATP, 0.3 Na-GTP, 65 KCl. 0.1% biocytin was included in both intracellular solutions. Acetylcholine is hydrolysed in the brain by acetylcholinesterase, hence a non-hydrolysable acetylcholine analogue, carbachol, was used in the experiments. Carbachol was prepared as stock solution in distilled water and stored at -20°C; for the experiments, carbachol was diluted in aCSF to working

concentration. Carbachol was used at 10μM to match a previously used concentration in *in vitro* experiments investigating the connection between fast-spiking interneurons and pyramidal neurons within the mPFC (Pafundo et al., 2013).

## 2.4 Whole-cell electrophysiology

### 2.4.1 Data acquisition

Recordings were sampled at 40kHz and filtered at 4kHz using Axon Multiclamp 700B amplifier and WinLTP 2.20 data acquisition software.

### 2.4.2 Paired recordings

During recordings, temperature was maintained between 31-33°C and slices were perfused with oxygenated aCSF solution at 2ml/min. In both current- and voltage- clamp, both pre- and postsynaptic cells were held at -70mV. Throughout the experiments, series resistance was compensated by bridge balance. Liquid junction potential was not corrected. Paired recordings were performed between pyramidal neurons and PV+ interneurons within layers 5 and 6 of the prelimbic area of the medial prefrontal cortex (mPFC). Recording electrodes were simultaneously lowered onto both cells, following formation of gigaohm seals, whole-cell configuration was established in both neurons. Only cells with a stable resting membrane potential that was more negative than -60mV after break-in were used. Recordings were conducted in layer 5/6 of the prelimbic region of the mPFC. PV+ interneurons were identified by expression of the fluorescent marker, tdTomato. Pyramidal cells were selected based on their characteristic large, triangular shaped soma. The cell bodies of targeted PV+ and pyramidal neurons were within 100μm. The experiments were conducted in current clamp to allow evoking action potentials in the presynaptic neurons during recordings of reciprocally connected neurons. Once patched, the recordings were abandoned if cells were not synaptically connected. If the neurons were connected, ten minutes was allowed between whole-cell configuration and data collection to allow for diffusion of the intracellular solution into the cells. The existence of reciprocal and unilateral connections was tested in both cells by injecting a single presynaptic action potential and observing the resulting postsynaptic deflection in the membrane potential of the postsynaptic cell within a 5ms time window. To ensure that relatively weaker connections are not omitted, if no clear postsynaptic response was observed, higher frequency trains of action potentials was used to verify the lack of connection. During data collection, 2ms long 1000pA current injections were used to evoke action potentials in the presynaptic cell. The intrinsic properties of both cells were tested with a series of hyper-

and depolarising current injections (-100, -50, 50, 100, 300, 500 and 700pA). Frequency trains were evoked at 5, 10, 20, 50, 100Hz in both PV neurons, and additionally at 5, 10, 20, 50, 100, 200Hz in pyramidal neurons. The frequencies were sequenced in an increasing order from 5 to 100/200 Hz, and each stimulation frequency was applied 10 times. Trains were applied at 0.1Hz, i.e. 10 seconds was allowed between each stimulation train.

## 2.5 Data analysis

Data were analysed using custom-written code in MATLAB (Mathworks).

### 2.5.1 Pre- and postsynaptic peak detection

Peak of the presynaptic APs were detected using peakdet package (http://www.billauer.co.il/peakdet.html). Postsynaptic peaks were detected within a 5ms time window set at the start of the presynaptic AP peak time. It was monitored whether a postsynaptic response reached its peak by the end of 5ms time window by checking if the detected postsynaptic peak was in the last 0.25ms of the peak window. In cases where the postsynaptic response did not reach its peak by the end of 5ms, the peak window was incrementally increased by 1ms until peak location was not within the last 0.25ms of the window as this indicated that the peak of PSP has been reached. This incremental increase was implemented in recordings of both single PSPs and also in frequency trains. However, in frequency trains, a maximum peak window size would not increase above a limit set by the interval between the presynaptic APs. For instance, during 50Hz frequency trains where the interval is equal to 20ms, the peak detection window would not increase above 20ms.

### 2.5.2 Intrinsic properties analysis

The cells were held at -70mV and hyper- and depolarizing current steps were applied for 500ms to characterise the intrinsic properties of the cells. The injections included -100, -50, 50, 100, 300, 500 and 700pA current steps. Sag was determined by measuring the difference between the peak of the hyperpolarization and the steady-state hyperpolarisation in the last 100ms of the -100pA current injection. % sag was determined by dividing sag by the peak of the hyperpolarization. Membrane time constant ($\tau_m$) was determined by fitting a single exponential model to the 10-90% voltage response to a hyperpolarising step of -100pA. Input resistance ($R_{in}$) was measured from a steady-state response to -100pA hyperpolarizing current injection. A schematic with measurements of sag, $\tau_m$ and $R_{in}$ is shown in Figure 2-1.

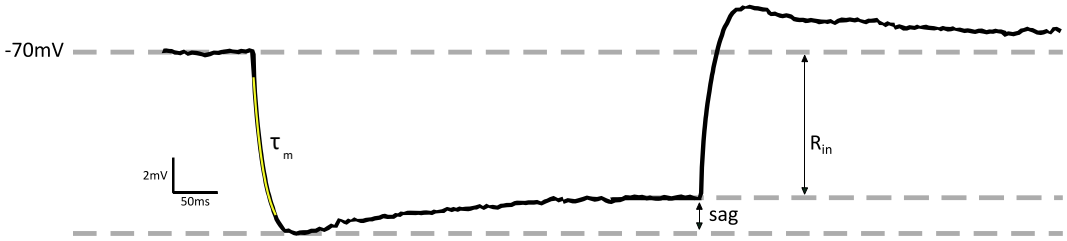


**Figure 2-1 Measurements of membrane properties.** Black trace shows a typical voltage deflection in response to -100pA current injections. The yellow line represents a single exponential fit to the 10-90% portion of membrane charging curve. The top grey line shows the membrane holding potential of -70mV.

The number of action potentials was counted in response to the depolarising currents injections (50 - 700pA). Action potential properties were measured using the first spike evoked by depolarising current injections. AP threshold was measured at a point where the velocity of the AP crossed 10mV/ms (Naundorf et al., 2006). The amplitude of the AP was measured as a difference between the peak and the threshold of the AP. The half-width of AP was measured at the point half way between the threshold and the peak. Afterhyperpolarising potentials (AHP) were measured as a difference between resting membrane potential (-70mV) and the most negative deflection in a 250ms window after 500pA current injections. A schematic with measurements of AP properties is shown in Figure 2-2.

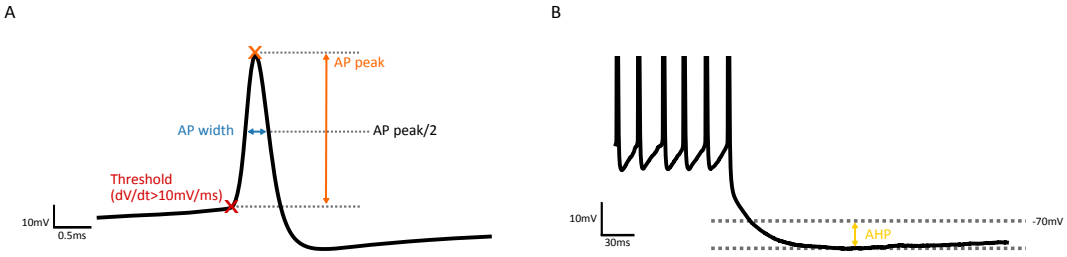


**Figure 2-2 Measurements of action potential properties.** (A) Black trace shows a typical AP and how AP threshold, peak and width were measured. (B) Black trace shows the end of a depolarizing 500pA current injection and how the AHP was measured.

## 2.5.3 PSP analysis

### *2.5.3.1* Baselining

Postsynaptic traces were baselined by subtracting the mean of the trace in a 1ms window centred around the peak of the presynaptic AP.

### *2.5.3.2* Single PSP peak detection

Peaks of single PSPs were measured by detecting a maximum value in 5ms window. To avoid the inclusion of background noise in the analysis, exclusion criteria were applied that were indicative of a postsynaptic failure:

- Detected PSP peak was smaller than three times the peak-to-peak value of the background noise.
- Detected PSP peak was smaller than 0.5mV and the difference between the location of the detected peak and the peak window was less than 0.25ms.
- 10% onset time was detected outside of the onset window of 0.2 and 2.5ms.
- Peak location and 10% onset time were within 0.25ms.

The bounds of these criteria were decided upon visual inspection of the analysed recordings. Occasionally, the presynaptic AP would evoke an AP in the postsynaptic cell. The recordings where an AP was consistently evoked in the postsynaptic cell due to presynaptic stimulation were discarded.

#### *2.5.3.3* Background noise

Typically, background noise is estimated on the basis of a short time window (~1-2ms) of the postsynaptic trace. The window is usually centred around the presynaptic action potential. This value is then used as a detection threshold to distinguish between synaptic successes and failures, i.e. all events less than a multiple of that value are considered as synaptic failures. However, if a spontaneous postsynaptic peak occurs during that time, this method is liable to overestimation of the background noise. To circumvent this problem, the 200ms trace before the postsynaptic PSP was divided into 2ms windows, peak-to-peak noise was calculated for each window, and the value of noise was taken as a median of the resulting 100 values. Median was chosen as it is less sensitive to outliers.

#### *2.5.3.4* Onset time

Onset time of each individual PSP was taken as the time from presynaptic AP peak to the first point were the PSP reach 10% of the postsynaptic peak. This method was preferable when analysing smaller PSPs (<1mV) over other methods such as finding the peak of a first-derivative of the postsynaptic PSP which corresponds to the onset time but can be highly occluded by the background noise. The onset jitter was calculated as a standard deviation of the detected onset times.

#### *2.5.3.5* Kinetic analysis

Kinetic analysis was conducted on averaged PSPs. Rise time was measured as the time from 10% to 90% of single PSPs. Decay time constant was calculated by fitting a single exponential model ($a * e^{(-t/\tau)} + c$) to the 10-90% portion of the decay of an averaged PSP. PSPs were aligned to 10% onset time for averaging. PSPs were only averaged if at least six sweeps passed the exclusion criteria. PSPs that were considered as synaptic

failures were not included in the averaged PSP. Additionally, sweeps where PSP was occluded by obvious spontaneous activity were excluded from averaged PSP.

### 2.5.4 Frequency trains analysis

Trains of PSPs were evoked to examine the short-term dynamics of the synaptic connections between PV+ and pyramidal neurons. Brief, 2ms, 2000pA current injections were used to evoke timed action potentials in the presynaptic neuron. The current injections were repeated ten times at regular intervals to yield frequency stimulations of 5, 10, 20, 50, 100 and 200Hz. The voltage of the postsynaptic neuron was recorded, and the trains of PSPs were analysed.

#### *2.5.4.1* Baselining of the postsynaptic trace

All postsynaptic traces were baselined by subtracting the mean of the trace based on 100ms before the time of the peak of the first AP evoked in the presynaptic neuron. However, if the PSP had decayed by the time of next AP during 5,10 and 20Hz stimulations, the sweep was rebaselined again by subtracting the mean of the 0.5ms window after the peak of the corresponding AP. The rebaselining was conducted to ensure that small fluctuations in the baseline are not considered when measuring the amplitude of PSPs.

#### *2.5.4.2* Peak measurement in frequency trains

Amplitude of the PSPs in frequency trains was measured by taking into account the specific contributions of previous PSPs to the current measured voltage. A single, averaged PSP was used as a template to interpolate the values of the decaying phases of previous PSPs in the train. Care was taken to ensure the template PSPs did not include spurious activity due to spontaneous and background noise. All the template PSPs were fit with a single exponential model, if the goodness-of-fit metric, R2, was below 0.99, the frequency data set was not analysed. The 0.99 threshold was decided upon visual inspection of exponential fits.

#### *2.5.4.3* Exclusion criteria for frequency analysis

Frequency stimulations were repeated at least ten times. The frequency train was excluded from analysis, if, based on the exclusion criteria, less than six sweeps were retained. Recordings were discarded if any of the following criteria were met:

Spurious action potentials: If extra presynaptic action potentials were detected during the train of stimuli, the corresponding postsynaptic trace was excluded from further analysis.

Additionally, if the presynaptic stimulation resulted in a postsynaptic action potential, these postsynaptic traces were excluded.

Baseline stability: Sweeps with unstable baseline were excluded from analysis as any substantial changes in baseline might affect the recorded PSPs. Baseline stability of frequency trains was assessed by comparing the mean of the trace before the start of the stimulation to the mean of the trace after the end of the stimulation. The mean after the end of the stimulation was calculated from 100ms after the last presynaptic AP peak to allow a full decay of the last PSP.

Spontaneous activity: Spontaneous activity in some recordings interfered with the analysis of the trains. This was particularly problematic when the amplitude of the spontaneous activity was similar or higher than the evoked transmission, and when the frequency of spontaneous activity was relatively high. These frequency trains recordings were excluded from the analysis by visually inspecting the recordings.

### 2.5.5 Statistical analysis

Statistical analyses were conducted in JASP software and using the SciPy package in Python. Shapiro-Wilk normality test was used to test for normality. If the normality assumption was violated, alternative non-parametric tests were used. Data are reported as mean and standard error of mean unless stated otherwise. Significance level was set at 0.05.

### 2.5.6 Data visualisation

Graphs were plotted in Python using matplotlib and seaborn graphing packages.

# Chapter 3. Modelling short-term plasticity of inhibitory and excitatory transmission

## 3.1 Introduction

The aim of this chapter is to select short-term plasticity models that capture the short-term dynamics of excitatory and inhibitory synaptic transmission between PV+ interneurons and pyramidal neurons within the mPFC. Over the past two decades, a range of factors have been identified that account for short term plasticity (STP) including vesicle depletion (Thomson et al., 1993), non-uniform release probabilities across release sites (Rosenmund et al., 1993; Taschenberger et al., 2016), changes in action potential waveform (Geiger et al., 2000; Kawaguchi and Sakaba, 2015), calcium channels inactivation (Forsythe et al., 1998; Patil et al., 1998) and postsynaptic receptor desensitisation and saturation (Wadiche et al., 2001; Koike-tani et al., 2008). As discussed in the general introduction (section 1.5), the PV+ inhibitory synapse onto pyramidal neurons in the cortex shows short-term depression while the excitatory synapse onto pyramidal neurons shows both short-term depression and facilitation (Angulo et al., 2003; Beierlein, 2003). Evidence from recordings in the hippocampus suggests that the synapse formed by PV+ interneurons onto excitatory cells can not be described with a simple model of short-term plasticity that assumes constant vesicle depletion and replenishment rates (Kraushaar et al., 2000; Stone et al., 2014). It is unknown if these cells also show unusual short-term plasticity in the neocortical structures such as the medial prefrontal cortex (mPFC).

A range of deterministic STP models have been previously proposed that characterise the dynamic properties of synaptic transmission (Hennig, 2013). These models provide a straightforward framework that helps to uncover the underlying mechanisms that shape the STP patterns at a particular synapse. This chapter uses a selection of these models to understand the mechanisms of the STP between PV+ and pyramidal neurons. The overarching difference between implemented models is whether the presynaptic release probability of vesicles is homogeneous or heterogeneous at rest. The parameters of models were constrained using experimental data from paired recordings between PV+ and pyramidal neurons in layer 5/6 within the mPFC.

The results show that while a simple model that assumes homogeneous release probability replicated the short-term dynamics of the excitatory connection, it failed to reproduce the

dynamics of inhibitory transmission. Inhibitory short-term depression was best described with models that assumed heterogeneous release probabilities.

Therefore, these results suggest that synaptic transmission at the excitatory synapse between pyramidal and PV+ interneurons is mediated by release sites with homogeneous release probability and short-term depression at this synapse is controlled by depletion of vesicles and their recovery kinetics. In contrast, the modelling results suggest that at the inhibitory synapse the release sites have heterogeneous release probabilities that differentially contribute to synaptic transmission during repetitive activity. The lower and higher release probability vesicles mediate the initial stages of synaptic transmission, and the later steady-state transmission is supported by the lower release probability vesicles.

## 3.2 Methods

### 3.2.1 In-vitro electrophysiology

The STP models were constrained using experimental data from whole-cell paired recordings between PV+ and pyramidal neurons. For a detailed description of data collection and analysis see Chapter 2: Materials and Methods.

### 3.2.2 Short-term plasticity models with homogeneous release-probability

#### *3.2.2.1* Tsodyks-Markram short-term plasticity models

The simplest version of Tsodyks-Markram (TM) models accounts for synaptic depression by modelling the fraction of available vesicles, *R* (Tsodyks and Markram, 1998). *R* is a continuous variable bounded between 0 and 1. At rest, *R* is set to 1 which corresponds to all release sites being occupied by a vesicle, i.e. 100% of vesicle resources are available. When the action potential arrives a proportion of the vesicles are released reducing *R* by a fraction dependent on current value of *R* and the release probability, $p$. After release, *R* recovers to 1 as vesicles dock to the vacant sites. These dynamics are captured by following equation:

$$\frac{dR(t)}{dt} = \frac{1-R(t)}{D} - p(t^-)R(t^-)\delta(t - t_{AP}) \qquad \text{Equation 3-1}$$

The variable $D$ represents the depression time constant that controls the rate of the recovery of the vesicles. The Dirac delta function, $\delta(t)$, is infinite when $t = 0$ and equal to 0 for all other $t$, the function integrates to 1 hence it models the instantaneous input such as an action potential at time $t_{AP}$. $t^-$ refers to the value of variables prior to the arrival of an action potential. Hence, $p(t^-)$ is the value of the release probability just before the arrival of an action potential and thus, controls the proportion of $R(t^-)$ that is released.

The depression-only model can be extended to include facilitation by letting the release probability, $p$, increase at spike time and decay back to its value at rest, $p_0$, between spikes:

$$\frac{dp(t)}{dt} = \frac{p_0 - p(t)}{F} + f[1 - p(t^-)]\delta(t - t_{AP}) \qquad \text{Equation 3-2}$$

At spike time, release probability is increased by $f[1 - p(t^-)]$, where $f$ is a facilitation rate parameter that controls the strength of facilitation. Between spikes, $p$ decays back to its initial value, $p_0$, with a facilitation time constant $F$.

*3.2.2.2* Release-independent depression models

Release-independent depression has been described at hippocampal and cortical synapses (Kraushaar et al., 2000; Fuhrmann et al., 2004). The main assumption of the model is that the release probability decreases at spike arrival, regardless of whether vesicles were released. The release-independent depression (RID) is modelled as follows (Fuhrmann et al., 2004):

$$\frac{dp(t)}{dt} = \frac{p_0 - p(t)}{\tau_{RID}} - r_{RID}p(t^-)\delta(t - t_{AP}) \qquad \text{Equation 3-3}$$

Release probability, $p$, is decreased at spike arrival, $t_{AP}$, the proportion of decrease is controlled by a depression rate parameter, $r_{RID}$. Between spikes, release probability relaxes to its initial value, $p_0$, with a time constant $\tau_{RID}$. Therefore, the depression of postsynaptic responses is mediated by depletion of the available vesicles and by decreases in the release probability.

At synapses showing RID, it was observed that the rate of recovery of release probability can be activity-dependent. This frequency-dependent recovery (FDR) was proposed to be mediated by decreases of $\tau_{RID}$

$$\frac{d\tau_{RID}(t)}{dt} = \frac{\tau_0 - \tau_{RID}(t)}{\tau_{FDR}} - r_{FDR}\tau_{RID}(t^-)\delta(t - t_{AP}) \quad \text{Equation 3-4}$$

In this model, $\tau_{RID}$ is decreased at spike time by $r_{FDR}\tau_{RID}(t^-)$, where $r_{FDR}$ controls the proportion of the $\tau_{RID}$ decrease. Between spikes $\tau_{RID}$ recovers to its initial value, $\tau_0$, with a time constant $\tau_{FDR}$.

### 3.2.3 Short-term plasticity models with heterogeneous release-probability

#### 3.2.3.1 Two independent pools model

The two independent pools model (2P) assumes there are two vesicle pools with lower and higher release probability and their replenishment is controlled by one time constant, $D$. This model is implemented using the equations of the Tsodyks-Markram model (Equation 3-1 and 3-2). Both pools are modelled as a fraction of synaptic resources available in each pool, $R_1$ and $R_2$, and at rest $R_1 + R_2 = 1$. The model is extended with an extra parameter, $\alpha_1$, that indicates the proportion of release sites in $R_1$. The proportion of vesicles in $R_2$, denoted as $\alpha_2$, is $\alpha_2 = 1 - \alpha_1$. Between spikes, the recovery of $R_1$ and $R_2$ are bounded by $\alpha_1$ and $\alpha_2$ respectively. The replenishment and release of both pools, $R_1$ and $R_2$, follow Equation 3-1:

$$\frac{dR_1(t)}{dt} = \frac{\alpha_1 - R_1(t)}{D} - p_1(t^-)R_1(t^-)\delta(t - t_{AP}) \quad \text{Equation 3-5}$$

$$\frac{dR_2(t)}{dt} = \frac{\alpha_2 - R_2(t)}{D} - p_2(t^-)R_2(t^-)\delta(t - t_{AP}) \quad \text{Equation 3-6}$$

Both pools release independently with independent release probabilities and replenish independently with depression time constant $D$.

The 2P model can be extended to include facilitation of both pools by following Equation 3-2:

$$\frac{dp_1(t)}{dt} = \frac{p_{1_0} - p_1(t)}{F_1} + f_1[1 - p_1(t^-)]\delta(t - t_{AP}) \quad \text{Equation 3-7}$$

$$\frac{dp_2(t)}{dt} = \frac{p_{2_0} - p_2(t)}{F_2} + f_2[1 - p_2(t^-)]\delta(t - t_{AP}) \quad \text{Equation 3-8}$$

Following the equation of the TM model (Equation 3-2), facilitation rate parameter, $f_1$ and $f_2$, control the strength of facilitation at spike time, and facilitation time constants, $F_1$ and $F_2$, control the decay of release probabilities back to the initial values of $p_{1_0}$ and $p_{2_0}$.

In contrast to the replenishment kinetics, the facilitation parameters were assumed to be different for each pool. This is due to evidence suggesting that release sites with different release probabilities show different levels of facilitation (Hessler et al., 1993; Murthy et al., 1997).

#### *3.2.3.2* Sequential model

The sequential model is an extension of the 2P model and is a phenomenological interpretation of kinetic models introduced to account for the short-term dynamics in the cerebellum and the calyx of Held (Trommershäuser et al., 2003; Hallermann et al., 2010; Taschenberger et al., 2016; Turecek et al., 2016). Taschenberger et al. (2016) and Trommershäuser et al. (2003) assume calcium dependent recovery of the higher release probability pool, however, this mechanism is not considered in this chapter.

There are two differences between the sequential model and 2P model. The first is, in the sequential model, the higher release probability vesicles are a mature version of lower release probability vesicles while in 2P model, the pools arise independently. Both models, however, assume the existence of a special molecular or positional modification that renders some vesicles to have higher release probability. The second difference is that the 2P model assumes the same replenishment kinetics while the sequential model has different replenishment kinetics for each pool.

In the sequential model, when vesicles dock to the presynaptic membrane, their release probability, $p_1$, is relatively low. From this low probability state, vesicles can transition into a mature state that has a higher probability of release, $p_2$. Furthermore, vesicles can transition back from the fully primed mature state into the earlier low probability state. The dynamics of low and high release probability pool, $R_1$ and $R_2$ respectively, are described with following differential equations

$$\frac{dR_1(t)}{dt} = \frac{1 - R_1(t) - R_2(t)}{D_1} - \frac{R_1(t)}{D_2} + \frac{R_2(t)}{D_3} - p_1(t^-)R_1(t^-)\delta(t - t_{AP}) \qquad \text{Equation 3-9}$$

$$\frac{dR_2(t)}{dt} = \frac{R_1(t)}{D_2} - \frac{R_2(t)}{D_3} - p_2(t^-)R_2(t^-)\delta(t - t_{AP}) \quad \text{Equation 3-9}$$

Where $D_1$ is the time constant that controls the replenishment of low release probability vesicles, $D_2$ controls the rate of transition of low release probability vesicles into high release probability vesicles, and $D_3$ controls the transition of high release probability vesicles to low release probability vesicles. The sequential model can be extended to include facilitation of release probabilities of both pools. The facilitation of each pool obeys Equation 3-2 with each pool having its own facilitation parameters.

In contrast to the two independent pool model, the steady-state ratio of low to high release probability vesicles is not explicitly modelled. However, it can be calculated using the time constants. The proportion of lower release probability vesicles, $\alpha_1$, is equal to

$$\alpha_1 = \frac{D_3}{D_2 + D_3} \quad \text{Equation 3-10}$$

where $D_2$ is the time constant that controls the transition of reluctant vesicles into mature higher probability vesicles, and $D_3$ is the time constant controlling the transition back from mature to reluctant vesicles. The proportion of vesicles in higher release probability state, $\alpha_2$, is $\alpha_2 = 1 - \alpha_1$.

### 3.2.4 Parameter inference

Parameters of the STP models were constrained with experimental recordings between connected PV+ and pyramidal neurons within the mPFC. To increase implementation efficiency, all the differential equations describing STP were solved analytically (see Appendix I for solutions).

All of the described STP models were fit by modelling the distribution of averaged decorrelated peak amplitudes following a method introduced by Costa et al., (2013). Additionally, one-pool models were fit by modelling quantal amplitude distributions following a method introduced by Bird et al., (2016). This method, however, was not extended to modelling two-pool models.

The main difference between the two optimisation methods is whether the correlations between consecutive peaks are considered during optimisation. The correlations arise due

to the fact that the amplitude of the current peak in a train of peaks will be dependent on the available number of vesicles which will be dependent on the number of vesicles released in previous peaks and the number of vesicles that were replenished between the spikes.

#### *3.2.4.1* Fitting decorrelated average peak amplitudes

Parameter inference of STP models that ignores the correlations between consecutive postsynaptic peaks (PSPs) in a train was based on an approach introduced by Costa et al. (2013). As the correlations are ignored it means that each average PSP in the train can be modelled independently. Gaussian distribution was used to model PSPs and the STP models were to used account for the dynamic properties of the synapse.

As described above, the variables that control the peak strength in the STP models are the proportion of available vesicles just before the spike, $R(t^-)$, and the release probability, $p(t^-)$. Hence, the model peak, $m$, in one pool models is equal to the product of these variables

$$m = p(t^-)R(t^-) \qquad \text{Equation 3-11}$$

And, similarly, in two pool models the model peak is dependent on values of $R$ and $p$ of both pools:

$$m = p_1(t^-)R_1(t^-) + p_2(t^-)R_2(t^-) \qquad \text{Equation 3-12}$$

The likelihood function that quantifies the probability of the observed mean experimental data, $\vec{d}$, given the parameters, $\vec{\theta}$, is formulated as follows

$$P(\vec{d}|\vec{\theta}) = \prod_{i=1}^{N} \frac{1}{\sqrt{2\pi\sigma_i^2}} e^{-(d_i - m_i)^2 / 2\sigma_i^2} \qquad \text{Equation 3-13}$$

where $i$ refers to the number of the peak in the train, $N$ is the total number of peaks, and $\sigma_i$ is the standard deviation of the $i$th peak calculated from the experimental data. To increase the numerical stability during the likelihood calculation, the log of the likelihood function is used. Additionally, as the normalising constant $(1/\sqrt{2\pi\sigma^2})$ is not dependent on the parameters, it is omitted in the likelihood calculation.

The STP models account for the short-term dynamics of the synapse and not the overall strength of the connection. Therefore, as in Costa et al. (2013), the model responses, $m$, were scaled with a synaptic efficacy parameter $A$

$$A = \frac{\sum_{i=1}^{N} d_i m_i / \sigma_i^2}{\sum_{i=1}^{N} m_i^2 / \sigma_i^2} \qquad \text{Equation 3-14}$$

where, as before, $i$ refers to the peak number in the train of N peaks, $d$ represents the experimental data, and $\sigma$ is the standard deviation of the experimental peaks.

### *3.2.4.2* Fitting correlated peak amplitudes

Optimisation of STP models that accounts for correlations between consecutive peaks was based on an approach by Bird et al. (2013). The study implements a stochastic model of synaptic transmission by combining phenomenological STP models with binomial models of vesicular release and replenishment.

The stochasticity of the model introduces correlations between peaks in the train and these correlations pose the main difficulty in the likelihood calculation. As discussed in Bird et al. (2013), if the likelihood is to be formulated using the probability distribution of released vesicles, the number of terms in the calculation would grow exponentially with the number of pulses in the train. Therefore, to make the calculation more efficient, the likelihood function is formulated in terms of the probability distributions of the release sites before and after a spike that fully captures the state of the system.

Therefore, in this approach the consecutive spikes are modelled as a Markov chain. This means, that at each spike, an occupancy vector that describes the probability of the number of vesicles currently docked and ready for release, is multiplied by two transition matrices. The first transition matrix corresponds to release and the second corresponds to replenishment of vesicles.

Release and replenishment matrices are dependent on release probability and depression time constant. The probability of vesicle release is derived from the STP models, and the vesicle replenishment probability, $g$, is modelled with a Poisson process controlled by a depression time constant parameter, $D$:

$$g_n = 1 - e^{-\Delta t/D} \quad \text{Equation 3-15}$$

where $\Delta t$ is the time between the action potentials. The quantal amplitude distribution of the postsynaptic response to a single vesicle follows Gaussian noise. This is a simplification to the approach in Bird et al. (2013) where the quantal distributions were modelled with gamma process. The change to Gaussian noise was introduced to increase the computational efficiency of the likelihood calculation. Background noise is also modelled with a Gaussian noise. Therefore, the total observed amplitude, $a$, given number of released vesicles, $k$, is modelled by a linear sum of quantal distributions and background noise:

$$P(a|k) = \frac{1}{\sqrt{2\pi\sigma_k^2}} e^{(\mu_k - a)^2/2\sigma_k^2} \quad \text{Equation 3-16}$$

where $\mu_k = k\mu_a$ and $\sigma_k^2 = k\sigma_a^2 + \sigma_b$, $\mu_a$ is the quantal mean, $\sigma_a$ is the quantal noise $\sigma_b^2$ is the variance of the background noise.

It is important to note that this optimisation approach was not extended to the two-pool models.

#### *3.2.4.3* Sampling

The parameter space was sampled with Metropolis-Hastings Monte Carlo Markov Chain algorithm (MCMC). MCMC was implemented using the PyMC2 package in Python with the tuning interval of the algorithm set to every 2% of the total number of samples. For deterministic models, eight Markov chains were initialised using randomly generated parameters, 100 000 samples were taken. The initial samples will be dependent on the initial condition of the sampling algorithm, i.e. the initial parameter values, hence first 50 000 samples were discarded as burn-in.

For stochastic models, four Markov chains were initialised using randomly generated parameters, 10 000 samples were taken and 5000 were discarded as burn-in. The parameter set that maximised the likelihood function was chosen as the point estimate of parameters for a given cell. All of the parameters were bounded with uniform priors. The upper bound of time constant parameters was set at 5s. Lower release probability in the 2P models was used as a lower bound for the higher release probability parameter.

Maximum a posteriori estimator was taken as the most likely parameter set ($\theta_{MAP} = \text{argmax}\, P(D|\theta)P(\theta)$ where D is data and $\theta$ refers to parameters).

#### *3.2.4.4* Model selection

The mean squared error (MSE) was calculated to quantify the accuracy of the models in describing the data. Additionally, Akaike Information Criterion (AIC) was calculated to select the most parsimonious model (Burnham and Anderson, 2004), this analysis was based on Pine et al (2009). AIC was calculated for each cell:

$$AIC = -2lnL + 2k \qquad \text{Equation 3-17}$$

where $L$ is the maximum likelihood and $k$ refers to the number of free parameters in the model. The AIC values of all cells were summed for each model, $m$

$$AIC_m = \sum_i^n AIC_i \qquad \text{Equation 3-18}$$

### 3.2.5 Data analysis

Experimental data collection and analysis is described in Chapter 2. Steady-state and paired-pulse ratio (PPR) values were calculated to compare simulated data to experimental data. These two measures capture the main synaptic dynamics in the trains and thus, are a good indicator of model performance. PPR was calculated as a ratio of the second averaged PSP to the first averaged PSP. Steady-state is defined as a ratio of the mean last two peaks in the train to the first averaged PSP. Correlation was assessed using the Spearman rank-order correlation was implemented in Python with the Scipy package.

# 3.3 Results

## 3.3.1 Paired recordings

Paired recordings of inhibitory and excitatory transmission between connected PV+ and pyramidal neurons within layer 5/6 in the medial prefrontal cortex (mPFC) were used to constrain the parameters of short-term plasticity (STP) models. The connection probability for the inhibitory synapse was higher at 34% than for the excitatory synapse at 19% (Figure 3-1).

| Connection type |  |  |  |
|---|---|---|---|
| Total connected | 27 / 585 | 118 / 585 | 82 / 585 |
| Connection probability | 5% | 20% | 14% |

**Figure 3-1 Connection probability between PV+ and pyramidal neurons**. Whole-cell paired recordings between PV+ and pyramidal neurons were performed in layer 5/6 within the mPFC. The overall connection probability of unilateral or reciprocal connection was 39%.

Current steps were injected into PV+ and pyramidal neurons ranging from -100pA to 700pA to characterise the hyper- and de-polarising responses of both types of cells used for the STP optimisation. The electrical properties were measured and are shown in Figure 3-2 for pyramidal neurons and Figure 3-3 PV+ neurons. Table 3-1 lists the mean properties of both cell types. It has been reported that neocortical pyramidal neurons can be divided in two subgroups: type A that has a prominent sag and AHP amplitude, and type B that shows minimal sag and AHP amplitude (Lee et al., 2014). It has been also shown that fast-spiking interneurons form synapses preferentially with type A neurons. The recorded pyramidal neurons showed substantial %sag (17±0.9%) and AHP (8±0.4mV) (Table 3-1; Figure 3-2B, D). Therefore, this suggests that the pyramidal neurons reported in this thesis belong to type A subtype.

| | AHP (mV) | AP amplitude (mV) | AP threshold (mV) | AP width (ms) | $R_i$ (MΩ) | % sag | $\tau_m$ (ms) |
|---|---|---|---|---|---|---|---|
| **PV (n = 23)** | 5.6±0.4 | 68.9±1.5 | -44.1±0.6 | 0.3±0.02 | 127.4±6.7 | 11.2±0.5 | 5.1+0.2 |
| **Pyr (n = 38)** | 8±0.4 | 88±1.5 | -46.5±0.6 | 0.8±0.02 | 101.4±5.5 | 17±0.9 | 17±0.8 |

**Table 3-1 Intrinsic properties of PV+ interneurons and pyramidal neurons.**

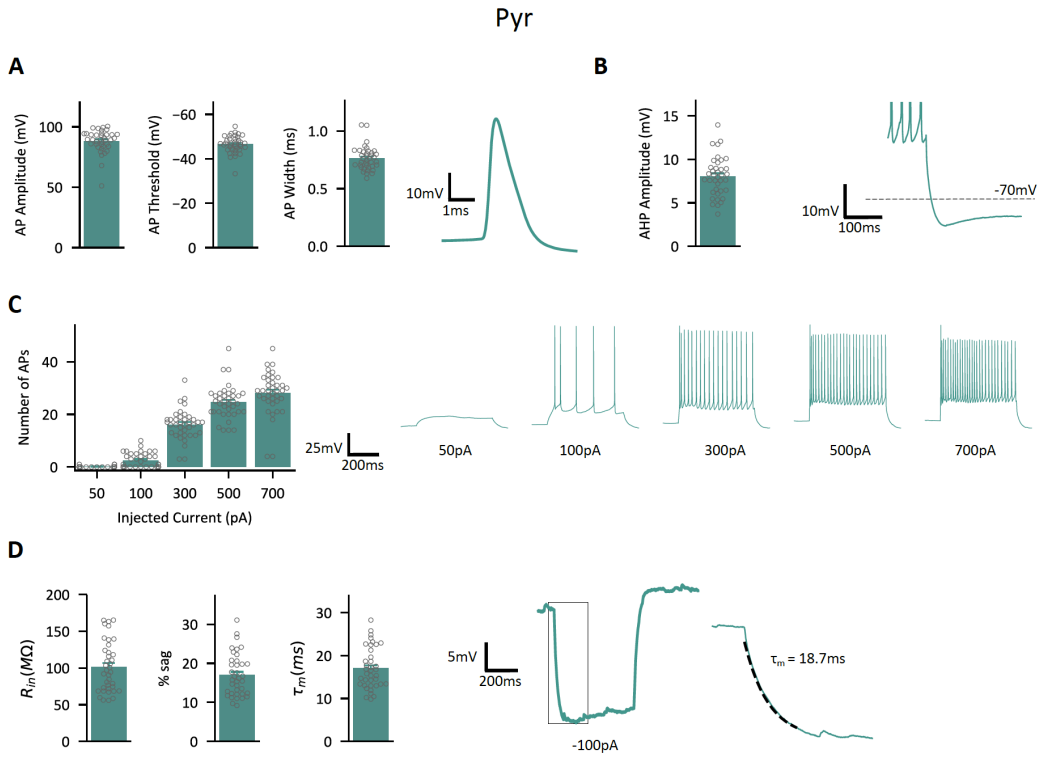


**Figure 3-2 Intrinsic properties of pyramidal neurons.** (A) Action potential (AP) amplitude, threshold and width properties of pyramidal neurons. (B) AHP amplitude of pyramidal neurons. (C) Number of APs fired during 500ms current injection to pyramidal neurons. (D) Input resistance ($R_{in}$), %sag and $\tau_m$ of recorded pyramidal neurons. Data are presented as mean ± SEM.

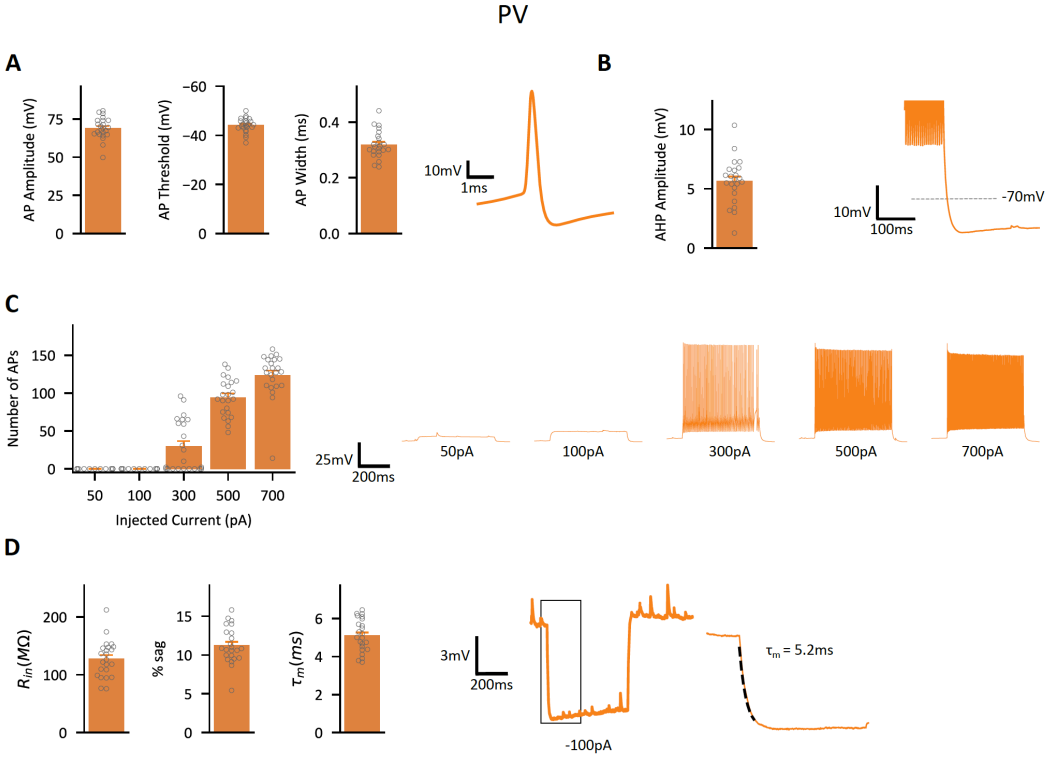


**Figure 3-3 Intrinsic properties of PV+ interneurons.** (A) Action potential (AP) amplitude, threshold and width properties of PV+ interneurons. (B) AHP amplitude of PV+ interneurons. (C) Number of APs fired during 500ms current injection to PV+ interneurons. (D) Input resistance ($R_{in}$), %sag and $\tau_m$ of recorded PV+ interneurons. Data are presented as mean ± SEM.

To ensure the synaptic dynamics were probed at a sufficiently broad stimulation range, the inhibitory connection was tested at the following six frequencies: 5, 10, 20, 50, 100 and 200 Hz (n = 38, Figure 3-4A). For excitatory transmission, it was not possible to evoke action potentials at 200Hz in the presynaptic pyramidal neuron in 12/26 pairs, therefore, recordings that included five test frequencies were used to constrain model parameters of the excitatory connection (n = 26, Figure 3-4B).

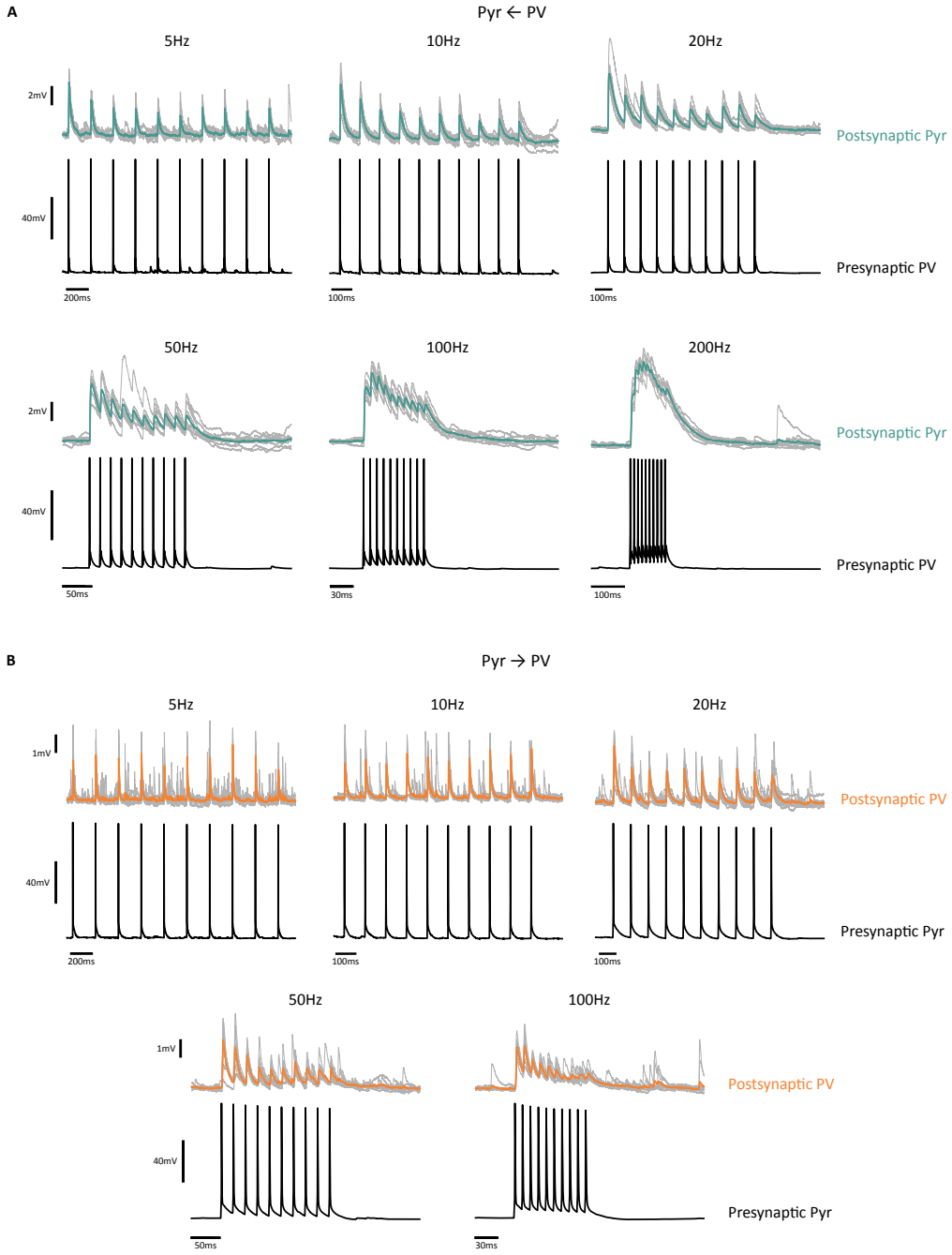


**Figure 3-4 Example traces of frequency trains.** Raw traces (grey) and averaged traces (bold orange/teal) of trains IPSPs in (A) and EPSPs in (B) at frequency stimulations. The presynaptic APs (black) were evoked from -70mV holding potential.

### 3.3.2 Fitting one pool TM models

Two versions of Tsodyks-Markram (TM) models were implemented that assume one pool of vesicles with homogeneous release probability (Tsodyks and Markram, 1997; Tsodyks and Markram, 1998). The first model only accounts for synaptic depression, hereafter referred to as $TM_D$. The second model, $TM_{D+F}$ is an extension of the $TM_D$ model that also accounts for synaptic facilitation by increasing the probability of release at the arrival of an action potential. Parameters of these models were constrained following the method introduce by Costa et al. (2013). A detailed description of the method is in section 3.2.4.1.

Point estimates of the parameters for each cell were used to simulate the model for each cell across all frequencies. To assess model performance, paired-pulse ratio (PPR) and steady-state values were compared to the PPR and steady-state values of the simulated data. The PPR was defined as the ratio of the second peak in the train compared to the first, and the steady state was defined as the mean of the two last peaks normalised to the first peak in the train.

#### *3.3.2.1* Fitting one-pool TM models to inhibitory data

Inhibitory transmission data were fit with both TM models. The point estimate parameters were used to simulate the models for each cell at frequencies used experimentally (5-200Hz). The modelled and experimental data were averaged across the cells and the average observed and predicted peaks were compared (Figure 3-5). As shown in the Figure 3-5A, both TM models fail to follow the dynamics of the recorded inhibitory data. The models overestimate the transmission at lower frequencies (5-20 Hz), and largely overestimate the transmission at higher frequencies (50-200Hz), with the exception of the last three peaks at higher frequencies where the peaks are underestimated (Figure 3-5A).

Next, PPR and steady-state values were compared between the experimental and simulated data. As shown, both models overestimated the PPR values at all frequencies (Figure 3-6A), and the steady-state values for frequencies between 5-20 Hz, but underestimated the steady-state values for 50-200 Hz frequencies (Figure 3-6D). As shown in Figure 3-6A and D, the PPR and steady-state curves have two phases. The initial phase at lower frequencies between 5 to 20Hz where these values decrease rapidly, and a second phase at frequencies between 50Hz to 200Hz where steady-state decreases more slowly. This biphasic pattern in the steady-state transmission of inhibitory transmission has been previously reported in the visual cortex and striatum (Varela et al., 1999; Gittis et al., 2010). The normalised

steady-state at 20Hz was equal to 0.353±0.01 compared to 0.235±0.01 at 100Hz. This small decrease in steady-state means that at frequencies between 20-100Hz inhibition onto pyramidal cells will be less sensitive to the change in firing frequency of PV+ cells. Similarly, at lower frequencies, as the initial relationship between steady-state and frequency is steep, the levels of inhibition will be affected by small changes in firing frequency.

The individual observed and predicted PPR and steady-state values were compared for each cell at all frequencies (Figure 3-6 B, C, E and F). Perfect concordance is achieved if the observed and predicted data follow the identity line (dashed lines in Figure 3-6B and E). If the data fall below or above the identify line it indicates the model is overestimating or underestimating the short-term dynamics, respectively. Both models overestimated the PPR values at all frequencies as shown by the majority of values lying below the identity line in Figure 3-6B. The ratio of overestimated PPR values was calculated by computing the difference between experimental PPR and modelled PPR values and calculating the ratio of the differences >0 to the total number of PPR values. The ratio, shown in Figure 3-6C, shows that both models consistently overestimated between 85-92% of PPR values.

As far as the steady state transmission is concerned, the models consistently overestimated the steady-state values for lower frequency trains (5-20Hz) and underestimated the steady-state values for higher frequency trains (50-200Hz; Figure 3-3D). This lack of fit is highlighted in Figure 3-6E where individual steady-state values for observed and modelled data are plotted. The majority of steady-state values for higher frequencies (50-200Hz) lie above the identity line and the majority of values for higher frequencies lie below the identity line, suggesting under- and overestimation respectively. Both models overestimated ~70% the lower frequency steady-state values and ~30% of higher frequency steady-state values (Figure 3-6F). Overall this indicates that a simple, depression-only TM short-term plasticity model does not account for the dynamics at the inhibitory synapse between PV+ and pyramidal neurons. Moreover, the addition of facilitation to the model does not improve the model performance in capturing the synaptic dynamics.

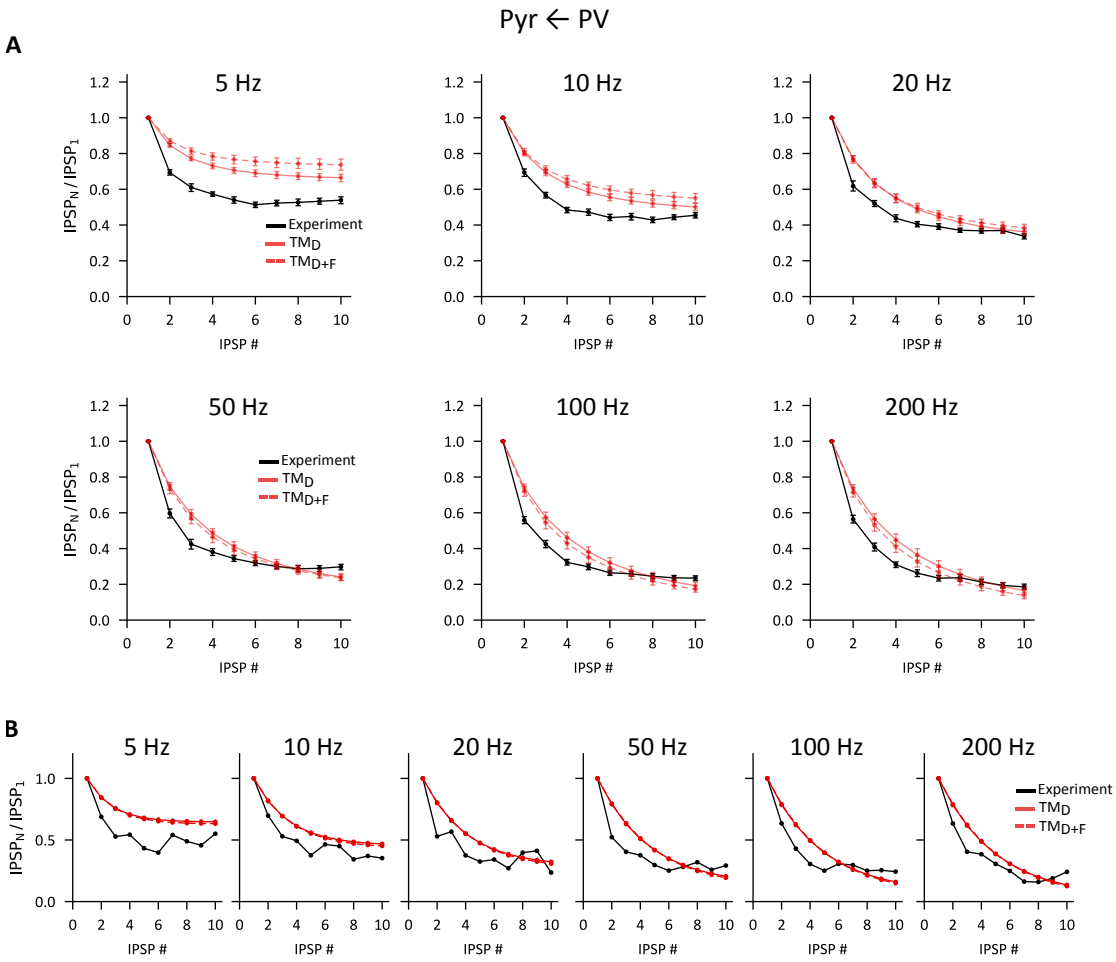


**Figure 3-5 One pool TM models fail to replicate inhibitory transmission between PV+ and pyramidal neurons.** (A) Data from 38 recordings of inhibitory transmission between pairs of PV+ and pyramidal neurons was used to constrain parameters of TM models. Graphs show pooled data from experimentally recorded peaks and pooled data from model simulations. Both models largely underestimate the short-term depression at all frequencies. Data are presented as mean ± SEM. (B) Example of a fit of $TM_D$ and $TM_{D+F}$ models to a single cell across the frequencies used in optimisation, 5 to 200Hz.

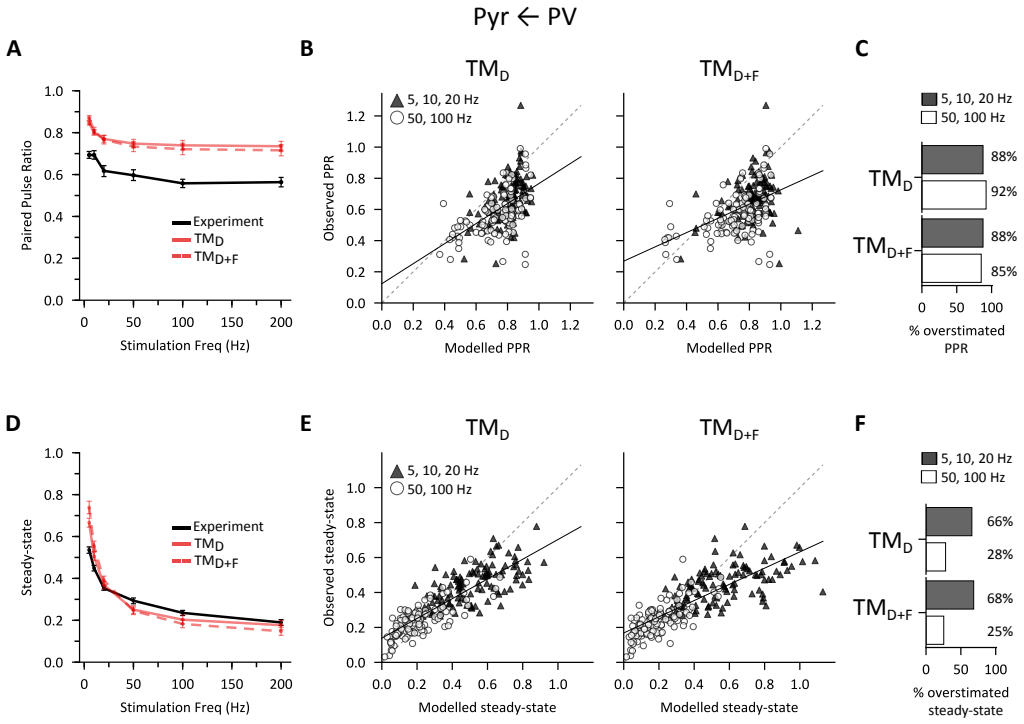


**Figure 3-6 Examining performance of TM models in capturing PPR and steady-state values of inhibitory connection.** (A) Averaged PPR values across frequencies from 5 to 200Hz for modelled and observed data. The individual PPR values for each cell are plotted in (B). (C) Proportion of overestimated PPR values at lower and higher frequencies. (D) Averaged steady-state transmission values for experimental data and modelled data. Individual data points for each cell are in (E) and show that majority of values for low frequency fall below the identity line, and majority of values for high frequency fall above the identity line indicating over- and underestimation respectively. (F) Proportion of overestimated steady-state values for each model at lower and higher frequencies. Data are presented as mean ± SEM.

### *3.3.2.2* Fitting one-pool TM models to excitatory data

Next, the performance of the one-pool TM models was assessed for the excitatory synapse between pyramidal neurons and PV+ interneurons. As described before, the experimental data contained trains of stimulations at frequencies between 5-100Hz. These data were used to optimise the parameters of two TM models, $TM_D$ model that only models depression and $TM_{D+F}$ that also accounts for facilitation. The parameters were optimised independently for each data set (n = 26) and the point estimates of the parameters were used to simulate the models at frequencies used in the experimental recordings to allow direct assessment of the model performance in capturing the data.

Figure 3-7A shows averaged experimental recordings compared to averaged simulations from all the recordings of excitatory transmission. At 5 and 10Hz the experimental EPSPs show little depression, however, increasing frequency of stimulation reveals marked short-term depression. In contrast to the inhibitory data, the depression-only $TM_D$ model successfully captured short-term dynamics of this connection (Figure 3-7A). The model

generates close fits to all the peaks across all the tested frequencies. Addition of facilitation to the $TM_D$ model deteriorates the fit of the model to the data. While $TM_{D+F}$ model closely followed the experimental data at frequencies of 20Hz and above, it largely overestimated the dynamics of recorded EPSPs at lower frequencies of 5 and 10Hz (Figure 3-7A).

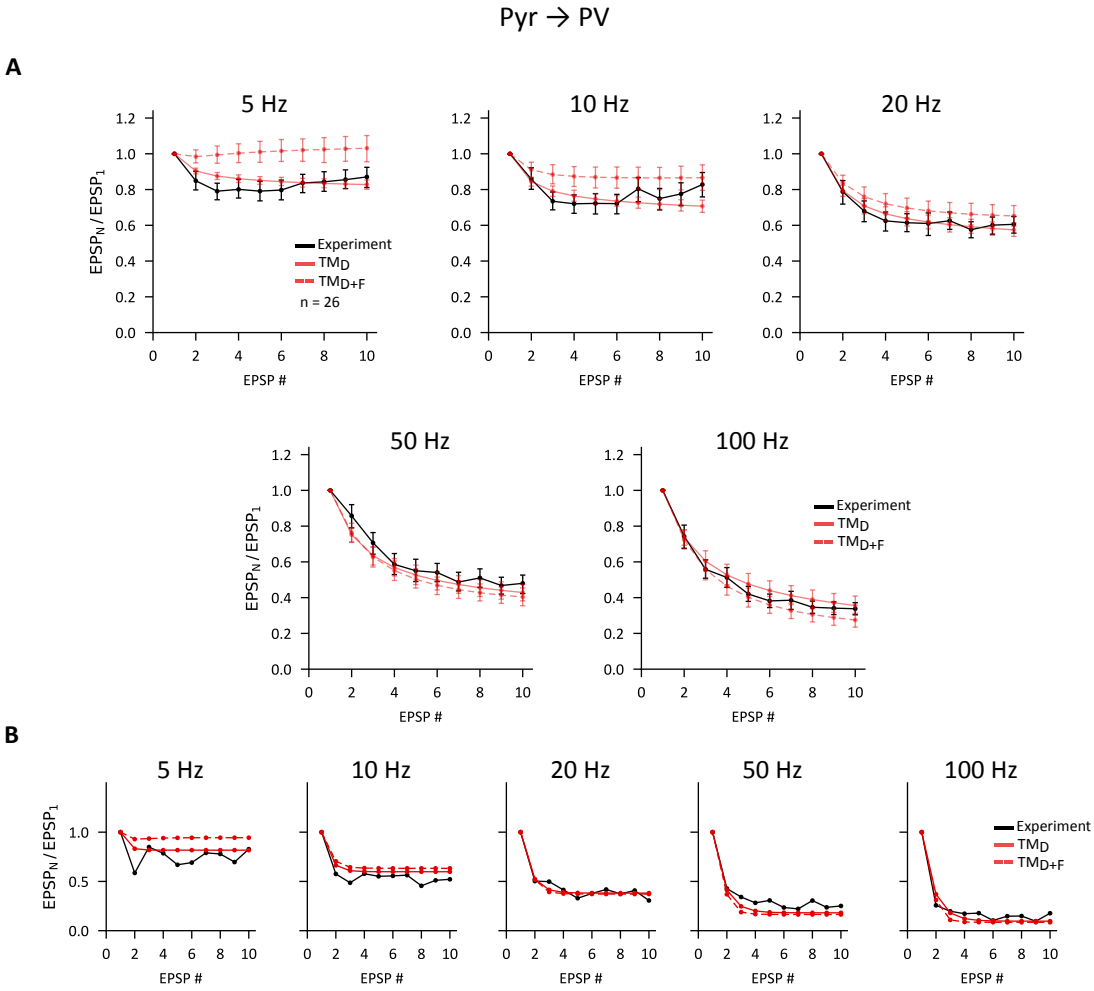


**Figure 3-7 $TM_D$ but not $TM_{D+F}$ models capture the dynamics of excitatory synaptic transmission formed by PV+ and pyramidal neurons.** (A) Data from 26 recordings was used to constrain parameters of TM models. Graphs show pooled data from experimentally recorded peaks and pooled data from model simulations. $TM_D$ model closely follows the peaks while extending the model with facilitation ($TM_{D+F}$) deteriorates the fit. Data are presented as mean ± SEM. (B) Example of a fit of $TM_D$ and $TM_{D+F}$ models to a single cell across the frequencies used in optimisation, 5 to 100Hz. Note how the model with facilitation, $TM_{D+F}$, overestimates the peaks at 5Hz.

Next, the performance of the models was examined specifically at capturing PPR and steady state values. As shown in Figure 3-8A, both models follow the PPR values at higher frequency of 100Hz, however, while the $TM_D$ model accurately captures PPR and steady-state at lower frequencies between 5 and 20Hz, the $TM_{D+F}$ model overestimates both the PPR and steady-state values at lower frequencies. The experimental data show a peak in PPR values at 50Hz (Figure 3-8A), however, neither of the models are able to replicate this

feature. The PPR values across the stimulation frequencies are remarkably stable and are only significantly different between 50 and 100Hz ($p = .01$; One-way repeated measures ANOVA with post-hoc Bonferroni correction). This suggests that a pyramidal neuron firing two action potentials provides the same levels of excitation to PV+ interneurons at each pulse across the frequencies between 5-50Hz. In the $TM_D$ model this relationship is achieved by a low release probability (0.27±0.2) and a relatively fast depression time constant that controls the recovery dynamics of vesicles (0.73±0.1s).

Figure 3-8B shows individual experimental PPR data points plotted against modelled PPR values for both models for each cell. PPR values are split into two groups, PPR values at lower frequencies between 5-20Hz and higher frequencies of 50 and 100Hz. The fact that there is no clustering of lower frequency values and higher frequency PPR values and that values at low and high frequencies span a similar range of values further highlights the frequency-independence of PPR values at this synapse. The ratio of overestimated PPR values for each frequency group was calculated by computing the difference between modelled PPR and experimental PPR values, if the model overestimated PPR values, the difference was >0, whereas, if PPR was underestimated the difference was <0. The ratio, shown in Figure 3-8C, was computed as the number of values >0 divided by the total number of PPR values. Both models show a similar trend in overestimation, where lower frequency PPR values are more likely to be overestimated ($TM_D$: 62%; $TM_{D+F}$: 79% overestimated) and higher frequency PPR values are more likely to be underestimated ($TM_D$: 31%; $TM_{D+F}$:25% overestimated).

Figure 3-8B also shows that a proportion of cells show paired-pulse facilitation as their PPR values are >1. It was identified that 16 out of 26 cells showed PPR>1 at at least one frequency. However, PPR values of synapses with no facilitation can occasionally be above 1. This can be attributed to the stochastic nature of synaptic transmission and lower release probabilities. If, for instance, the first pulse in the train only releases a small proportion of vesicles then by the second pulse in the train the empty release sites are likely to be replenished. This might be particularly problematic at lower frequency trains where the time between spikes is longer, hence the vesicles are more likely to be fully replenished by the second pulse. PPR values at each stimulation frequency were examined (Figure 3-9A, B). As can be seen in Figure 3-9A, there is some consistency of PPR>1 across frequencies for individual cells, for example, 6 out of the 16 cells showed values of PPR>1 at both 50Hz and 100Hz, and 3 out of 16 cells showed PPR>1 at 20, 50 and 100Hz. At each frequency between 20-35% of cells show paired-pulse facilitation (Figure 3-9B). This suggests that a subset of synapses formed by pyramidal neurons onto PV+ interneurons

show facilitation. PPR at synapse between these synapses have been previously reported to be age-dependent with the level of short-term depression decreasing with age (Angulo, Rossier, et al., 1999). Therefore, the correlation of PPR values and age was examined for PPR values at 50Hz (Figure 3-9C). No correlation between age and 50Hz PPR values was observed in the age range of postnatal day 26-45 (Spearman's $\rho = 0.036$, $p = .86$). Therefore, paired-pulse facilitation between postnatal day 26 and 45 is independent of age.

In conclusion, PPR values suggest that the excitatory inputs onto PV+ cells facilitate in a small subset of connections (20-35%) a feature that the $TM_D$ model can not account for. However, despite the fact that the $TM_{D+F}$ includes facilitation by modelling increases in release probability at spike time, the model does not replicate this facilitation. This is clear in Figure 3-8B where the modelled vs observed values for observed PPR values >1 do not follow the identity line.

Next, the performance of TM models in capturing steady-state transmission was evaluated. Steady-state transmission was calculated as a mean of peaks 9 and 10 normalised to the first peak of any given stimulation frequency. In contrast to the inhibitory steady-state transmission (Figure 3-6D), the excitatory steady-state decays monoexponentially, almost linearly, with increasing stimulation frequency (Figure 3-8E). This means that during steady-state transmission PV+ are more sensitive to changes in firing rate of pyramidal neurons (Silver, 2010). As in the case of PPR values, a subset of cells showed steady-state values >1. The PPR values and steady-state transmission were positively correlated (Figure 3-10; Spearman's $\rho = 0.716$, $p < .001$). This means that if the synapse showed paired-pulse facilitation it was more likely to show facilitation in steady-state

Individual modelled steady-state transmission values were plotted against experimental steady-state values (Figure 3-8E). In contrast to PPR values at this synapse, the lower and higher frequency steady-state values show clear clustering which highlights their frequency-dependence. As shown in Figure 3-8F, a similar trend was observed as in PPR values where steady-state transmission was mostly overestimated by both models ($TM_D$: 77%; $TM_{D+F}$:83% overestimated) and underestimated for lower frequencies ($TM_D$: 34%; $TM_{D+F}$:32% overestimated). As in the case of PPR values, the model that included facilitation, $TM_{D+F}$, does not replicate the facilitated steady-state transmission at this synapse. This is highlighted by the fact that steady-state values >1 do not follow the identity line (Figure 3-8E).

Therefore, the $TM_D$, model that only models depression, performs better than $TM_{D+F}$ model at replicating the short-term dynamics at this synapse. This is despite the fact that a subset of cells (20-35%) shows facilitation. Hence, the $TM_D$ model is viewed as favourable in accounting for the short-term dynamics of excitatory transmission between pyramidal and PV+ interneurons within the mPFC.

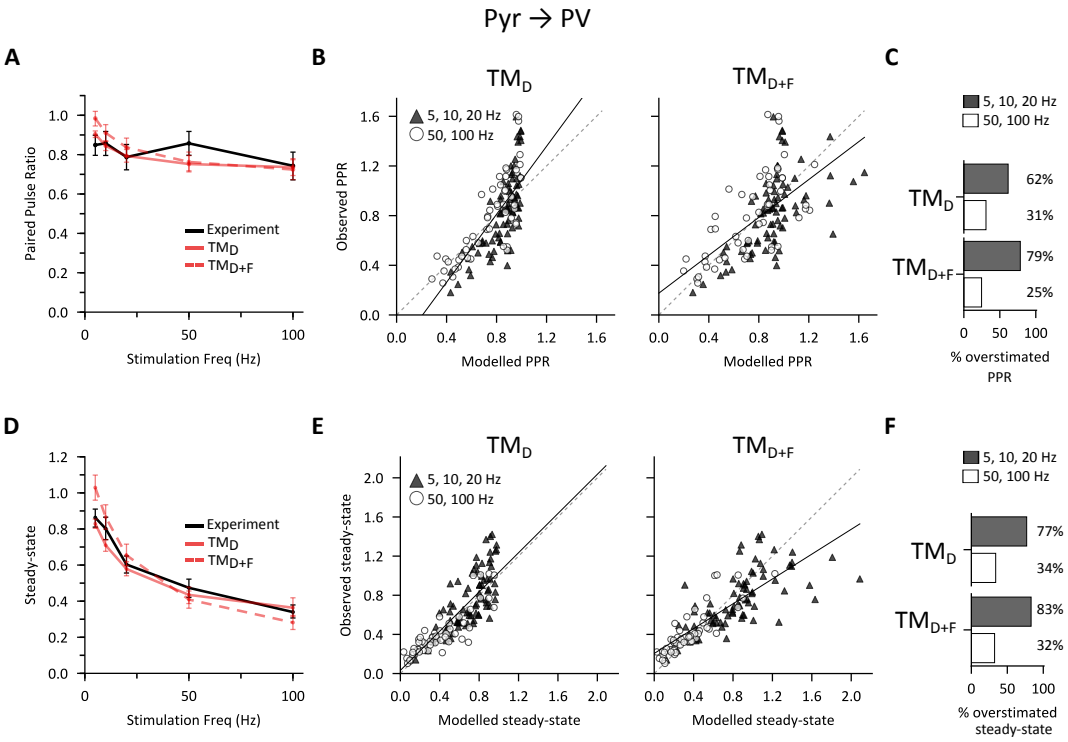


**Figure 3-8 Examining performance of TM models in capturing PPR and steady-state values of excitatory connection** (A) Averaged PPR values across frequencies from 5 to 100Hz for modelled and observed data. The individual PPR values for each cell are plotted in (B). (C) Proportion of overestimated PPR values at lower and higher frequencies. (D) Averaged steady-state transmission values for experimental data and modelled data. Individual data points for each cell are in (E). (F) proportion of overestimated steady-state values for each model at lower and higher frequencies. Data are presented as mean ± SEM.

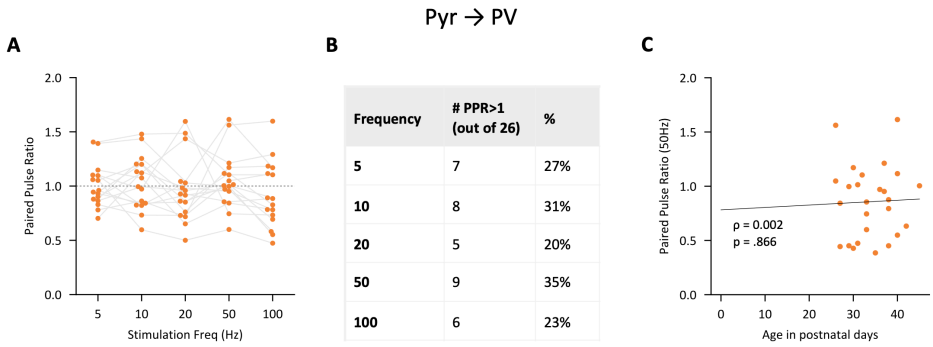


| Frequency | # PPR>1 (out of 26) | % |
|---|---|---|
| 5 | 7 | 27% |
| 10 | 8 | 31% |
| 20 | 5 | 20% |
| 50 | 9 | 35% |
| 100 | 6 | 23% |

**Figure 3-9 PPR values of excitatory transmission across range of frequencies.** (A) PPR values across a range of frequencies. Each dot represents one PPR value for one cell. Light grey lines connect PPR values across the frequencies for individual cells. (B) Proportion of synapses showing paired-pulse facilitations. (C) Using Spearman rank test, PPR values were tested for correlation with age, no relationship was found.

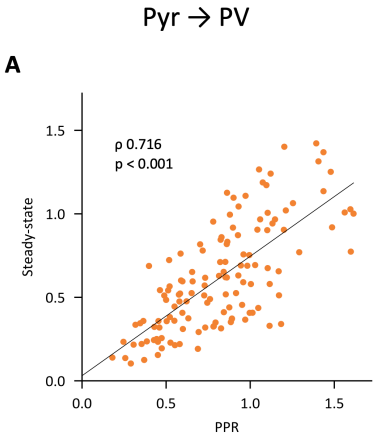


**Figure 3-10 Correlation of PPR and steady-state values of excitatory transmission.** PPR values and steady-state values are positively correlated at the excitatory synapse between pyramidal and PV+ neurons within the mPFC. Correlation tested with a Spearman rank order test.

### 3.3.3 Alternative STP models

Next, alternative STP models were fit to the recorded data to test if different models can capture the synaptic dynamics of inhibitory transmission and furthermore, to verify the robustness of the fit by one pool depression-only $TM_D$ model to the excitatory data. The candidate models were selected based on studies investigating mechanistic details of STP in cortical, cerebellar and calyceal synapses (Fuhrmann et al., 2004; Hallermann et al., 2010; Taschenberger et al., 2016). Table 3-2 lists the tested models and highlights the main differences between their assumptions about the number of vesicle pools and the release probability dynamics. Figure 3-11 shows schematics of the models listed in Table 3-2. All the models are phenomenological, the differential equations controlling the variables in the

models are described in methods section 3.2.2 and 3.2.3 and the analytical solutions to the equations are provided in Appendix I.

As described in the general introduction (section 1.5), synaptic transmission is mediated by the release of vesicles containing neurotransmitter. Vesicles transition through a number of steps before the release (Sudhof, 2004). Vesicles are replenished from a reserve pool which in all of the implemented models is infinite and homogeneous, i.e. there are no molecular/intrinsic differences between the vesicles and any release probability differences only arise once the vesicle docks to the presynaptic membrane. Vesicles dock to the presynaptic membrane where they become primed for release and at spike time, vesicles can be released with certain release probability. The docking and priming steps are modelled as one step and the release is instantaneous.

Three alternative classes of STP models were implemented (Figure 3-11). First class, release-independent depression models (RID), models a decrease in release probability at a spike time which then recovers back to its initial value between spikes. Physiologically, decrease in release probability is mediated by decreases in calcium influx with repetitive activity due to inactivation of calcium channels and/or changes in action potential waveform (Patil et al., 1998; Thomson and Bannister, 1999; Kirischuk et al., 2002; Kawaguchi and Sakaba, 2015). Some evidence shows that the recovery from depression may be activity-dependent (Stevens and Wesseling, 1998; Wang and Kaczmarek, 1998; Fuhrmann et al., 2004). It has been proposed to be mediated by either activity dependent recovery rate of vesicles or by activity dependent recovery of the release probability. To the test latter hypothesis, the RID model is further extended to include a frequency-dependent recovery (FDR) of the release probability ($RID_{FDR}$ model) (Fuhrmann et al., 2004).

The RID models assume that during activity synaptic transmission will be mediated by release sites with different release probabilities, however, at rest, release probability will be homogeneous across all release sites. An alternative hypothesis, based on work in the cerebellum and calyx of Held, is that the release sites have heterogeneous release probabilities at rest (Trommershäuser et al., 2003; Hallermann and Silver, 2013; Taschenberger et al., 2016; Turecek et al., 2016). Across the literature, these models are implemented in two ways. One way is to model the heterogeneous release sites as independent and one is to model the higher release probability release sites arising from low release probability release sites. In the results described in this chapter, the second way

is tested where lower release probability vesicles transition into a higher state of release probability, referred to as a sequential model (Seq).

The sequential, Seq, model is a phenomenological simplification of models used previously to account for short-term dynamics at cerebellar and calyceal synapses (Trommershäuser et al., 2003; Hallermann and Silver, 2013; Taschenberger et al., 2016; Turecek et al., 2016). In this model, vesicles transition through stages of maturation where the first step is associated with a lower release probability and the higher release probability vesicles are a mature version of the lower release probability vesicles. Additionally, vesicles can transition back from high to low release probability. This means that the proportion of low to high release probability vesicles at rest will be controlled by the depression time constants of the forward and backward rate associated with this transition. Whether the step in the sequential model corresponds to molecular priming or positional priming is not well understood. However, as the model is phenomenological, it can account for either or both at the same time.

The models that assume heterogeneous release probability at rest implemented in the aforementioned studies, such as the Seq model, assume different speeds of replenishment of lower and higher release probability vesicle pools. The low release probability vesicles are replenished rapidly while the higher release probability vesicles are replenished more slowly. Here, a simplification of these recovery kinetics is also tested where both pools are replenished with the same time constant, referred to as 2P model hereafter. In the 2P model, release sites can have lower or relatively higher release probability at rest. The proportion of low to high probability release sites is modelled with an extra parameter, $\alpha_1$.

Therefore, in summary, in all of the models depletion of vesicles contributes to depression of postsynaptic responses. In release-independent depression models, decrease in release probability at the arrival of the presynaptic action potential also contributes to depression. In models that include facilitation, facilitation is implemented by increases of release probability at spike time. Both the 2P and Seq model were tested either assuming no facilitation of the release probability of both pools, or assuming facilitation of both pools with differing facilitation parameters for each pool.

| Model # | Notation | Model description | Pool # | Release probability dynamics |
|---|---|---|---|---|
| 1 | $TM_D$ | Tsodyks-Makram model | 1 | - |
| 2 | $TM_{D+F}$ | | 1 | Facilitation |
| 3 | $RID_D$ | Release-independent depression model | 1 | - |
| 4 | $RID_{FDR}$ | | 1 | Release-independent depression and frequency-dependent recovery |
| 5 | $2P_D$ | Two independent pools model | 2 | - |
| 6 | $2P_{D+F}$ | | 2 | Facilitation of both pools |
| 7 | $Seq_D$ | Sequential model | 2 | - |
| 8 | $Seq_{D+F}$ | | 2 | Facilitation of both pools |

**Table 3-2 List of STP models fit to excitatory and inhibitory transmission data.**

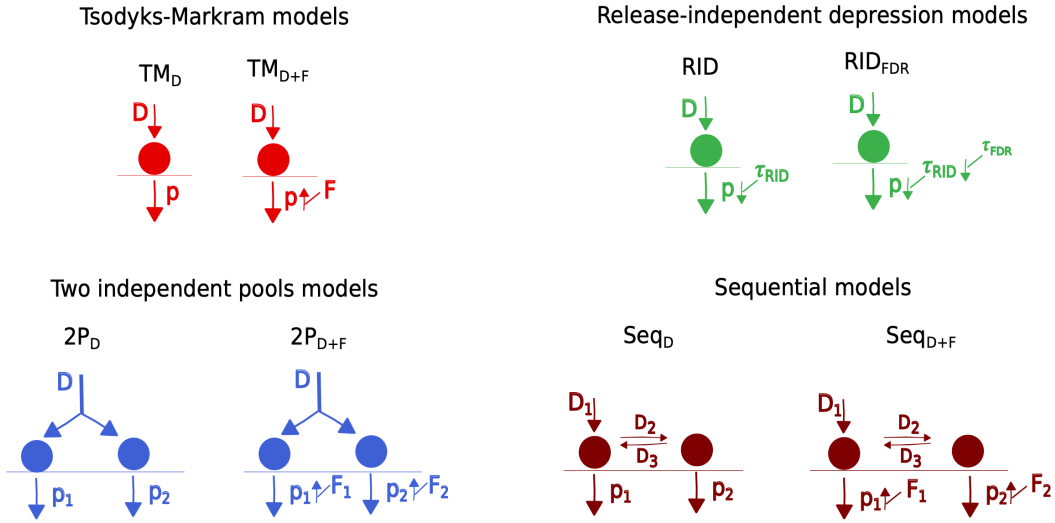


**Figure 3-11 Schematics of tested STP models.** TM models assume heterogeneous release probability, $p$, that controls the release of vesicles. Between spikes vesicles recover with time constant $D$. Three main classes of STP models were tested in addition to one-pool TM models. The RID models model decreases in release probability, $p$, that recovers with $\tau_{RID}$. The RID model can be extended to include activity dependent recovery from the depression by modelling decreases in $\tau_{RID}$, in that formalism $\tau_{RID}$ recovers back to its initial value with time constant $\tau_{FDR}$. Two classes of models were tested that assume heterogeneous release probabilities, $p_1$ and $p_2$, at rest. First, the 2P models, assumed the two release sites release and replenish with the same dynamics but release with different release probability. The Seq models assume that the higher release vesicles are a mature version of lower release vesicles. This transition of low to high release probability state is controlled with $D_2$. Vesicles can transition back to low release probability state with time constant $D_3$.

### 3.3.4 Model selection

The aim of this chapter is to determine which model best describes excitatory and inhibitory short-term dynamics between PV+ and pyramidal neurons within the mPFC. The candidate STP models (Table 3-2) were optimised using experimental recordings of trains of postsynaptic amplitudes in response to range of stimulation frequencies between 5-200Hz. The parameter inference followed an approach by Costa et al., (2013). This method models

average decorrelated peaks with Gaussian noise, see methods section 3.2.4.1 for a detailed description of the implementation of this method.

To select the most parsimonious model, two measures were used to quantify model performance. First, the mean squared error (MSE) was used that quantifies the mean squared difference between the modelled and observed data. If the model was selected based on how closely it follows the recorded data, then the models with the lowest MSE would be selected. However, it is important to note that measures such as MSE will most likely favour the most complex models that have more parameters and thus pose a higher risk of overfitting the data, i.e. the model fits the noise rather than the actual experimental features. Therefore, this quantification was only used as a general indication of the improvement offered by fitting the alternative models.

Hence, to decide which model is the most parsimonious whilst considering its complexity, the Akaike Information Criterion (AIC) was also calculated (Burnham and Anderson, 2004; Wagenmakers and Farrell, 2004). AIC provides a principled method for model selection which evaluates the evidence for each model while penalising the more complex models. The model with the lowest AIC score is the best at approximating the data in the set of the tested models. In the results presented in this chapter, as each model was fit independently for each cell, the AIC scores were calculated for each cell and the individual AIC scores were summed for each model following the approach in Pine et al. (2009). The summed AIC scores were used to compute ΔAIC scores for each model which is the difference between the AIC of a given model and a model with the lowest AIC score. ΔAIC is an indicator of information lost by selecting a given model compared to the best model with the lowest AIC. Rule of thumb has been proposed in regards to ΔAIC values where $\Delta AIC < 2$ suggests that the models are indistinguishable and values >10 suggest that model has no support given the data (Anderson, 2004; Wagenmakers and Farrell, 2004)

#### *3.3.4.1* Model selection - Excitatory transmission

First, MSE was compared between the models for the recordings of the excitatory synapse between pyramidal and PV+ interneurons (Figure 3-12A). As the first peak was normalised for both experimental and modelled data, MSE was calculated using peaks 2-10 across five frequencies between 5-100Hz for the data from 26 recorded pairs of pyramidal and PV+ neurons.

As shown in Figure 3-12A MSE values are very similar for all the tested STP models. The alternative STP models did not produce substantial improvement in the fit of the modelled peaks to the experimental EPSPs compared to the TM models. The $TM_D$ and $2P_D$ model have the lowest MSE scores (Figure 3-12A). Similar to the TM models, addition of facilitation to 2P and Seq models did not improve the fit of the model to the data. It is important to note that all the tested models are nested. This means that if parameters in a more complex model that are not in the simpler models are set to zero then the more complex model behaves like the simpler model. Therefore, the similar MSE values are likely a result of the fact that the models are nested.

MSE values suggest that the $TM_D$ model is sufficient to describe the data. To confirm this, AIC values were computed for each model. The model AIC values were obtained by first calculating the AIC values for each cell independently and then summing the individual AIC values for each of the models. As shown in the table in Figure 3-12A, AIC is the lowest for the $TM_D$ model and ΔAICs for all other models are >10. This indicates depression-only TM model is the most parsimonious model to explain the excitatory data.

The models were simulated using the optimised parameter sets at the experimental frequencies of 5-100Hz. Figure 3-13A, C and E show PPR and steady-state values for the three alternative classes of STP models that were tested. The models that do not include facilitation of release probability performed similarly to depression-only $TM_D$ model that, as shown before in Figure 3-7 and Figure 3-8, captured short-term dynamics of the excitatory synapse. Similar to the TM model with facilitation, both of the two-pool models with facilitation overestimate synaptic transmission at lower frequencies of 5, 10 and 20Hz (dashed lines in Figure 3-13C and E). This shows that facilitation of release probability does not account for the paired-pulse facilitation reported at this synapse (section 3.3.2.2).

Therefore, using model simulations, the performance of four classes of models in capturing the STP of the excitatory connection between pyramidal and PV+ interneurons within the mPFC was compared. Model simulations and AIC values demonstrate that the one-pool, depression only TM model provides the best description of the excitatory connection when compared to all the other tested models.

### 3.3.4.2 Model selection - Inhibitory transmission

As shown in section 3.3.2.1, TM models largely underestimated the short-term depression at the inhibitory synapse formed by PV+ and pyramidal neurons. To find a model that explains the dynamics observed at this synapse three alternative classes of models were fit to the data, models are described in detail in section 3.3.3. The models were fit using experimental recordings following approach by Costa et al. (2013).

To assess a general improvement offered by alternative models, MSE was calculated for peaks 2-10 across six stimulation frequencies between 5-200Hz to quantify the error between the observed and modelled data. The first peak was normalised for both modelled and experimental data hence it was not included in the calculation. MSE quantifies the mean of the squared differences between the modelled and experimental data. As shown in Figure 3-12B, all of the alternative models had substantially lower MSE values compared to the TM models, hence all of the alternative models offered an improvement in model performance. Compared to the $TM_D$ model, the biggest improvement in MSE was observed with the $Seq_D$ model (58%) and the smallest improvement was observed with the $RID_D$ model (39%). The $2P_D$ model improved the fit by 45%. Importantly, all the alternative models improved the MSE score, and MSE favours the $2P_D$ model as the best model to describe the data.

Next, to assess the performance of the models while considering the number of free parameters in each model, AIC values were calculated for each cell and summed over the models (table in Figure 3-12B). On the basis of these values, AIC favours the $Seq_D$ model as the most parsimonious with $2P_D$ model in the second place. However, the small difference in the AIC score between these models ($\Delta AIC = 0.3$) indicates that the two models are indistinguishable (Burnham and Anderson, 2004). Nevertheless, the fact that AIC favours these models over the one-pool models suggests that the short-term dynamics at the inhibitory synapse are explained with heterogeneous release probabilities, and that the TM and RID models are not an appropriate phenomenological approximation of inhibitory transmission.

AIC score ranks the tested model and helps to select the most parsimonious model in the set of the tested models. Hence, this means that even in a set of badly informed models that do not replicate the data, AIC will still select a ‘winner’. Therefore, it is important to simulate the models and validate if the models replicate the features of the experimental data. As shown previously (Figure 3-5 and Figure 3-6), the one pool TM models failed to

capture the dynamics of the inhibitory connection between PV+ and pyramidal neurons. The PPR values were largely overestimated and the steady-state values were either over- or underestimated dependent on the frequency of stimulation. The replication of these features was examined for the three classes of alternative models (Figure 3-14).

As shown in Figure 3-14, both RID models improve the fit of the steady-state values across all the frequencies. The depression only RID model, $RID_D$, while it improves the fit of PPR values over the TM models, it still largely overestimates the PPR values at all frequencies. The addition of an activity-dependent recovery of release probability, the $RID_{FDR}$ model, improves the fit of PPR values and accurately captures the PPR values at lower frequencies between 5-20Hz, however, it still slightly overestimates the PPR values at frequencies between 50-200Hz. It is important to note that the $RID_{FDR}$ model performs well at capturing the data. However, AIC favours the 2P and Seq models because these models have less parameters than the $RID_{FDR}$ model, hence offer a more parsimonious explanation of the dynamics at this synapse.

The depression only two-pool models, $Seq_D$ and $2P_D$, mostly capture the PPR and steady-state values, while slightly overestimating the PPR values at higher frequencies of 50-200Hz (Figure 3 14C, E). Similar to TM models, addition of facilitation does not substantially change the quality of these fits, suggesting there is no facilitation at this synapse.

In contrast to excitatory transmission, one pool TM models did not reproduce the inhibitory data and the alternative models offered substantial improvements on the fits to the data. Based on the AIC ranking, it can be concluded that the models with heterogeneous release probabilities, $2P_D$ and $Seq_D$ models, are the most parsimonious models to describe the short-term dynamics at this synapse.

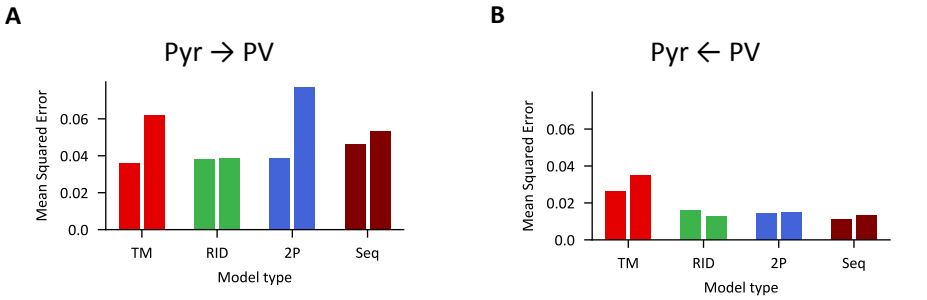


| Model # | Model | k | sum AIC | delta AIC |
|---|---|---|---|---|
| **1** | $TM_D$ | 2 | 394 | 0 |
| **2** | $TM_{D+F}$ | 4 | 544 | 150 |
| **3** | $RID_D$ | 4 | 487 | 93 |
| **4** | $RID_{FDR}$ | 6 | 609 | 215 |
| **5** | $2P_D$ | 5 | 487 | 93 |
| **6** | $2P_{D+F}$ | 9 | 724 | 330 |
| **7** | $Seq_D$ | 5 | 552 | 158 |
| **8** | $Seq_{D+F}$ | 9 | 770 | 376 |

| Model # | Model | k | sum AIC | delta AIC |
|---|---|---|---|---|
| **1** | $TM_D$ | 2 | 980 | 163 |
| **2** | $TM_{D+F}$ | 4 | 1246 | 430 |
| **3** | $RID_D$ | 4 | 916 | 100 |
| **4** | $RID_{FDR}$ | 6 | 937 | 121 |
| **5** | $2P_D$ | 4 | 816.5 | 0.3 |
| **6** | $2P_{D+F}$ | 8 | 1114 | 298 |
| **7** | $Seq_D$ | 5 | 816.2 | 0 |
| **8** | $Seq_{D+F}$ | 9 | 1203 | 387 |

**Figure 3-12 STP model selection for excitatory and inhibitory data.** (A) MSE values (top) calculated using experimental frequency train data of frequency trains for excitatory connection between pyramidal and PV+ interneurons for four tested classes of models. AIC values (bottom) for each tested model for excitatory data. (B) MSE values (top) calculated for inhibitory transmission between PV+ and pyramidal neurons using experimental and modelled data. AIC values (bottom) for each tested model for inhibitory data. k – number of free parameters in a model.

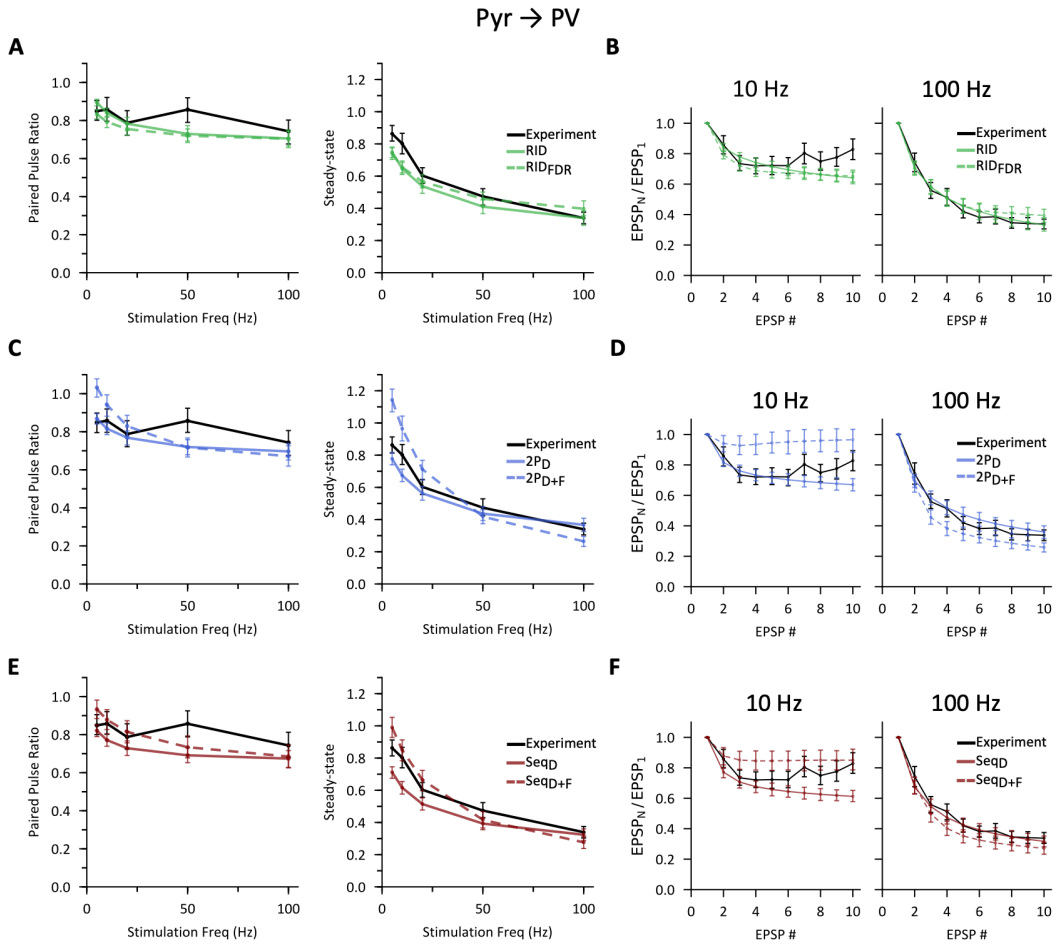


**Figure 3-13 Comparison of model performance of all tested STP models in capturing the short-term dynamics of excitatory transmission.** Three alternative classes of model were optimised to test if they improve the fit of TM models of short-term dynamics of excitatory transmission. The simulated and experimental PPR and steady-state values across all tested frequencies (5-100Hz) are plotted A, C and F. Panels B, D and F show model performance of three classes of models for two example frequencies of 10 and 100Hz. Data are presented as mean ± SEM.

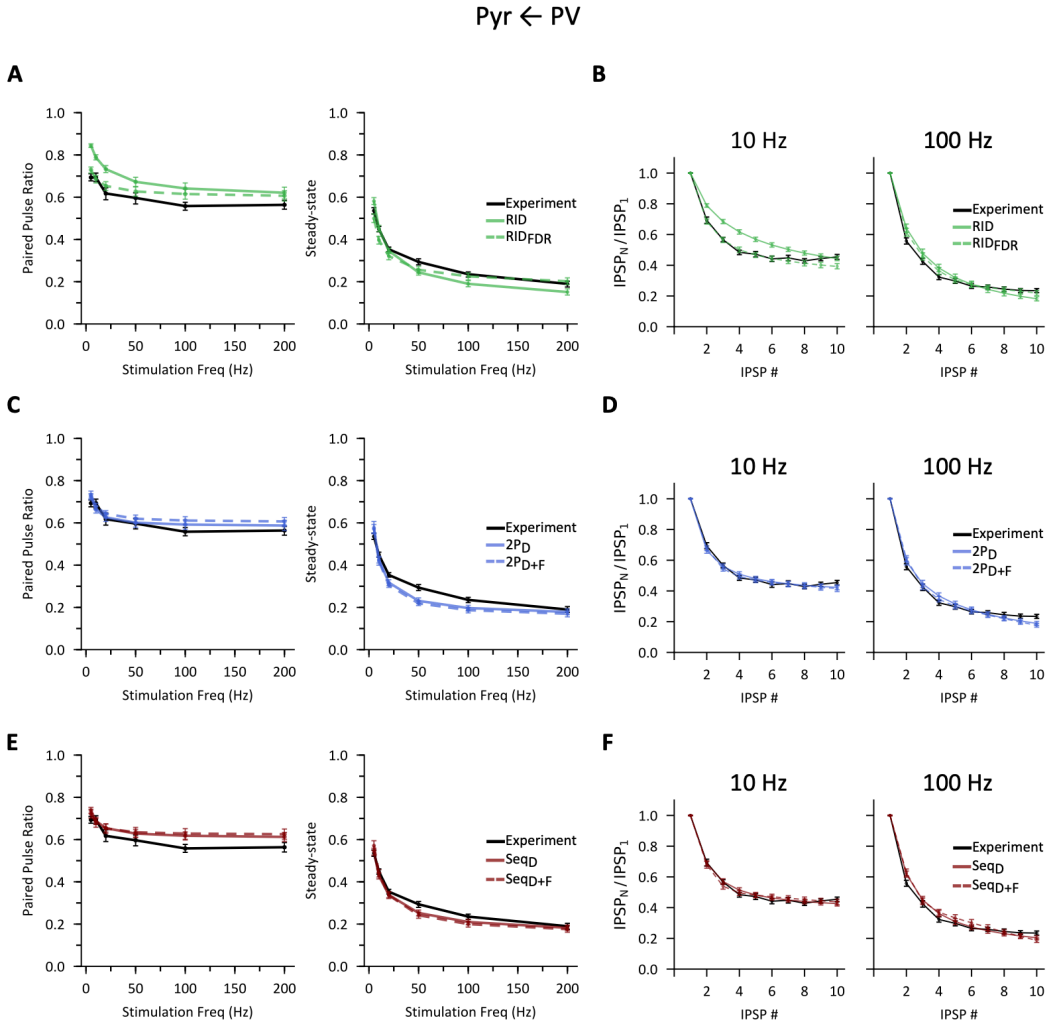


**Figure 3-14 Comparison of model performance of all tested STP models in capturing the short-term dynamics of inhibitory transmission.** Three alternative classes of model were optimised to test if they improve the fit of TM models of short-term dynamics of inhibitory transmission. The simulated and experimental PPR and steady-state values across all tested frequencies (5-100Hz) are plotted A, C and F. Panels B, D and F show model performance of three classes of models for two example frequencies of 10 and 100Hz. Data are presented as mean ± SEM.

## 3.3.5 Comparison of two-pool models for inhibitory data

As concluded in the section before, AIC ranking indicates that the heterogeneous release probability models, $2P_D$ and $Seq_D$ models, are the best at describing the inhibitory short-term plasticity between PV+ and pyramidal neurons (Figure 3-12). As shown in Figure 3-14C and E, both models produce very similar fits to the data.

The parameters of the models were compared to test if the similar performance in capturing inhibitory transmission is driven by similar parameters. The $Seq_D$ model does not explicitly model the ratio of low to high release probability vesicles, hence this proportion is

calculated using the time constants that control the transition to and back between lower release probability vesicles and higher release probability vesicles (Equation 3-10). As shown in Figure 3-15, the parameters for both models yield the same values, as confirmed with Wilcoxon signed-rank test ($p_1$: p = .518; $p_2$: p = .699; $\alpha_1$: p = .087; $\alpha_2$ was not tested as $\alpha_2 = 1 - \alpha_1$; $D_1$: p = .667). This suggests that using this experimental protocol, it is not possible to differentiate between these two models of STP.

Therefore, based on these observations, it is not possible to unequivocally state what might be the mechanism of the existence of heterogeneous release probabilities at the inhibitory synapse between PV+ and pyramidal neurons. The fact that both models replicate the STP, supports the hypothesis that the release probability is not homogeneous, however, confirming the existence of heterogeneous release probabilities and establishing if higher release probability vesicles arise independently or sequentially requires further experiments.

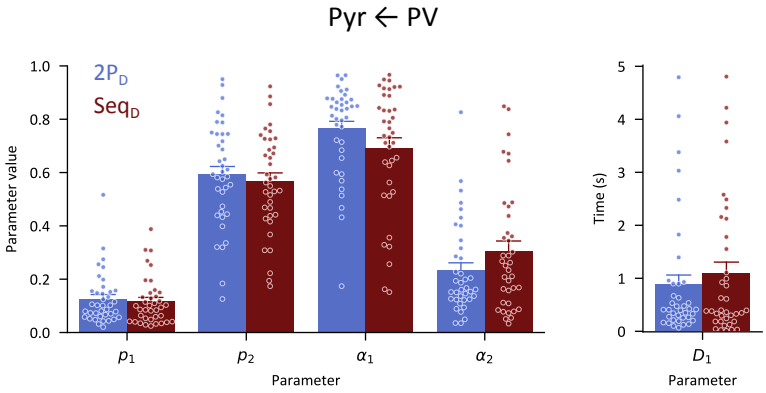


**Figure 3-15 Heterogeneous release probability models yield the same parameter values.** Comparison of optimised parameters for inhibitory data of 2P and Seq models. The parameters showed no differences when tested with Wilcoxon signed-rank test. Data are presented as mean ± SEM.

### 3.3.6 Inhibitory steady-state transmission is sustained by low-release probability vesicles

The previous sections showed that STP at inhibitory synapse formed by PV+ and pyramidal neurons is best explained by assuming heterogeneous release probabilities. Model simulations were used to understand the underlying mechanisms that might support the repetitive transmission at this synapse. Only $2P_D$ model was used to investigate the mechanisms of synaptic transmission as, as discussed in section 3.3.5, the parameters of $2P_D$ and $Seq_D$ are similar, hence, simulations would yield the same answers. It is important to note that, due to two time constants of recovery, $Seq_D$ model will differ from $2P_D$ model

in its recovery after repetitive stimulation, however, the recovery is not examined in this section.

To determine how different heterogeneous release probability vesicles mediate synaptic transmission at inhibitory synapse, the optimised parameters for 38 cells were simulated at 50Hz and the relative contribution of low and high release probability vesicles was determined. The relative contribution of each vesicle pool was quantified by calculating a ratio of the released vesicles in each pool to the total peak. The average difference between low and high release probably vesicles is almost six-fold ($p_1$= 0.13±0.02 vs $p_2$= 0.6±0.03), and at rest the low release probability vesicles constitute 77±3% of total vesicles.

As shown in Figure 3-16, the higher release probability contributes to the initial transmission at the synapse. The higher release probability vesicles contribute to 57±3% of the first peak, compared to 43±3% of transmission mediated by the lower release vesicles. With consecutive peaks, the higher release probability vesicles are depleted and their contribution to the synaptic transmission is smaller relative to the lower release probability vesicles. Once the synapse reaches steady-state transmission, the higher release probability vesicles contribute to only 21±3% of the total peak, while the lower release probability vesicles contribute to 79±3% of the peak. Consequently, the initial synaptic transmission is mediated by both types of vesicles, higher release probability vesicles deplete after ~5 stimuli and lower release vesicles sustain the steady-state transmission.

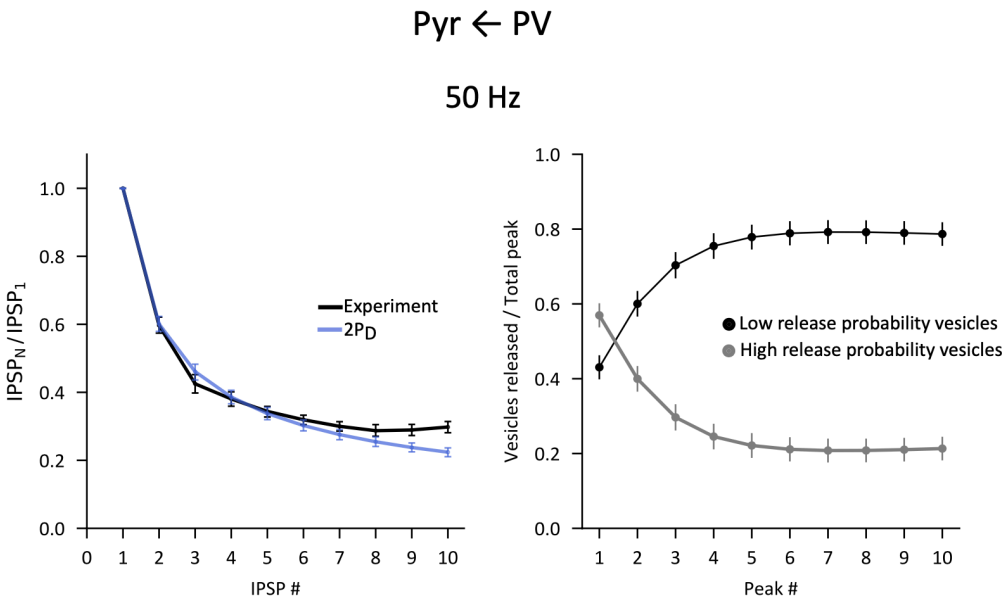


**Figure 3-16 Higher release probability release sites contribute to first initial peaks of the inhibitory synaptic transmission.** Optimised parameters for 38 paired recordings of inhibitory transmission were simulated to assess relative contribution of low and high release probability vesicles to synaptic transmission. Right panel shows the low and high release probability vesicles contribution to the modelled data presented on the left.

### 3.3.7 Optimisation considering correlations between peaks

So far, the STP models were optimised using decorrelated averaged peak values. The correlations between consecutive peaks arise because each peak will be influenced by the number of released and replenished vesicles at previous stimulation times before each next given peak. Therefore, next, it was tested whether the results reported using the deterministic modelling of decorrelated peaks are consistent with results obtained by modelling the correlations between the peaks. The method employed here is based on an approach introduced by Bird et al. (2013) with the exception that Gaussian noise was used to account for the quantal amplitude distributions rather than a gamma process that was used in the study by Bird et al. (2013). This method was not extended to two-pool models and only one-pool models, the TM and RID models, were optimised using this approach.

#### *3.3.7.1* Comparing parameters of optimisation approach with and without peak correlations

The parameters obtained using both methods were compared for both the inhibitory data (Figure 3-17) and excitatory data (Figure 3-18). As the optimisation with no correlations does not model the quantal properties of the synaptic transmission, quantal parameters were not compared.

The differences in parameter values were largely consistent for both excitatory and inhibitory datasets. The facilitation time constant of the TM model that controls the decay of release probability to its initial value, showed differences between the two optimisation methods. The facilitation time constant was higher using the approach with no correlations for the inhibitory and excitatory data compared to the approach that considers correlations (0.42±0.17s vs 2.15±0.27s $p = .002$ for inhibitory; 0.31±0.1s vs 2.24±0.24s $p = .001$ for excitatory). However, it is important to note that the parameter that controls the rate of the facilitation at spike arrival, facilitation rate, showed no differences between the two approaches for both the inhibitory data (no correlations: 0.05±0.02; correlations: 0.07±0.02) and the excitatory data (no correlations: 0.2±0.05; correlations: 0.12±0.03). These two parameters need to be considered together because if one of the parameters is relatively small it means it will counteract the facilitation produced by the other parameter. Hence, both methods of optimisation are in agreement about the lack of presynaptic facilitation at these synapses.

Notable differences between parameters obtained with the two methods were observed in parameters of the RID models. Optimisation with no correlations of the $RID_D$ model yields higher estimates of the depression time constant for the excitatory data (no correlations: 1.49±0.28s vs correlations: 0.26±0.07s, p=.016) and the inhibitory data (no correlations: 1.38±0.2s vs correlations: no correlations: 0.54±0.14s, p=.018). Additionally, in the RID model that also models frequency-dependent recovery, $RID_{FDR}$, the depression time constant was higher for the inhibitory data using the approach with no correlations compared to the approach with correlations (1.62±0.23s vs 0.59±0.14s, p=.001).

Therefore, both optimisation methods yield largely similar parameter values for the four of the tested models. This means that considering the decorrelated, averaged peak amplitude values is a powerful approach to optimising the STP models. The implementation of the deterministic models and their optimisation using decorrelated values is computationally efficient and a large number of parameter samples can be obtained in relatively short periods of time. The optimisation with correlations is more demanding computationally, however, its advantages may become more apparent when dealing with smaller data sets for example of *in vivo* recordings, as discussed in Bird et al. (2013).

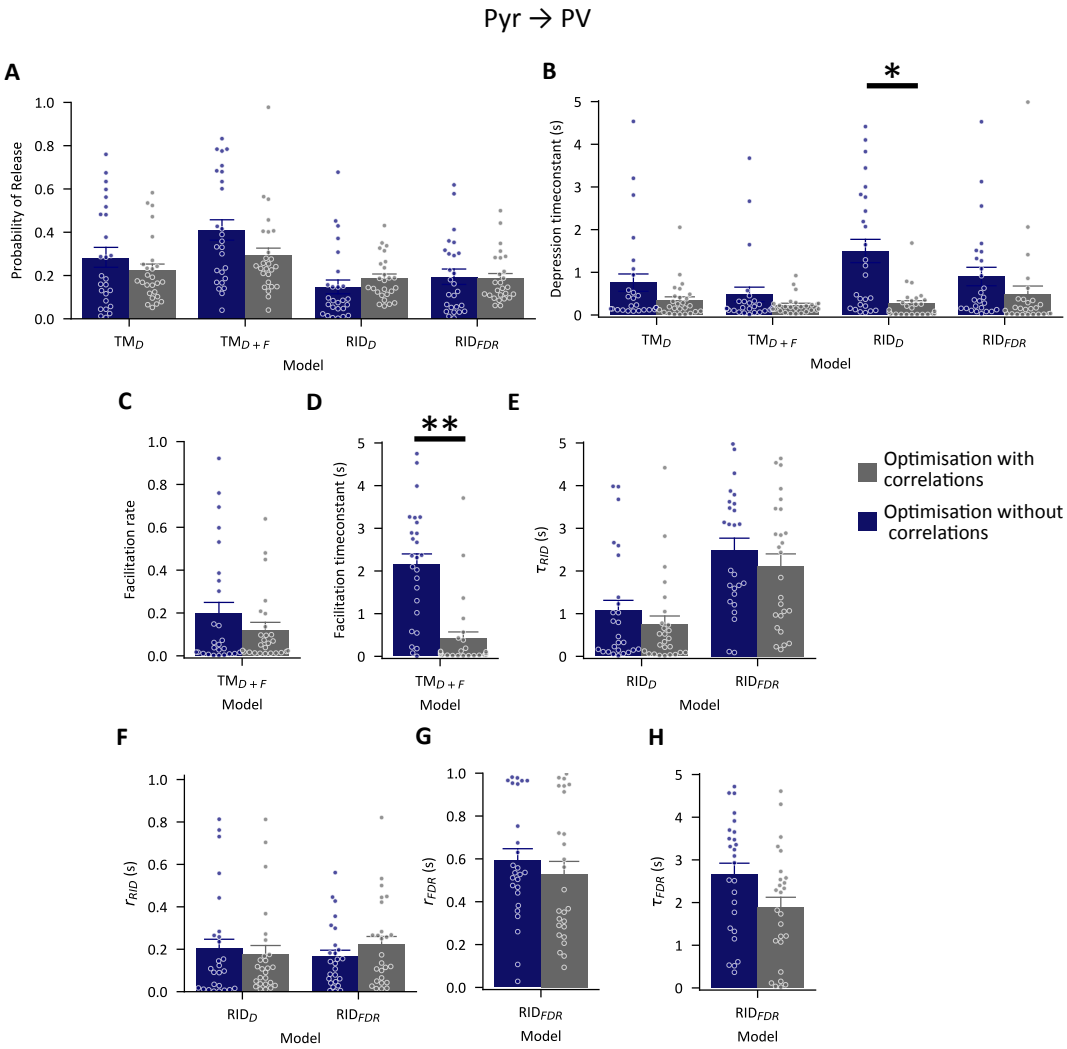


**Figure 3-17 Comparing parameters obtained by optimisation with and without correlations between peaks for excitatory data.** Point estimates of parameters were obtained for a data set of 26 recordings using optimisation approaches that either consider or do not consider correlations between consecutive peaks. Data are presented as mean±SEM, each dot represents one cell; Wilcoxon signed-rank test with Bonferroni correction * = p<.05, ** = p<.01

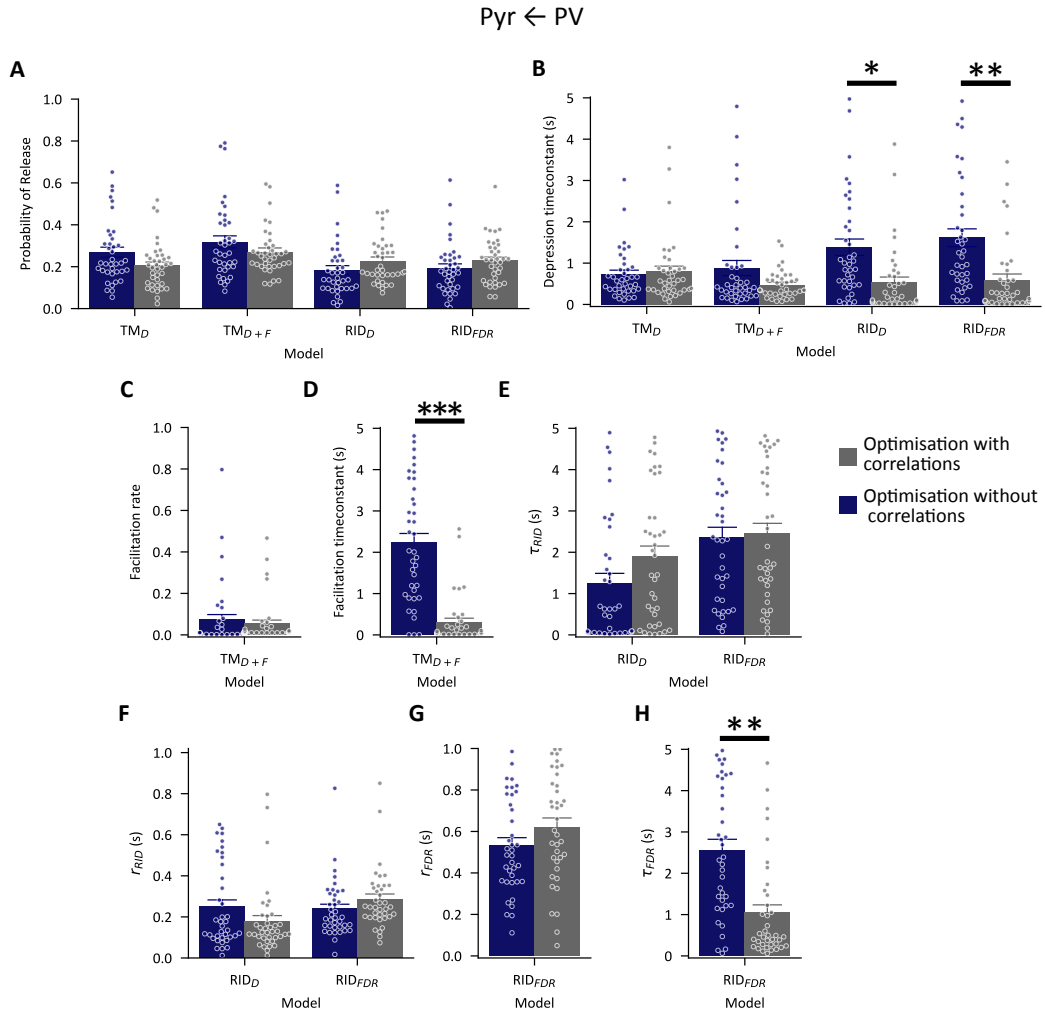


**Figure 3-18 Comparing parameters obtained by optimisation with and without correlations between peaks for inhibitory data.** Point estimates of parameters were obtained for a data set of 38 recordings of inhibitory transmission using optimisation approaches that either consider or do not consider correlations between consecutive peaks. Data are presented as mean±SEM, each dot represents one cell; Wilcoxon signed-rank test with Bonferroni correction * = p<.05, ** = p<.01, *** = p<.001

#### *3.3.7.2* Comparing simulations of optimisation approach with and without peak correlations

The parameters obtained by optimisation method that considers peak correlations were simulated and compared to experimental recordings. The optimisation with correlations also returns quantal parameters hence a stochastic STP model was used to simulate the data. The stochastic STP models were simulated using the point estimates of the parameters for each cell. Each frequency was simulated 100 times for each cell, and the simulated data were averaged and compared to the averaged experimental data for both excitatory and inhibitory transmission (Figure 3-19 and Figure 3-20). As the parameter values obtained by the optimisation with correlations were largely similar, it was expected that the models simulations will perform similarly to the deterministic models in capturing the data.

As shown in Figure 3-19, the excitatory data were captured by simple one-pool TM models. The depression-only TM model, $TM_D$, closely follows the PPR and steady state-values across all the stimulation frequencies between 5-100Hz. As was observed with the optimisation with no correlations, addition of facilitation to the TM model does not improve the fit of the model to the data. The RID models also capture the excitatory data, as previously noted the RID and TM models are nested, this means that if RID parameters, which are not included in the TM models, are set to zero, the RID model behaves like the TM model. Nevertheless, the optimisation considering correlations further validates the observation that the extension of the depression-only TM model is not necessary and does not substantially improve the fit to the data.

Similar to the optimisation with no correlations, inhibitory data were not accounted for by simple TM models (Figure 3-20). The TM models overestimated the synaptic transmission across all the frequencies between 5-200Hz (Figure 3-20A-D). As before, the RID models overestimated the synaptic transmission during initial peaks across all the frequencies, but both models captured the steady-state values of inhibitory transmission. As seen in Figure 3-20C and D, the RID models also overestimate the synaptic transmission between peak 2-8 at both lower and higher frequencies. The optimisation considering correlations was not extended to modelling heterogeneous release sites, hence it can not be tested how the optimisation with correlations of the two pools models performs in capturing the data. Nevertheless, optimisation that considers correlations shows that the one-pool models are inadequate in describing the inhibitory data.

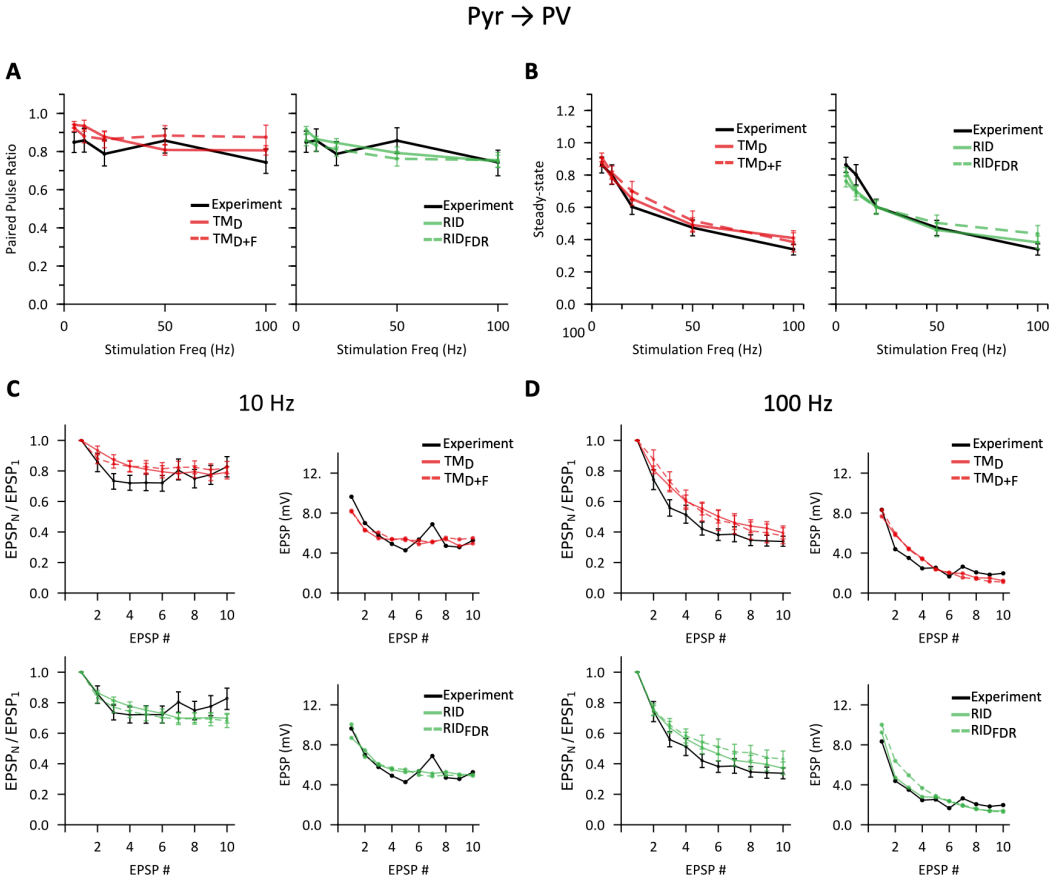


**Figure 3-19 Simulations of stochastic STP models of excitatory transmission.** Best fit parameters were obtained by optimisation that considers correlation between consecutive peaks. Each parameter set for each cell (n = 26) was used to simulate a stochastic STP. Resulting averaged modelled data are plotted against averaged experimental data. Data are presented as mean ± SEM.

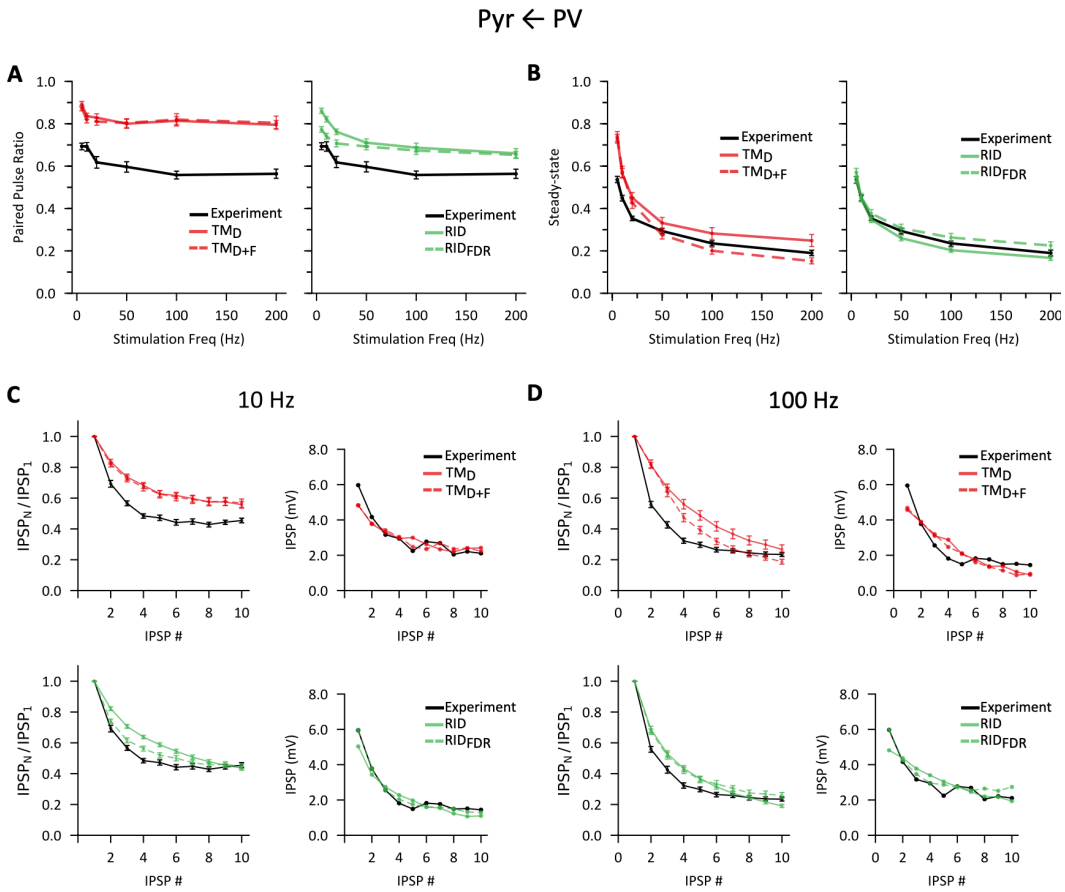


**Figure 3-20 Simulations of stochastic STP models of inhibitory transmission.** Point estimates of parameters were obtained by optimisation method that considers correlation between consecutive peaks. Each parameter set for each cell (n = 38) was used to simulate a stochastic STP. Resulting averaged modelled data are plotted against averaged experimental data. Data are presented as mean ± SEM.

## 3.4 Discussion

This chapter adopted a model-based approach to examine the short-term plasticity (STP) of inhibitory and excitatory transmission between PV+ interneurons and pyramidal neurons within the mPFC. The main finding is that the excitatory data were captured by a simple STP model – Tsodyks-Markram model - that assumes short-term depression is mediated by a balance of depletion and replenishment of a pool of vesicles with homogeneous release probability. Inhibitory transmission, however, is only accurately described by models that assume two pools of vesicles with different release probabilities. As a consequence, these results suggest that the short-term dynamics of inhibitory transmission might be controlled by release sites with differing release probabilities where lower release probability release sites would support the steady-state transmission while the release sites with high release probability would be mostly recruited during the initial synaptic transmission.

### 3.4.1 Model selection

To identify the most parsimonious model that describes excitatory and inhibitory synaptic transmission between PV+ and pyramidal neurons two broad classes of STP models were used. The main difference between these was their assumption about the uniformity of release probability of vesicles at rest.

The Tsodyks-Markram models and the release-independent depression models assume a homogeneous release probability while the sequential and two-parallel pool models assume heterogeneous release probability at rest. The Tsodyks-Markram models can account for simple depression driven by vesicle depletion and can be extended to include facilitation by increases in release probability at spike time. Release-independent depression models assume depression is driven by vesicle depletion and decreases in release probability. The release-independent depression model can also be extended to include an activity-dependent recovery component. The other two classes of models assume that at rest the release probability of vesicles is heterogeneous which arises either by a sequential maturation of low release probability vesicles into high release probability state or the pools arise independently.

It is important to note that all the implemented models assumed a homogeneous recycling pool from which the vesicles were replenished. In the model with two independent pools this meant that the release probability differences only arise once the vesicles are docked

to the presynaptic membrane. The choice to model homogeneous recycling pool was motivated by two reasons. First, in a model with two molecularly distinct recycling pools, i.e. their release probability is dictated before the vesicle docks to the presynaptic membrane, there is a need for a mechanism that sorts the vesicles to different release sites to maintain a constant ratio of low to high release probability at rest. Currently, no such mechanism has been identified (Wen et al., 2015). The second reason is that a number of studies has identified physiologically plausible explanations of heterogeneity in release probability between the release sites once the vesicle is docked to the membrane. These differences have been proposed to be either positional due to calcium channel coupling distances, or molecular, which would arise from priming by different proteins (Schluter et al., 2006; Wadel et al., 2007; Wolfel et al., 2007; Ishiyama et al., 2014).

To identify the most parsimonious models for each synapse, the Akaike Information Criterion (AIC) was calculated. The AIC penalises the complexity of the models hence, it helps to avoid overfitting. Additionally, all the tested models were validated with simulations to ensure that the models capture the features of the experimental data. On the basis of this model selection approach, the STP of excitatory synapse between pyramidal and PV+ interneurons was best explained by a simple, depression only Tsodyks-Markram model while the STP of inhibitory synapse was best captured by models with heterogeneous release probability at rest.

### 3.4.2 Short-term dynamics of excitatory transmission

The short-term dynamics of excitatory transmission was captured by a simple one-pool Tsodyks-Markram model. The model accounted for the dynamics of the synapse across a wide range of frequencies between 5 and 100Hz. This indicates that excitatory STP arises through a balance of vesicle depletion and replenishment.

A subset, ~30%, of excitatory synapses onto PV+ interneurons showed paired-pulse facilitation. However, this facilitation was not captured by any of the models that modelled facilitation by increases in release probability at spike time. This suggests a different presynaptic facilitation mechanism or a contribution of postsynaptic receptors to STP at this synapse. PV+ interneurons express calcium permeable AMPA receptors (Isaac et al., 2007). Previous study has shown that the excitatory synapses onto PV+ cells within the mPFC that express these receptors also show short-term facilitation (Wang and Gao, 2010). Therefore, it is possible that the observed paired-pulse facilitation can be attributed to a

postsynaptic component. Future models of STP could incorporate an activity dependent increase in postsynaptic contribution to test the validity of this explanation.

### 3.4.3 Short-term dynamics of inhibitory transmission

The findings demonstrate that inhibitory transmission is best captured by models with two pools of vesicles with non-uniform release probability. As described in the introduction (section 1.5.4) heterogeneity in release probabilities has been previously described at glutamatergic and GABAergic synapses (Trommershäuser et al., 2003; Hallermann, et al., 2010; Jackman et al., 2016; Taschenberger et al., 2016). Furthermore, the synapse between PV+/fast-spiking and pyramidal cells has been previously reported to not follow simple one-pool vesicle depletion models (Kraushaar et al., 2000; Lawrence et al., 2015). According to inferred parameters, the average difference between the release probability of low and high release probability pools was almost six-fold and the proportion of low release probability vesicles to high release probability vesicles was ~80%. Interestingly the proportion of low to high release probability and the magnitude of differences between release probabilities is comparable to a recent report from the glutamatergic synapse at the calyx of Held (Taschenberger et al., 2016). This suggests similarities across brain regions. The existence of heterogeneous pools of vesicles will also have implications for other forms of plasticity. For example, it has been previously shown that post-tetanic potentiation increased the first peak in the train but the steady-state transmission was unaffected, hence it was suggested that the post-tetanic potentiation modified the proportion of higher release probability vesicles while having no effect on the lower release probability vesicles (Taschenberger et al., 2016).

The results described show that two types of models provide a plausible mechanism for STP mechanisms at this synapse. The sequential model assumes that higher release probability vesicles are a mature version of lower release probability vesicles and both pools are replenished with different kinetics. The two independent pool model assumes that the processes responsible for lower and higher probability of release are independent and that both low and high release pools are replenished with the same kinetics. One of the differences between the two independent pools model and the sequential model is their assumption about the kinetics of replenishment of low and high release probability pools. The two-independent pools model assumes both types of vesicles are refilled with identical recovery kinetics, while the sequential model assumes different recovery kinetics of each pool. These assumptions can be tested experimentally with the use of recovery protocols

(Oline and Burger, 2014). Recovery protocols involve applying a stimulation train at high frequency that depletes the vesicles at the synapse followed by a single pulse at varying intervals. The ratio of the recovery pulse to the first peak in the train is a measure of how quickly the synapse recovers following sustained activity. If the synapses have two pools of vesicles with different replenishment kinetics, then the recovery curve will be biphasic. If the recovery kinetics of both pools are the same, the recovery curve will follow a single exponential pattern. Therefore, these experimental protocols can be used to further dissect which mechanism might be underlying the STP at this synapse. Recovery protocols can also be used to constrain model parameters as previous analysis has shown that the inclusion of a recovery pulse in the experimental protocol significantly improves the robustness of parameter inference (Costa et al., 2013). Therefore, to further understand the underlying mechanisms future experiments should include recovery pulses after frequency trains to improve the parameter inference of these two models and thus, help to differentiate between these two models.

The two independent pools model was simulated to determine the underlying synaptic processes controlling STP at this synapse. The results of these simulations suggest that high release probability vesicles contribute to the initial synaptic transmission and low release probability vesicles mediate steady state transmission. During 50Hz stimulation, high release probability vesicles are quickly depleted and contribute to ~20% of the peak strength during steady-state transmission. Hence, after the first initial peaks, the transmission will be mostly mediated by lower release probability vesicles. The fact that steady-state transmission is supported by lower release probability vesicles is in line with previous reports from cerebellar synapses and the calyx of Held (Trommershäuser et al., 2003; Hallermann et al., 2010; Jackman et al., 2016; Taschenberger et al., 2016).

The steady-state transmission of inhibitory synapse (Figure 3-3) showed relative stability across higher range of frequencies between 20 and 200Hz. This stability arises because of the heterogeneity in release probabilities and the different contribution of low and high release probability vesicles to different stages of transmission. Stable steady-state transmission across a range of frequencies implies that pyramidal neuron will be less affected by relative changes in firing of PV+ neurons, and will be more affected by the absolute rate of PV+ interneurons firing (Silver, 2010). This suggests that the heterogeneity of vesicles contributes to the stability of inhibition across a range of firing frequencies and the STP of PV+ interneurons is adapted to mediate sustained levels of inhibition during high-frequency firing. Future studies should explore the role of this identified stability of inhibition and its implications for oscillations in models of prefrontal circuitry.

The results demonstrate that the excitatory and inhibitory synapses are different. A recent network simulation study explored the influence of different STP models on cortical oscillations in networks of cortical excitatory and inhibitory neurons (McDonnell et al., 2012). The study showed that assuming the release-independent depression model for excitatory connection increases the power of gamma oscillations and beta oscillations emerge. Future modelling studies could implement the differences identified in this this chapter in short-term dynamics of excitatory and inhibitory synapses to establish how it would impact the prefrontal dynamics and the excitatory/inhibitory balance in the mPFC.

### 3.4.4 General limitations

A number of experimental limitations may affect the drawn conclusions. One of the potential confounding factors is the fact that the results use the postsynaptic responses as a measure of presynaptic neurotransmitter release. The recordings were conducted in basal conditions without controlling for receptor desensitisation and saturation. Postsynaptic receptor desensitisation and saturation can cause non-linearities in the recorded postsynaptic potentials, hence, future studies should evaluate the postsynaptic contribution to STP at these synapses. At larger synapses, such as the calyx of Held, the presynaptic bouton can be directly patch-clamped which allows measurements of membrane capacitance that allows direct quantification of released vesicles. Due to their small size, such direct presynaptic recordings are not possible at the synapses investigated here. However, a number of pharmacological agents can be used to relieve receptor saturation and desensitization. Therefore, to evaluate the contribution of the postsynaptic component to the observed patterns in the results, the recordings should be conducted in the presence of low-affinity AMPA receptor antagonist such γDGG (Wadiche et al., 2001) and a low-affinity competitive $GABA_A$ receptor antagonist, TPMPA (Jones et al., 2001).

### 3.4.5 Conclusions

Computational modelling enabled the analysis of STP mechanisms at the inhibitory and excitatory synapses between PV+ and pyramidal neurons within the mPFC. The excitatory data were well described by a simple model indicating that synaptic transmission at the excitatory synapse is mediated by release sites with homogeneous release probability. The synaptic transmission at inhibitory synapse formed by PV+ interneurons and pyramidal neurons could not be explained with one pool model, but was shown to be explainable by heterogeneous release sites with differing initial release probabilities. The heterogeneity in release probability imparts special properties onto inhibitory synapse that will translate into

providing stable inhibition across broader range of frequencies. In contrast, the excitatory synapse will be more sensitive to changes in frequency of firing of the presynaptic pyramidal neuron. These results can inform future modelling studies that include models of these synapses to dissect how these short-term plasticity properties regulate the activity within the mPFC.

# Chapter 4. Cholinergic modulation of excitatory and inhibitory transmission

## 4.1 Introduction

As described in the general introduction (section 1.4), the medial prefrontal cortex (mPFC) receives dense cholinergic projections from the basal forebrain and acetylcholine release in the mPFC is important in attentional processes (Mesulam et al., 1983; Bloem et al., 2014). Little is known about how acetylcholine modulates the synaptic transmission between PV+ and pyramidal neurons within the mPFC, particularly within the deeper layers.

The experiments presented in this chapter examined the cholinergic modulation of inhibitory and excitatory transmission within the prelimbic region of the mPFC. Paired recordings were performed between PV+ and pyramidal cells in layer 5/6 to investigate modulation of baseline transmission and of short-term plasticity. The computational modelling of short-term plasticity in Chapter 3 revealed that inhibitory transmission is best explained with models of heterogeneous release probability. Here, one of these models is used to uncover the underlying synaptic changes of inhibitory transmission induced by cholinergic modulation.

Activating cholinergic receptors caused a robust decrease in both excitatory and inhibitory postsynaptic potentials. The results showed that the failure rate of synaptic transmission increased for both connections, suggesting that the observed reduction was mediated presynaptically. Short-term depression of inhibitory transmission remained unchanged for lower frequencies (5-20Hz), however, it was reduced at higher frequencies (50-200Hz). The parameters of the short-term plasticity model revealed that acetylcholine reduces the release probability and increases the recovery times of vesicles at the presynaptic terminal of PV+ interneurons. The model uncovered that acetylcholine preferentially acts on release sites that show lower release probability in basal conditions.

## 4.2 Methods

The cholinergic modulation of synaptic transmission was examined by performing whole-cell recordings in connected pairs of PV+ and pyramidal neurons. For a detailed description of electrophysiological analysis see Chapter 2: Materials and Methods and for description of the computational modelling see Chapter 3.2: Methods.

### 4.2.1 *In-vitro* electrophysiology

Recordings were conducted in layer 5/6 in coronal slices of prelimbic region of mPFC. All cells were held in current-clamp configuration at -70mV. Baseline transmission was examined by evoking a single action potential in the presynaptic neuron and recording the excitatory or inhibitory postsynaptic potentials (E/IPSP) in the postsynaptic neuron. Between 10-41 peaks of postsynaptic potentials were recorded and used to estimate the mean baseline transmission before the acetylcholine agonist carbachol was applied. Carbachol, was bath-applied for 10 minutes at a concentration of 10μM. Following carbachol application, mean peak amplitude was measured by averaging peaks of 30 PSPs. PSPs classified as failures (section 2.5.3.2) were included in the calculation of the mean PSP amplitude. The effect of carbachol was quantified as a ratio of the mean PSP after carbachol application to the mean PSP in control condition. The effect of carbachol on the decay time of single PSPs was quantified by comparing the time constants before and after carbachol application. As described in section 2.5.3.5 in Chapter 2, a single exponential model was fit to the 10-90% portion of the decay, the fit was accepted if the goodness-of-fit statistic, R2, was above a threshold of 0.99, this threshold was decided by visually inspecting the quality of the fits.

Short-term plasticity was examined by evoking trains of ten action potentials in the presynaptic cell at 5, 10, 20, 50, 100, 200Hz. These frequencies were selected to ensure the synaptic dynamics were probed at a sufficiently broad stimulation range. For detailed description of train analysis see Chapter 2, section 2.5.4. Briefly, each frequency was repeated ten times every 10s. The data were analysed if at least six sweeps were collected per frequency that passed the predefined exclusion criteria (Section 2.5.4.3). If this was not reached, the data were not included in analysis. The trains of PSPs were deconvolved to account for the contribution of previous PSPs in the train to the measured peak amplitude (Chapter 2, section 2.5.4.2).

To test whether the peak detection method affects the reported results, two methods of peak detection were compared for baseline transmission. First method, described in Section 2.5.1, where the peak was taken as the maximum value in a 5ms window following the time of the presynaptic AP (Figure 4-1A). In the second method, the peak was detected at one time point, which was set to the peak latency of an averaged PSP (Figure 4-1B). Following the same principle as for the baseline transmission, the latencies of 10 peaks in frequency stimulations were established using an averaged postsynaptic train, these time points were then used to detect the peak values in each single train.

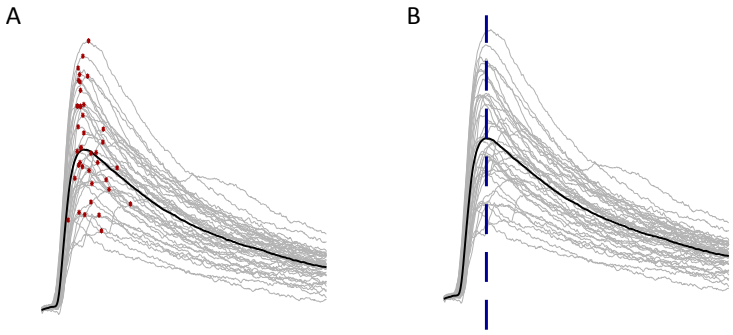


**Figure 4-1 Peak detection methods**. (A) Peak detection where the maximum (red star) in a 5ms window after a presynaptic AP was taken as a peak value. (B) Second method of peak detection were the latency (blue line) of an averaged PSP (bold black line) was used as a time point for peak measurement of single PSPs.

### 4.2.2 Computational modelling

Short-term plasticity (STP) models were implemented to explain the effects mediated by carbachol. Parameters of deterministic STP models were optimised following the approach by Costa et al. (2013). For a description of the models and parameter sampling routine see Chapter 3, section 3.2.4.

### 4.2.3 Statistical analysis

Statistical analysis was performed in JASP and Python. For frequency data, a pairwise comparison at each time point between control and carbachol conditions were first assessed using a Wilcoxon signed-rank test in Python. To control for multiple comparisons, the obtained p-values were corrected for using the Bonferroni correction the StatsModels package in Python. To test for differences between short-term plasticity between control and carbachol conditions, a two-way repeated-measures ANOVA was conducted for each frequency; significance was corrected using a Greenhouse–Geisser correction. Differences were considered significant if $p < .05$. Data are presented as mean ± SEM.

# 4.3 Results

## 4.3.1 Cholinergic modulation of baseline transmission

The medial prefrontal cortex (mPFC) receives dense cholinergic innervation from the basal forebrain (Mesulam et al., 1983; Zhang et al., 2010). The cholinergic modulation of the excitatory and inhibitory transmission between PV+ and pyramidal cells was investigated in acute mPFC slices by bath application of an acetylcholine agonist carbachol (10μM). To selectively stimulate the synapses, paired recordings between PV+ and pyramidal neurons were conducted.

### 4.3.1.1 Carbachol reduces excitatory transmission between pyramidal and PV+ interneurons

First the cholinergic modulation of excitatory transmission will be reported. Excitatory postsynaptic potentials (EPSPs) between synaptically connected pyramidal and PV+ neurons were examined before and after carbachol application to measure the effects of cholinergic modulation of excitatory transmission. A single action potential was evoked in the presynaptic pyramidal neuron and a subsequent EPSP was recorded in the postsynaptic PV+ neuron before and after carbachol application.

The amplitude of EPSPs began decreasing at ~4 minutes following carbachol application and reached a steady-state decrease after around 6 minutes (Figure 4-2C). Carbachol significantly reduced the recorded EPSPs from 2.54±0.98mV to 0.86±0.34mV ($p = .012$, $n = 9$, Wilcoxon signed-rank test). This was a decrease of 63±13% compared to the initial EPSP (Figure 4-2A, B). The magnitude of reduction is higher than the previously reported reduction of ~35% at the same connection within the mPFC (Pafundo et al., 2013).

The alternative peak detection method, where PSPs peaks are measured at a fixed timepoint, was used to confirm the depressing effects of carbachol on baseline transmission (Figure 4-3A). The results of this analysis were consistent with the peak detection method that measures the maximum value in a time window with of 54±13% decrease in EPSP amplitude compared to the initial control EPSP amplitude (control: 2.47±0.98mV; carbachol: 0.81±0.33mV; $p = .004$, $n = 9$, Wilcoxon signed-rank test).

In 3/9 cases carbachol caused a total suppression of recorded EPSPs resulting in a loss of detectable excitatory transmission (Figure 4-4). In these cases, the mean amplitude of post carbachol EPSP was set to zero. Setting the amplitude to zero was preferable as, as described in Chapter 2 (section 2.5.3), the analysis of PSPs was conducted by measuring the maximum value of a single PSP in a 5ms window. As can be seen in the raw traces in Figure 4-4, carbachol increased the spontaneous activity in recorded cells. Hence, the analysis was frequently classifying a spontaneous response as an evoked PSP. For this reason, the analysis was visually inspected for all the carbachol experiments to decide whether the synaptic transmission is abolished.

To examine the locus of carbachol induced effects, the failure rate was calculated by computing the percentage of failures in synaptic transmission to the total number of stimulations. The failure rate significantly increased from 12±6.8% to 50±14% (Figure 4-5A; $p = .03$, Wilcoxon signed-rank test). The increase failure in transmission suggests that the carbachol effects are presynaptic.

The decay time constant of single EPSPs was examined. The three experiments where excitatory transmission was no longer detectable were excluded from kinetic analysis. Analysing the results, the decay time constant showed no changes between control, 7.02±0.72ms, and carbachol conditions, 7.7±1.13ms (Figure 4-6A; $p = .563$, Wilcoxon signed-rank test).

Therefore, the results show that carbachol induces a robust average decrease of excitatory transmission between pyramidal and PV+ neurons within the mPFC and completely supresses the transmission in ~30% of the examined cells.

#### 4.3.1.2 Carbachol reduces inhibitory transmission between PV+ and pyramidal neurons

Cholinergic modulation of inhibitory postsynaptic potentials (IPSPs) was examined between connected pairs of PV+ and pyramidal neurons. A single IPSP was evoked in the postsynaptic pyramidal neuron by evoking a single action potential at 0.1Hz in the presynaptic PV+ interneuron. The mean amplitude of the IPSP was compared before and after application of 10μM carbachol with failures in transmission included in the calculation of the mean. The application of carbachol significantly reduced inhibitory transmission from 5.48±0.71mV to 2.57±0.41mV ($p < .001$, $n = 22$, Wilcoxon signed-rank test). This was a decrease of 53±5.6% compared to the initial control IPSP amplitude

(Figure 4-2A-C). The amplitude of IPSPs started decreasing after around 4 minutes of carbachol application and reached its maximal reduction within 1-2 minutes (Figure 4-2C).

The alternative peak detection method was used to confirm the depressing effects of carbachol on baseline transmission (Figure 4-3B). The results of both methods were consistent with the alternative method yielding with a decrease of 52±5.6% in IPSP amplitude compared to the initial control IPSP amplitude (control: 5.44±0.71mV; carbachol: 2.57±0.42mV; $p < .001$, $n = 22$, Wilcoxon signed-rank test).

The decrease of ~50% of inhibitory transmission reported here is larger than a previously reported decrease in the mPFC of ~35% (Pafundo et al., 2013). This difference may be indicative of regional and/or laminar differences in cholinergic modulation.

The failure rate of inhibitory transmission was examined before and after carbachol application. The failure rate significantly increased from 1.2±0.6% to 12±3.4% (Figure 4-5B; $p = .004$, Wilcoxon signed-rank test). The increase in failed transmission observed indicates that presynaptic modulation by carbachol contributes to the reduction of the IPSP amplitude.

Previous evidence shows that the decay time constant of hippocampal PV+ interneurons decreases after carbachol application (Szabó et al., 2010). The decay time constant was examined pre- and post-carbachol application. A single exponential model was fit to the 90-10% decaying phase of the single averaged PSP. The averaged PSP did not include synaptic transmission that was classified as failures and it excluded PSPs that showed obvious spontaneous activity during the decay. The decay time constant of the IPSP significantly decreased from 34.57 ±2.32ms to 30.51±2.28ms (Figure 4-6B; $p = .009$, Wilcoxon signed-rank test).

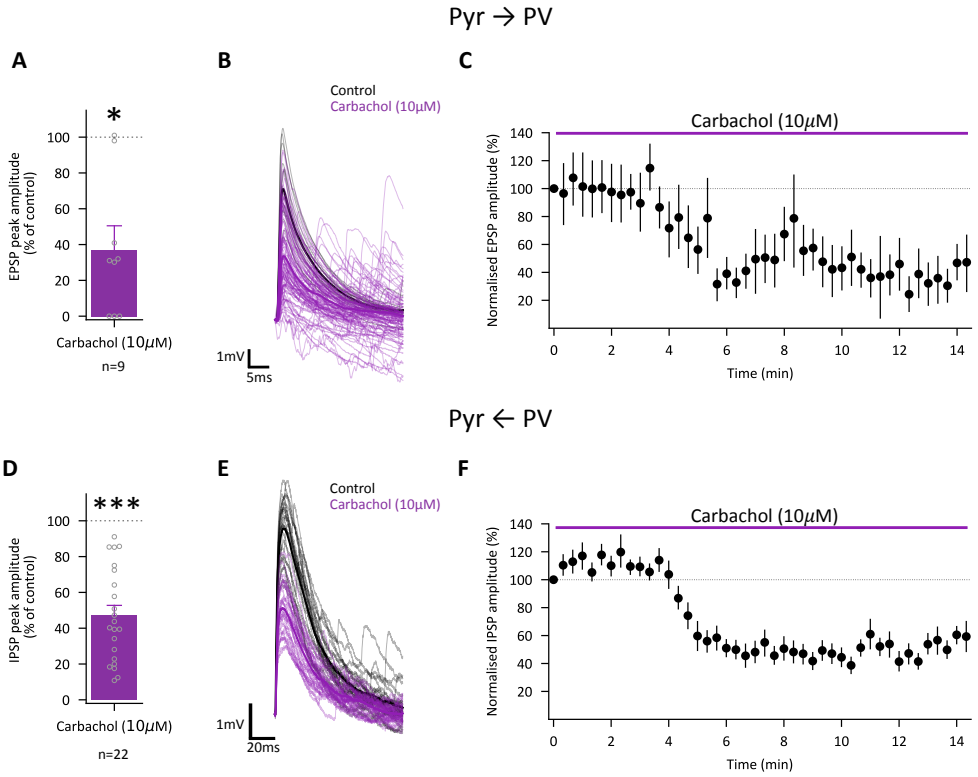


**Figure 4-2 Carbachol application reduces excitatory and inhibitory baseline transmission between PV+ and pyramidal neurons.** EPSPs and IPSPs were evoked every 10s, carbachol effects were quantified after 10 minutes of application. (A) Carbachol (10µM) significantly decreased the EPSP amplitude in the excitatory synapse onto PV+ interneurons; the transmission was no longer detectable for three cells, these are set to zero in the bar chart. (B) Example averaged EPSP (bold line) before and after carbachol wash. The individual traces are plotted in fine lines. (C) Effect of carbachol over time on EPSPs across all cells (n = 9), each data point represents two averaged EPSPs. EPSPs were set to zero in the graph after ten minutes of carbachol wash for the three experiments where the transmission was no longer detectable. (D) Carbachol (10µM) significantly decreased the IPSP amplitude in the inhibitory synapse onto pyramidal neurons. (E) Example averaged IPSP (bold) before and after carbachol wash, individual traces are plotted in fine lines. (F) Effect of carbachol wash on IPSP over time across all cells (n = 22), each data point represents two averaged IPSPs. Data are presented as mean ± SEM; each dot represents one cell. Wilcoxon signed-rank test * = p<.05, *** = p<.001.

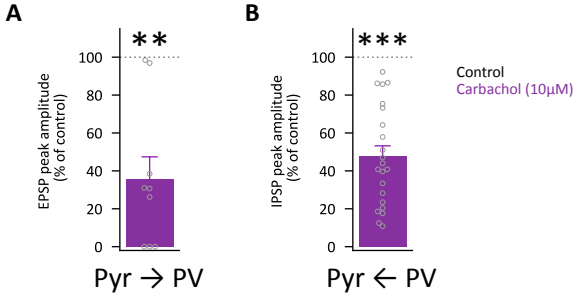


**Figure 4-3 Analysis of baseline transmission using alternative peak detection method.** Using a fixed time point to measure PSP peaks show reduction in excitatory (A) and inhibitory transmission (B) due to carbachol application (10µM). Data are presented as mean ± SEM; each dot represents one cell. Wilcoxon signed-rank test ** = p<.01. , *** = p<.001.

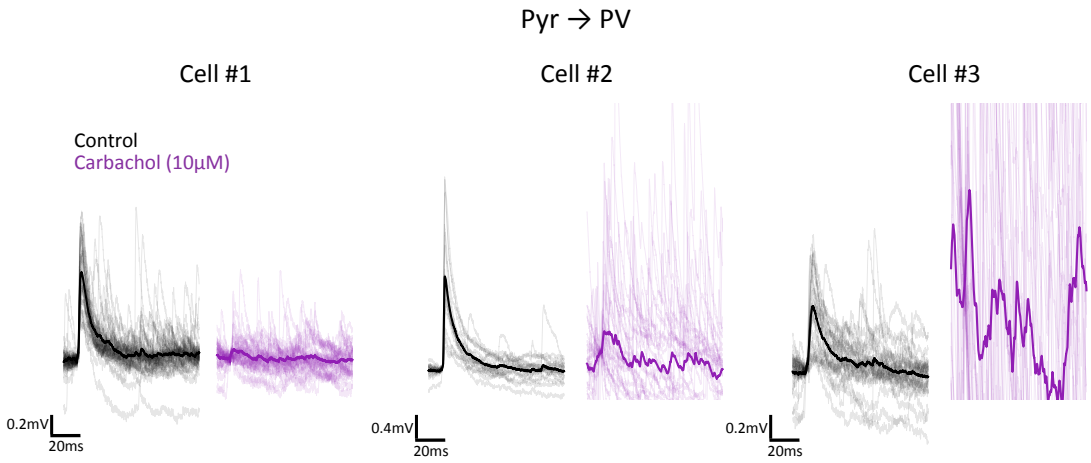


**Figure 4-4. Carbachol abolished excitatory transmission in a subset of cells.** Averaged (bold line) and individual (fine line) EPSPs of the cells where post-carbachol application the synaptic transmission was no longer detectable. Note the elevated spontaneous activity post-carbachol application, particularly in cell #3. The post-carbachol traces were truncated to match control. The individual traces are aligned to the peak of the presynaptic action potential.

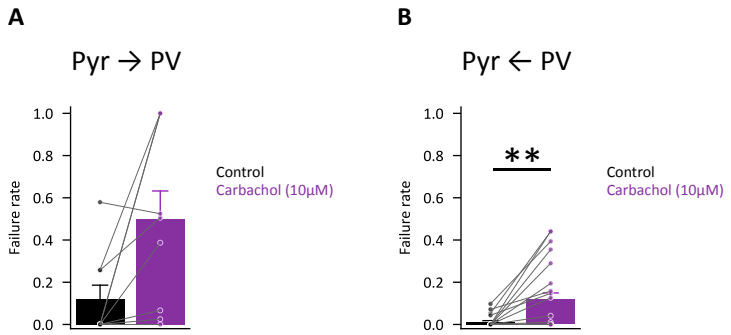


**Figure 4-5 Increased failure rate of excitatory and inhibitory transmission following carbachol application**. (A) Failure rate of inhibitory transmission between pyramidal and PV+ interneurons was increased by 10μM carbachol application. (B) Failure rate of excitatory transmission between pyramidal and PV+ interneurons increased after carbachol (10μM) application. Data are presented as mean ± SEM; each dot represents one cell. Wilcoxon signed-rank test, ** = p<.01.

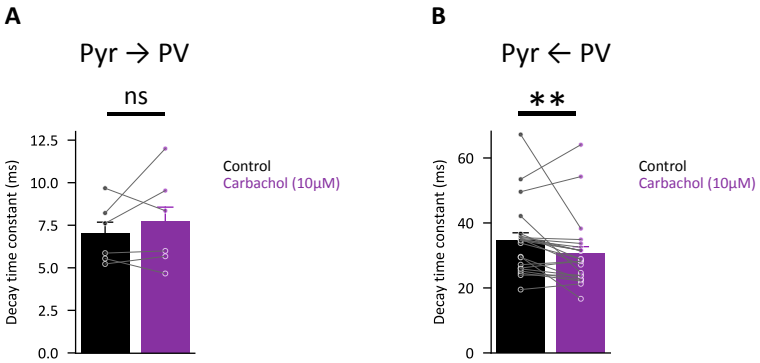


**Figure 4-6 Carbachol reduces IPSP decay time constant and has no effect on EPSP time constant.** (A) Carbachol (10μM) has no effect on EPSP decay. (B) Carbachol (10μM) application reduced the decay time constant of IPSP. Data are presented as mean ± SEM; each dot represents one cell. Wilcoxon signed-rank test ** = p<.01.

### 4.3.2 Cholinergic modulation of sustained activity

It has been shown before that activation of cholinergic receptors modulates short-term dynamics of excitatory and inhibitory connection within layer 2/3 of the mPFC (Pafundo et al., 2013). Therefore, cholinergic modulation of short-term dynamics was examined to verify if similar effects are observed at the connection between PV+ and pyramidal neurons within the layer 5/6 in the mPFC.

To investigate the changes of PSPs during sustained stimulation, ten trains of ten action potentials were evoked in the presynaptic cell at frequencies 5, 10, 20, 50, 100, and 200Hz and the resulting EPSPs and IPSPs in the postsynaptic cell were recorded before and after application of 10μM carbachol. Baseline PSPs between cells showed variable mean peak amplitudes. Hence, for each cell the control and carbachol PSPs were normalised to the average first peak in the control conditions of each given frequency. This was implemented to compare the relative changes in the strength of the connection for each cell after carbachol application. As described in methods (section 4.2.3), pairwise comparisons were made between normalised peak 2-10 in control vs carbachol conditions. The difference between the first peaks for each frequency was not tested to reduce multiple comparisons and furthermore, as it was shown previously the recorded baseline transmission is decreased (see section 4.3.1). An example of the experimental protocol is displayed in Figure 4-7, where action potentials were evoked at 50Hz in the presynaptic PV+ interneuron and the IPSPs were recorded in the postsynaptic pyramidal cell recorded before and after carbachol application.

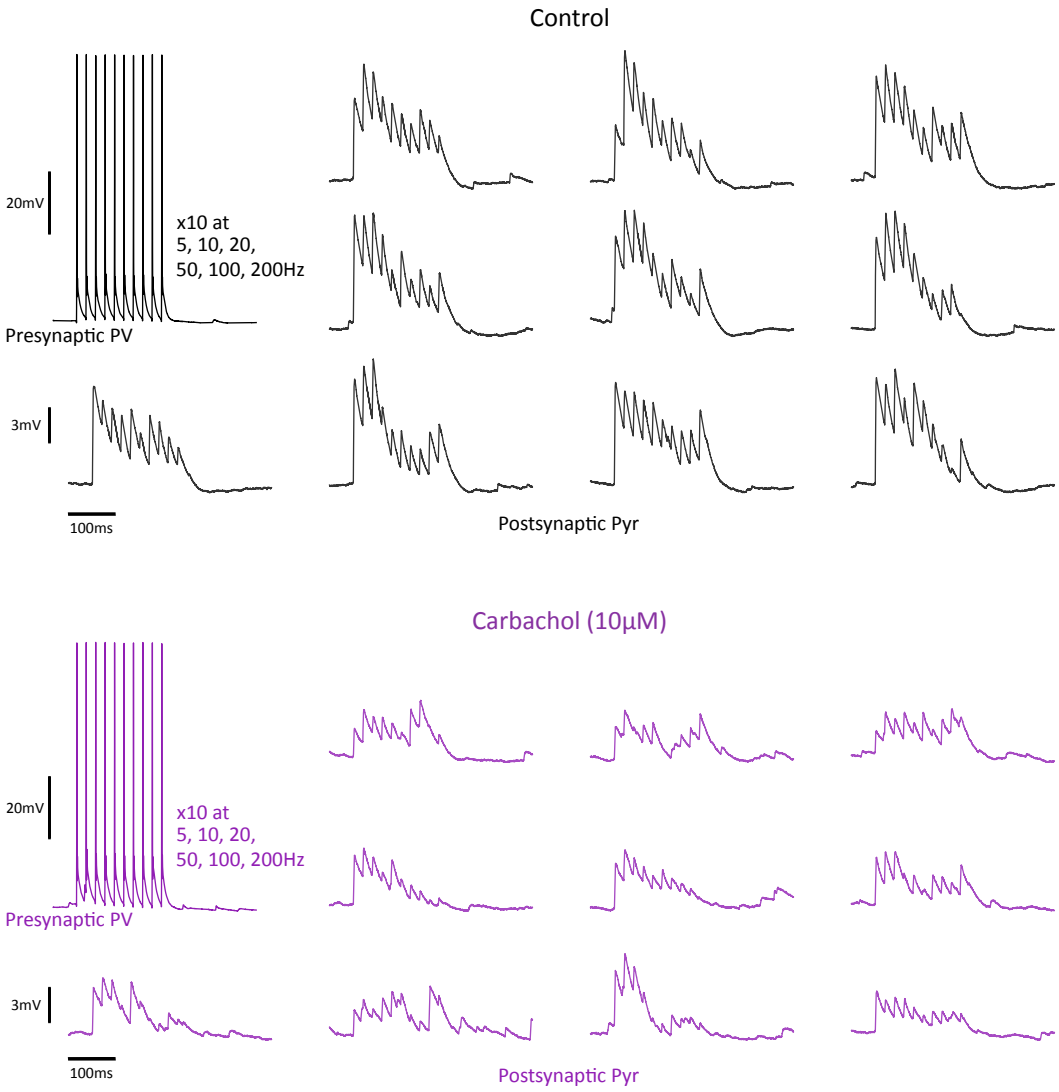


**Figure 4-7 Experimental protocol used to test cholinergic modulation of repetitive activity.** To investigate cholinergic modulation of sustained activity ten action potentials (represented in the left traces) were elicited in the presynaptic cell and the peaks of raw single traces were deconvolved to account for the contribution of the previous PSPs to the measured peak. The stimulation protocol was repeated at frequencies between 5 – 200Hz. The traces on the right are example single traces from one cell stimulated with a train of presynaptic action potentials at 50Hz.

#### 4.3.2.1 Carbachol effects on sustained excitatory transmission

As data from only three cells were collected for excitatory transmission, no statistical tests were conducted. The low number of experiments is partially due to the lack of detectable transmission in three out of nine experiments, as reported in section 4.3.1.1. Out of the six remaining experiments, three experiments were discarded due to deteriorating quality of the recordings.

The trains of EPSPs for the remaining data set of three cells are plotted in Figure 4-8. As stated before, the EPSPs in both conditions were normalised to the first peak in control condition. At lower frequencies of 5, 10 and 20Hz, carbachol reduced excitatory transmission. This pattern changes at higher frequencies between 50-200Hz where while the first EPSP is substantially different, the consecutive peaks are converging onto similar steady-state values at higher frequencies (Figure 4-8). This suggests that carbachol reduces the transmission at lower frequencies (5-20Hz), however, at higher frequencies it only reduces the initial peaks (50-200Hz).

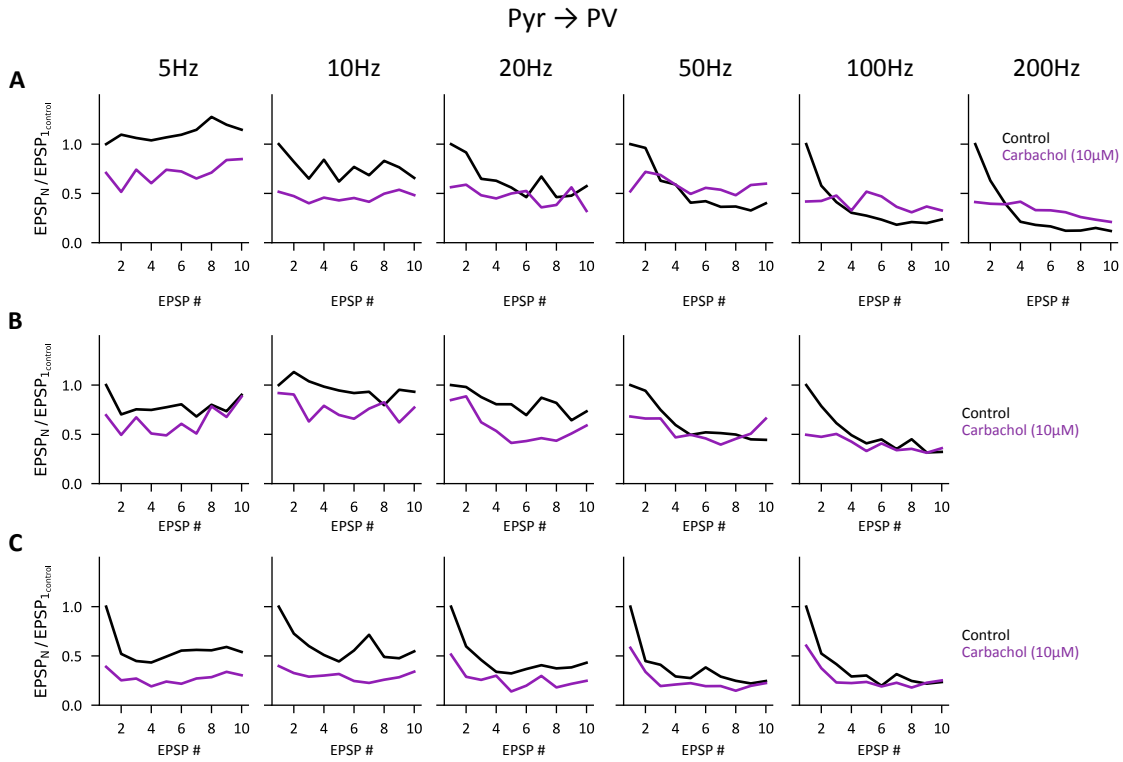


**Figure 4-8 Cholinergic modulation of sustained excitatory transmission.** The effect of carbachol was examined for excitatory transmission between pyramidal and PV+ neurons. (A-C) Deconvolved peak values for recordings of EPSPs from three PV+ cells across the five or six stimulation frequencies in control and carbachol conditions. Peaks are normalised to the first peak in control conditions ($EPSP_{1control}$). Carbachol consistently reduced the peaks across the train at lower frequencies of 5, 10 and 20Hz for all cells.

#### 4.3.2.2 Carbachol effects on sustained inhibitory transmission

The cholinergic modulation of sustained activity of inhibitory transmission between PV+ and pyramidal neurons within the mPFC was examined. Ten IPSPs evoked in postsynaptic pyramidal neurons were compared between control and carbachol conditions (Figure 4-9). As described above, recorded IPSPs in control and carbachol conditions were normalised to the mean peak amplitude of the first peak in each given frequency in control conditions. The individual pairwise comparisons between peaks 2-10 in both conditions were tested using a Wilcoxon signed-rank test followed by Bonferroni correction (see Appendix II for individual p-values for each peak at each frequency).

Relative to control transmission, activation of cholinergic receptors significantly decreased the IPSPs at all consecutive peaks at lower frequencies of 5 and 10Hz ($p < .05$; Figure 4-10A, B). However, as shown in Figure 4-10C-F, with increasing frequencies, inhibitory transmission converges onto the same steady-state transmission in control and carbachol condition. This effect is clear at frequencies of 50, 100 and 200Hz where only the second IPSP is different at 50 and 200Hz, while all other compared peaks show no changes for transmission at 100Hz. The 20Hz stimulation is somewhat ambiguous with 4/9 tested peaks showing differences. This, however, indicates that inhibitory transmission starts to equalise between control and carbachol around this stimulation frequency. The effects of carbachol are largely consistent when an alternative peak detection method is used where peaks are measured at a fixed time points based on latency of peak in averaged trace (Figure 4-11). The main difference in the results obtained by both peak detection methods is at 20Hz. This might suggest that around 20Hz is a transition frequency where the carbachol effects on sustained transmission become apparent.

Therefore, inhibitory PV+ neurons firing repetitively at higher frequencies mediate the same degree of inhibition onto pyramidal cells in control and carbachol conditions. In conclusion, these data show that cholinergic modulation reduces the steady-state inhibition at lower frequencies (5-20Hz) but has no effect on steady-state inhibition at higher frequencies (50Hz-200Hz).

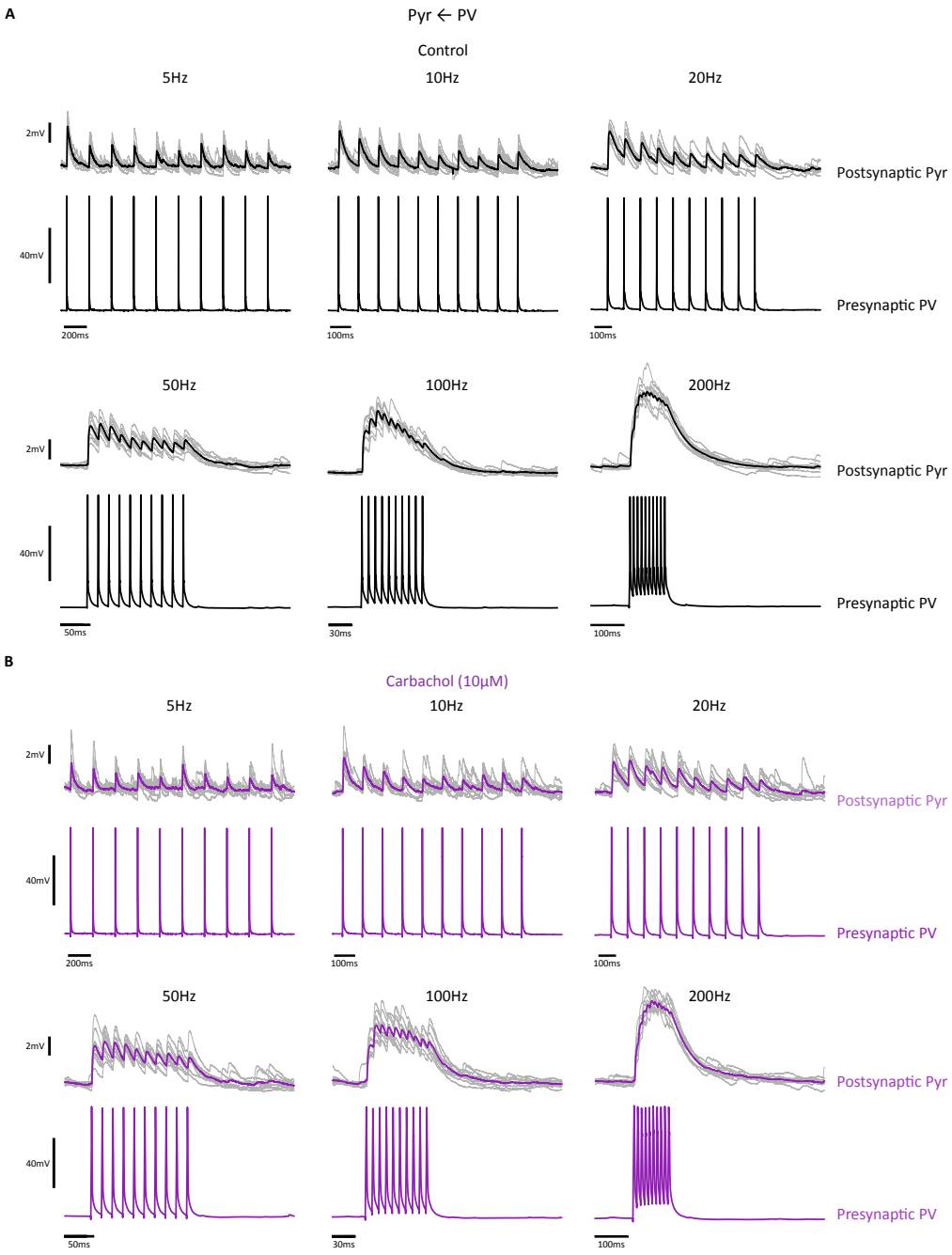


**Figure 4-9 Example effect of carbachol on sustained inhibitory transmission.** The graph shows single traces (fine line) and averaged traces (bold line) of inhibitory frequency trains in control (A) and carbachol conditions (B) for one connection between PV+ and pyramidal neurons.

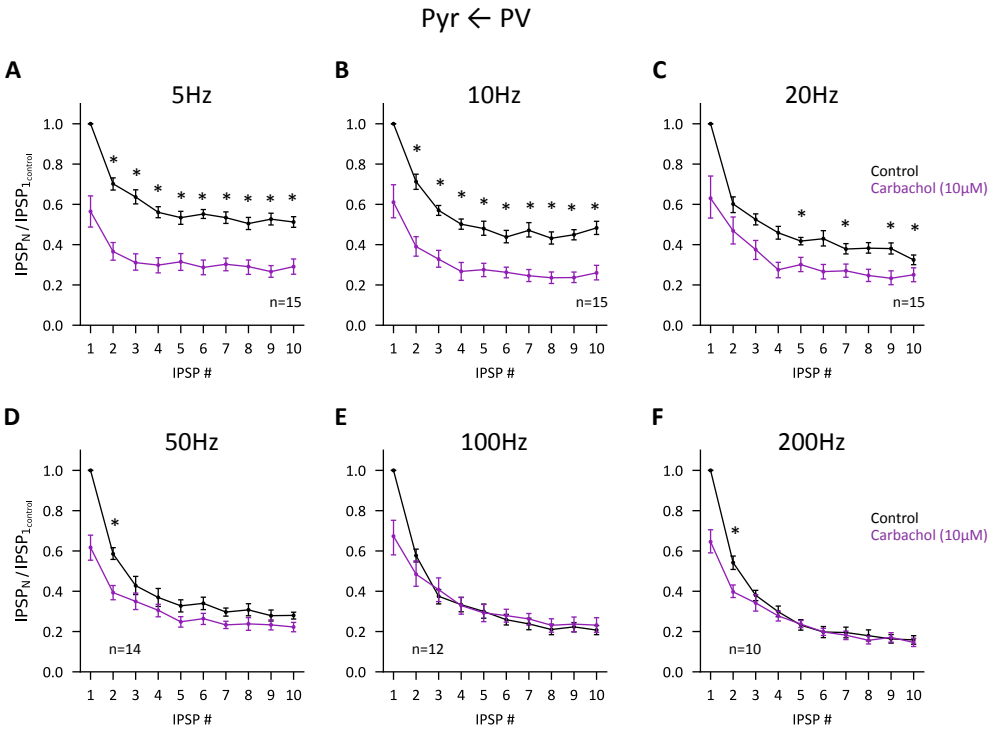


**Figure 4-10 Activation of cholinergic receptors does not affect steady-state inhibition at higher frequencies.** Cholinergic modulation of inhibitory transmission between PV+ and pyramidal neurons at frequencies between 5-200Hz. The graphs represent average deconvolved peak amplitudes across all cells. Peaks were normalised to the first peak in control conditions ($IPSP_{1control}$) for each frequency. (A – C) Carbachol significantly reduces inhibitory transmission at lower frequencies of 5, 10 and 20Hz. (D – F). Carbachol reduces the initial peaks at higher frequencies but the steady-state transmission is unaffected. Data are presented as mean ± SEM. Wilcoxon signed-rank test with post-hoc Bonferroni correction * = $p<0.05$. See Appendix II for individual p-values for each peak and frequency.

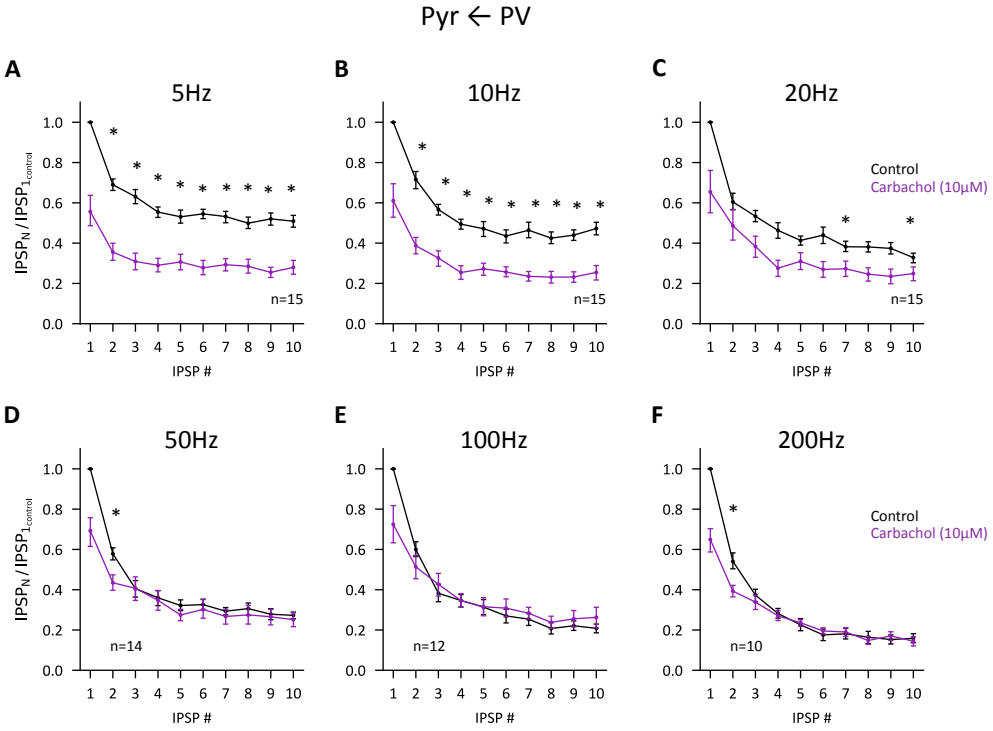


**Figure 4-11 Analysis of frequency transmission using alternative peak detection method.** (A-F) Using fixed latency to measure peaks of individual traces shows effects of carbachol that are largely consistent when peaks are measured as a maximum point in a time window. Wilcoxon signed-rank test with post-hoc Bonferroni correction * = $p<0.05$. See Appendix II for individual p-values for each peak and frequency.

### 4.3.3 Cholinergic modulation of short-term plasticity

Next, the changes in short-term plasticity that account for the changes in sustained activity across the lower and higher frequencies were investigated. As stated before, a data set of only three recordings was collected of excitatory transmission, hence, this dataset is not further analysed.

To compare the short-term dynamics between the control and carbachol conditions, the amplitude of all PSPs in the train was normalised to the first PSP in that condition. As stated previously (see section 4.3.1), the application of carbachol reduced the baseline amplitude. Normalising the trains to the IPSP within its condition controls for the change in the baseline amplitude in the connection and allows for comparison of short-term dynamics.

#### 4.3.3.1 Carbachol reduces short-term depression of inhibitory transmission

The short-term dynamics of inhibitory transmission were examined before and after carbachol application. In control conditions, inhibitory transmission between PV+ interneurons and pyramidal cells shows short-term depression at all examined frequencies (Figure 4-12).

As shown in Figure 4-12A and B, trains of IPSPs in the presence of carbachol condition closely follow the dynamics of those recorded in control conditions. At 20Hz and above the IPSPs start diverging, whereas in carbachol conditions the normalised IPSPs are consistently higher (Figure 4-12C-F). Two-way repeated measures ANOVA investigating carbachol and response number was used to investigate the effects of carbachol on short-term plasticity of the inhibitory connection. Carbachol had no effect on the short-term dynamics of inhibitory transmission at lower frequencies of 5 and 10Hz (Figure 4-13A, B; n = 15; 5Hz: $F(1,14) = 0.7$, $p = .43$; 10Hz: $F(1,14) = 0.0001$, $p = .991$). A significant effect of carbachol on short-term dynamics was revealed at 20Hz (Figure 4-13A; $F(1,14) = 8.9$, $p = .01$, n = 15). This effect persisted across higher frequencies of 50, 100 and 200Hz (Figure 4-13D-F; 50Hz: $F(1,13) = 16$, $p = .001$, n = 14; 100Hz: $F(1,11) = 49.1$, $p < .001$, n = 12; 200Hz: $F(1,9) = 6.3$, $p = .033$, n = 10).

Therefore, activation of cholinergic receptors, reduces the short-term depression of inhibitory transmission between PV+ and pyramidal neurons. This reduction of depression

is frequency dependent and is observed at frequencies between 20 – 200Hz. The observed reduction in short-term depression at higher frequencies is in line with previous evidence from layer 2/3 in the mPFC, showing that the inhibitory short-term depression is reduced at frequencies of 30Hz and above (Pafundo et al., 2013). The changes in short-term plasticity largely reduced the inhibition at lower frequencies (5-20Hz) while allowing the inhibition to remain unchanged at higher frequencies (50-200Hz). Therefore, the reduction in short-term depression explains how, as reported in 4.3.2.2, inhibitory transmission during sustained activity is the same in control in carbachol conditions despite the reduction in baseline transmission.

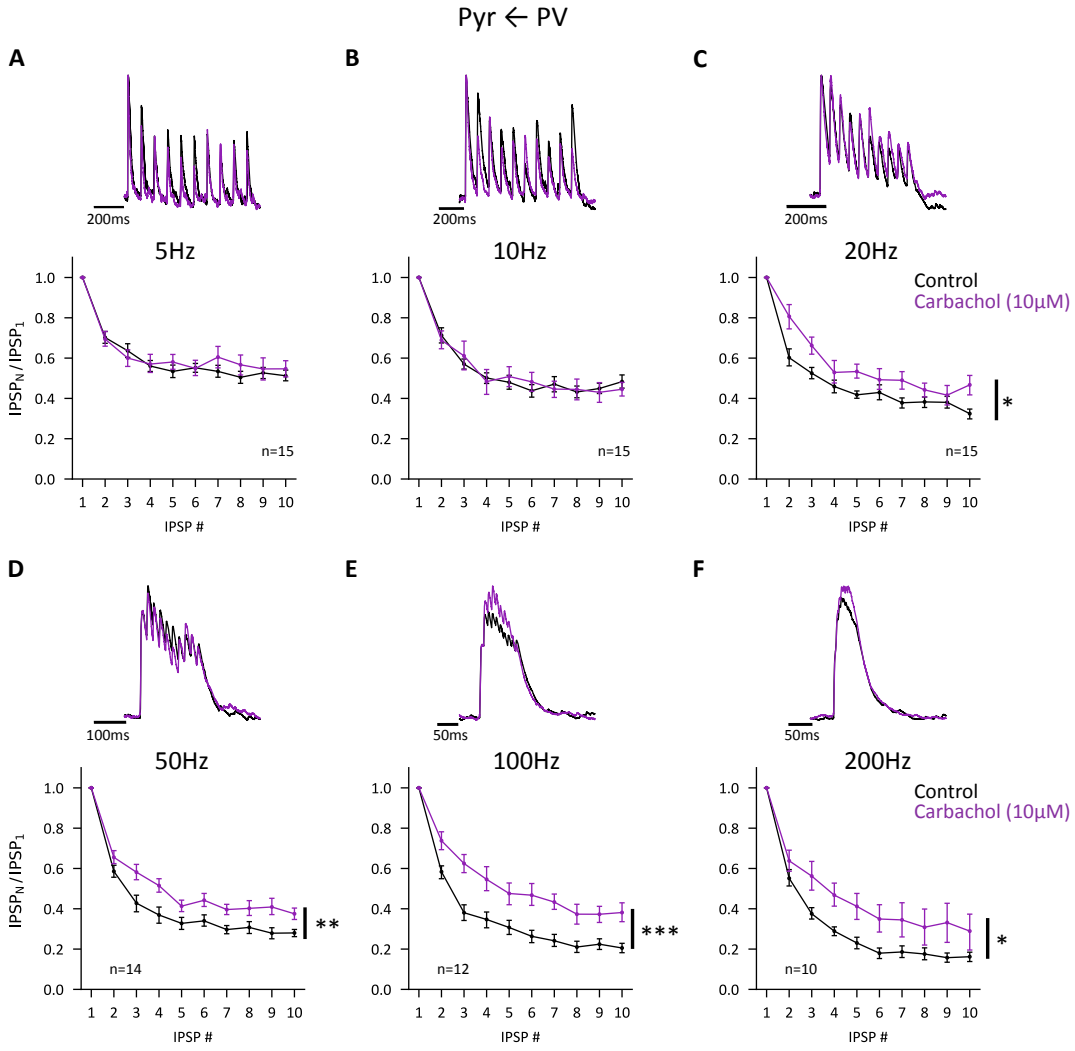


**Figure 4-12 Carbachol reduces the short-term depression of inhibitory synapse between PV+ and pyramidal neurons.** Cholinergic modulation of short-term plasticity was examined at 5-200Hz stimulations. Deconvolved peaks for each cell were normalised to the first peak within control or carbachol conditions. The example traces represent averaged recordings from one paired connection between PV+ and pyramidal cell in control and carbachol conditions. (A,B) Carbachol has no effect on short-term plasticity at lower frequencies of 5 and 10Hz. (C-F) Carbachol reduces the short-term depression at higher frequencies of 20, 50, 100 and 200Hz. Data are presented as mean ± SEM. Two-way repeated measures ANOVA with carbachol and response number as factors * = $p<0.05$, ** = $p<0.01$, *** = $p<0.001$.

### 4.3.4 Model based inference of synaptic changes post carbachol

Previous evidence suggests that carbachol acts via presynaptic mechanisms to induce the changes in short-term depression (Pafundo et al., 2013; Lawrence et al., 2015). To elucidate the mechanisms of the short-term plasticity changes induced by carbachol, short-term plasticity model was implemented. As concluded in Chapter 3, inhibitory transmission between PV+ and pyramidal neurons in the mPFC is not captured by short-term plasticity model that assumes a homogeneous release probability across release sites. Models that include two pools of vesicles with lower and higher probability replicated the short-term dynamics at this synapse. Two models with heterogeneous release probability were tested in Chapter 3 (see Figure 3-11 for model schematics). As discussed in section 3.3.5 of Chapter 3, it is challenging to differentiate between these two models as both capture the dynamics of inhibitory transmission.

The first model, the sequential model assumed the higher release probability vesicles are a mature version of the lower release probability vesicles. This represents a sequential maturation of vesicles, where the vesicle that dock at the presynaptic terminal has a lower release probability but has the propensity to transition into a higher release probability state. The second model was the two-independent pools model (2P). This model simulates two presynaptic heterogeneous release sites with differing release probabilities that are replenished independently but with the same recovery kinetics. As shown in Chapter 3 in section 3.3.4.2, both models performed equally well at capturing the dynamics of the synapse. However, as the mechanistic evidence supporting the sequential model is limited, the 2P model is viewed as favourable as it has less assumptions about the underlying synaptic dynamics. Additionally, as was shown in Figure 3-15 in Chapter 3 the common parameters between these two models for the optimised cells showed no difference, hence supporting the notion that a single recovery time constant is sufficient to replicate the short-term dynamics.

Therefore, the 2P model was used to account for the short-term plasticity changes of inhibitory transmission between PV+ and pyramidal neurons after carbachol application. The parameters of the 2P model were optimised using the frequency trains data presented in Figure 4-10 before and after carbachol application. To ensure that the data were consistent across the cells, only cells that were probed at all six frequencies (5 – 200Hz) were used to constrain the parameters of the models.

Parameters were constrained using an approach introduced by Costa et al., (2013) (see section 3.2.4). A dataset of recordings from ten cell was used in which inhibitory transmission was tested at all six frequencies (5-200Hz). As frequency stimulations were conducted in an increasing order during the experimental recordings, the limiting factor for the number of cells used for modelling was the number of cells that were tested at 200Hz in the presence of carbachol.

Repeated measures ANOVA confirmed that similar effects were observed for the dataset of ten cells as for the whole dataset at frequencies between 5-100Hz (Figure 4-13). As before, carbachol had no effect on the short-term dynamics of inhibitory transmission at lower frequencies of 5 and 10Hz (5Hz: $F(1,9) = 0.23$, $p = .645$; 10Hz: $F(1,9) = 1.09$, $p = .324$). The effects on short-term plasticity were revealed at frequencies of 50 and 100Hz (50Hz: $F(1,9) = 12.56$, $p = .006$; 100Hz: $F(1,9) = 36.34$, $p < .001$). However, carbachol did not influence the short-term dynamics at 20Hz for this subset of cells ($F(1,9) = 4.56$, $p = .061$). The lack of effect at 20Hz could be explained by variability between cells at lower frequencies. However, this subset does show the main feature: reduction of short-term dynamics at most of the higher frequencies. As such, it was deemed satisfactory to use this subset for optimising the short-term plasticity models.

Next, it was verified that the 2P model captures the short-term dynamics of this subset of recorded cells in control conditions. As this dataset was used in optimisation routines in Chapter 3, it was expected that the 2P model will follow the short-term plasticity at this synapse. The point estimates of parameters for the ten cells recorded in control conditions were used to simulate the short-term dynamics at experimental frequencies (5-200Hz). As shown in Chapter 3 section 3.3.2.1, the simple Tsodyks-Markram (TM) short-term plasticity model did not account for the inhibitory short-term dynamics at this synapse. In addition, the point estimates of the parameters of the TM model were also simulated to verify that a simple depression only model can not explain the dynamics in this subset of cells. Simulation of the two models was conducted for each cell at all six frequencies (5-200Hz) and the averaged traces of the modelled peaks were plotted against the averaged experimental data. As shown in Figure 4-14, the TM model does not capture the short-term plasticity of this subset of cells and largely underestimates the short-term depression. The 2P model, however, produces a fit that closely follows the experimental data. Therefore, showing that a model with heterogeneous release sites is appropriate to use to infer the short-term plasticity changes due to carbachol application.

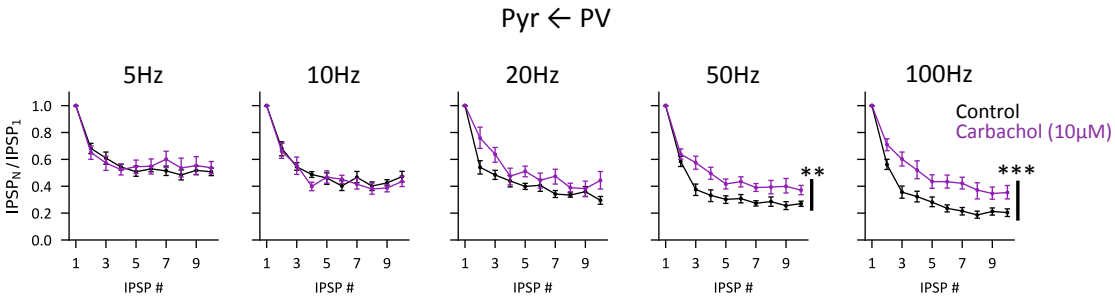


**Figure 4-13 Inhibitory data used for parameter inference.** A subset of ten recordings, previously presented in Figure 4-12, that were stimulated across all six frequencies (5-200Hz) was used for constraining the parameters. This subset captures the main effects of carbachol reduction short-term depression at higher frequencies while having no effect on short-term dynamics at lower frequencies. Data are presented as mean ± SEM. Two-way repeated measures ANOVA with carbachol and response number as factors ** = $p<0.01$, *** = $p<0.001$.

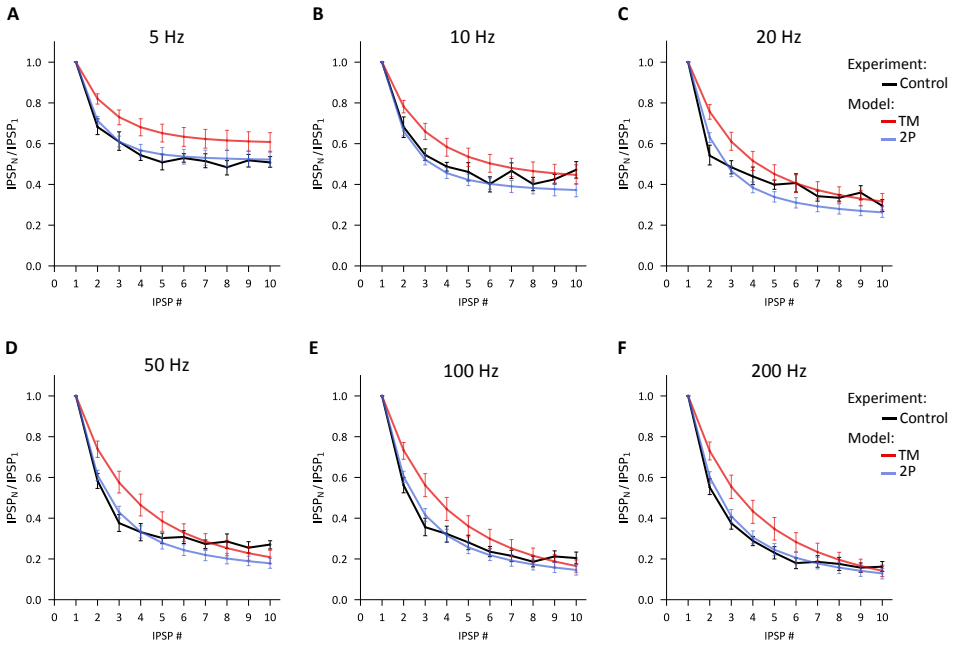


**Figure 4-14 Two pool model captures the dynamics of inhibitory transmission in control conditions**. Parameters of 2P and TM were optimised using frequency stimulation data of the inhibitory connection between PV+ and pyramidal neurons in control conditions. The optimised parameters were used to simulate the models at experimental frequencies. Simulation data were pooled and plotted against averaged deconvolved peak values of experimental data. (A-F) Model with heterogeneous release probabilities, 2P model, captures the dynamics of the data in control conditions. The one-pool model, TM model, underestimates the depression at this synapse. Data are presented as mean ± SEM.

#### 4.3.4.1 Two-pool model replicates the cholinergic modulation at higher but not lower frequencies

It was then investigated whether the 2P model can account for the short-term plasticity effects observed in the presence of carbachol. The trains of recordings at different frequencies (5-200Hz) in the presence of carbachol were used to constrain the model

parameters of the TM and 2P models. It is important to note that the point estimates of parameters were obtained independently for control and carbachol conditions.

The point estimates of the 2P model using the carbachol data were obtained and used to simulate the model at experimental frequencies (5-200Hz). The averaged simulated peaks for the ten cells were plotted against the experimental data (Figure 4-15). As in the case of the control data, the TM model largely underestimates the short-term depression at this synapse, therefore the TM model does not capture the dynamics of the short-term plasticity post carbachol application (Figure 4-15).

Surprisingly, while the 2P model produced close fits to the data at higher frequencies of above 20Hz (Figure 4-15D-F), the model performed poorly at describing the data at lower frequencies between 5-20Hz (Figure 4-15D-F). Similarly, to the TM model, the 2P model underestimated the magnitude of short-term depression, although the 2P model performs better than the TM model at capturing the short-term plasticity of this connection.

The poor fit of the 2P model to the lower frequencies (5-20Hz) indicates that the 2P models fails to account for an additional factor that influences the short-term dynamics at this synapse which is revealed or induced in the presence of carbachol. The short-term dynamics between PV+ and pyramidal neurons have been previously described with a model that assumes a frequency-dependent replenishment of vesicles (Stone et al., 2014). The 2P model does not include this feature and so it is possible that this is why it is a poor fit to the data.

So far, the modelled peaks were compared to the experimental data for each condition. The simulated data in control and carbachol conditions previously presented in Figure 4-14 and Figure 4-15 were plotted together to verify that the model captures the reduction of short-term depression at higher frequencies. Figure 4-16 shows the averaged modelled peaks across the experimental frequencies (5-200Hz). The 2P model captures the reduction of short-term depression at higher frequencies of 50, 100 and 200Hz and the lack of effect on STP at 5Hz. However, the model also predicts a degree of reduction in short-term depression at lower frequencies of 10 and 20Hz – a feature that was not observed in this subset of data (see Figure 4-13). This is a reflection of the model not capturing the short-term depression dynamics at lower frequencies as shown in Figure 4-15.

Therefore, the model can replicate the short-term depression dynamics at higher frequencies. However, carbachol application reveals a short-term plasticity mechanism that

is not captured by the 2P model. The potential reasons underlying the mechanisms not captured by 2P model in carbachol conditions are discussed in 4.4.5 section of discussion.

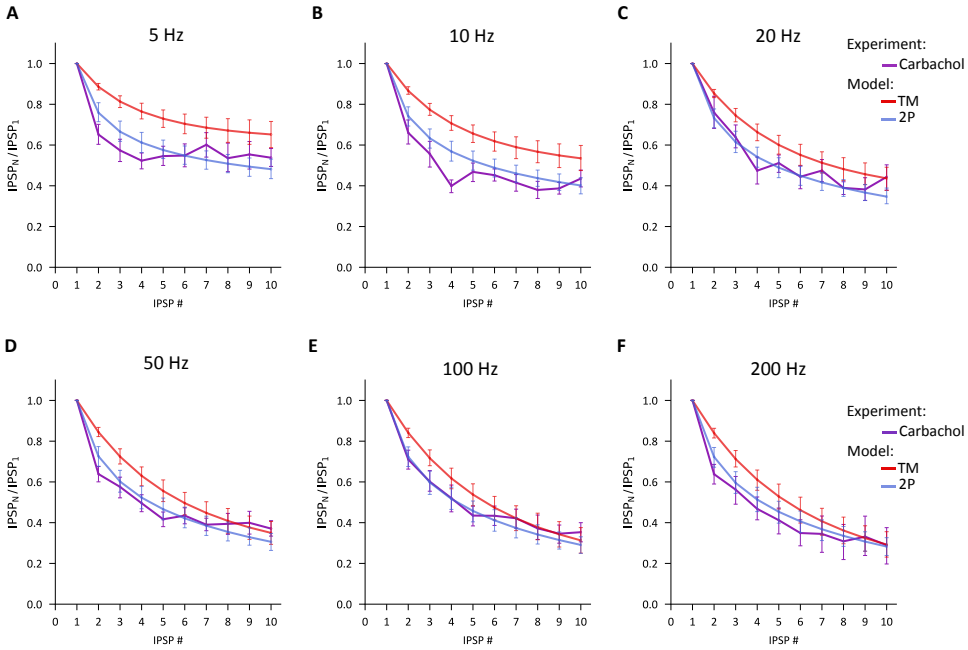


**Figure 4-15 Two pool model captures the inhibitory short-term dynamics in carbachol conditions at higher frequencies but not at lower frequencies.** 2P and TM parameters were optimised using frequency stimulation data of the inhibitory connection between PV+ and pyramidal neurons in carbachol conditions. The optimised parameters were used to simulate the models at experimental frequencies. Averaged simulation data are plotted against averaged deconvolved peak values of experimental data. TM model (red line) underestimated the short-term depression across all frequencies (A-F). Model with heterogeneous release probabilities, 2P model, captures the dynamics at higher frequencies between 20-200Hz (C-F), however, slightly underestimates the short-term depression at lower frequencies of 5 and 10Hz (A,B). Data are presented as mean ± SEM.

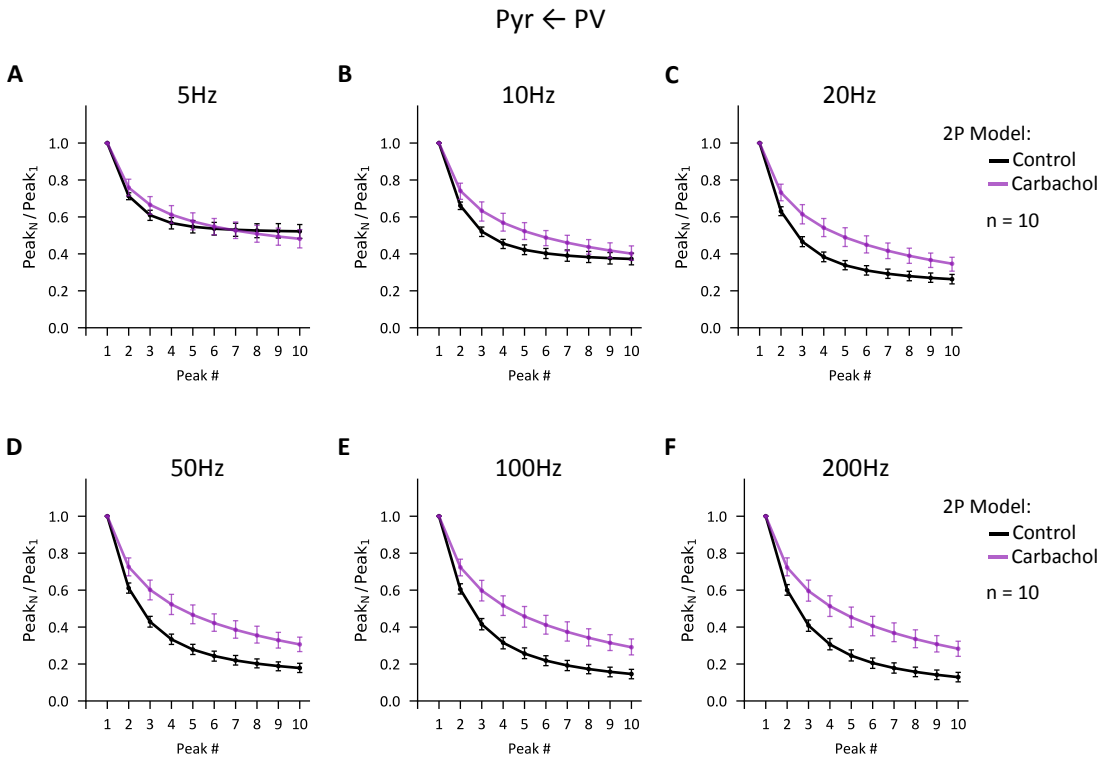


**Figure 4-16 Two independent pool model reproduces the main effects of carbachol on inhibitory short-term plasticity.** The parameters of 2P model were independently optimised using frequency stimulation dataset of the inhibitory connection between PV+ and pyramidal neurons. Simulations of the 2P in control and carbachol conditions were averaged and plotted. (A-C) The model does not capture the lack of effect of carbachol at lower frequencies of 10 and 20hz and predicts a slightly reduced short-term depression at these frequencies. (D-F) The model reproduces the reduction of the short-term depression observed in the experimental data at frequencies above 20Hz. Data are presented as mean ± SEM

#### 4.3.4.2 Two-pool model predicts carbachol reduces release probability and increase the recovery kinetics of vesicles

The parameters of 2P model before and after application of carbachol were tested with a Wilcoxon signed-rank test to examine the changes between the two conditions that underlie the changes in short-term plasticity at the inhibitory synapse between PV+ and pyramidal neurons within the mPFC. The parameters before and after carbachol application are shown in Figure 4-17A.

The 2P model revealed a significant reduction in the lower release probability ($p_1$: p = .036) and a significant increase in the depression time constant ($D$: p = .027). No significant changes were observed in the higher release probability ($p_2$: p = .322) or the ratio of low to high release probability vesicles ($\alpha_1$: p = .105).

The increase the recovery time constant, $D$, might be an indication that the replenishment of vesicles at this synapse is dependent on calcium, as suggested before by Lawrence et al. (2015). Therefore, computational modelling indicates that while the 2P model reproduces the short-term dynamics at higher frequencies, the model needs to be extended to ensure the peaks at lower frequencies are the same under the control and carbachol conditions. The 2P model suggests that the reduction in short-term depression by carbachol is mediated by a decrease in release probability of lower release probability vesicles and an increase in recovery time constant of vesicles (Figure 4-17B).

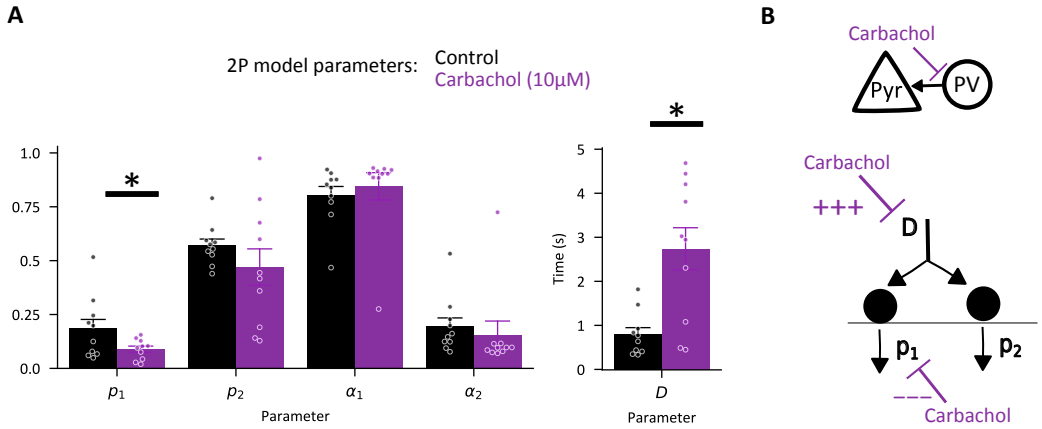


**Figure 4-17 Carbachol reduces release probability and increases the recovery kinetics of vesicles at inhibitory synapse between PV+ and pyramidal neurons.** (A) Parameters of a short-term plasticity model, 2P, with two pools of vesicles with heterogeneous release probabilities were optimised independently for control and carbachol conditions. The model predicts that the reduction in short-term depression is mediated by a decrease in $p_1$, which is a parameter that controls the release of the lower release probability vesicles. The model also predicts that $D$ is increased by carbachol which is a parameter that control the recovery of vesicles of all the release sites. Data are presented as mean ± SEM. Wilcoxon signed-rank test * = p<.05. (B) Schematic of results in (A), optimisation of the short-term plasticity model before and after carbachol reveals that carbachol reduces the release probability of the lower release probability vesicles and also increases the recovery rate of both pools of vesicles. These changes result in reduced short-term depression.

## 4.4 Discussion

The cholinergic modulation of excitatory and inhibitory synaptic transmission was examined between PV+ and pyramidal neurons within layer 5 and 6 of the mPFC. To selectively activate synapses, whole-cell paired recordings were conducted between these cells. Computational modelling was employed to uncover the synaptic changes underlying the cholinergic modulation of short-term plasticity. The main results were that activation of cholinergic receptors in the mPFC caused a robust depression in both excitatory and inhibitory baseline transmission between PV+ and pyramidal neurons within deeper layers of the mPFC. Additionally, activation of cholinergic receptors reduced the short-term depression of inhibitory transmission. The change in short-term depression showed frequency-dependent effects on inhibitory transmission. While at low frequencies carbachol suppressed the inhibition, at higher frequencies the activation of acetylcholine receptors had minor effects on inhibitory transmission. This is highlighted by the fact that during steady-state activity at higher frequencies the inhibition in carbachol conditions was the same as the inhibition in control conditions. Computational modelling revealed that carbachol reduced release probability and increased the recovery kinetics of the presynaptic vesicles which mediated the observed changes is in short-term dynamics.

### 4.4.1 The role of muscarinic receptors in suppressing synaptic transmission

Muscarinic receptors, M1-4, are expressed in the cortex (Levey et al., 1991) and M2 receptors are expressed on presynaptic terminals of PV+ cells in hippocampus and entorhinal cortex (Hajos et al., 1998; Chaudhuri et al., 2005). Current evidence suggests the suppression of inhibitory transmission is mediated by M2 receptors while the suppression of excitatory transmission may be mediated by M4 receptors. Co-application of non-selective muscarinic antagonists with carbachol has been shown to block the reduction of inhibitory transmission between pairs of PV+ and pyramidal neurons in the mPFC and insular cortex (Yamamoto et al., 2010; Pafundo et al., 2013). The specific receptors that might be involved include M2, as shown in CA3 (Szabó et al., 2010). As far as excitatory transmission is considered, in paired recordings between PV+ and pyramidal cells, non-selective muscarinic antagonists block the reduction of excitatory transmission in the mPFC and somatosensory cortex (Levy et al., 2008; Pafundo et al., 2013). The specific contribution of different types of muscarinic receptors to reduction of excitatory transmission between connections of PV+ and pyramidal neurons is currently not known. In cortical cultures the reduction of EPSPs was shown to be mediated by M4 muscarinic

receptors (Kimura and Baughman, 1997) and the reduction of EPSPs at Schaffer-collateral input to CA1 pyramidal cells has also been shown to be mediated by M4 receptors (Dasari and Gulledge, 2011). However, there have been no studies specifically examining the receptor contribution to the reduction in excitatory transmission mediated by carbachol between PV+ interneurons and pyramidal neurons. Further pharmacological experiments are required to verify the specific receptor contribution to carbachol-mediated changes in the mPFC, and immunolabelling studies need to confirm the existence of muscarinic receptors at presynaptic terminals of pyramidal cells and PV+ interneurons within the mPFC.

Nevertheless, overwhelming pharmacological evidence suggests that the suppressive effects of cholinergic modulation on excitatory and inhibitory transmission in paired recordings between PV+ and pyramidal neurons are mediated by presynaptic muscarinic receptors. Activation of M2-type muscarinic receptors, which include M2 and M4 receptors, inhibits presynaptic voltage-gated calcium channels (Thiele, 2013). Blocking presynaptic calcium channels will lead to reduced release probability and reduced neurotransmitter release. Therefore, given previous evidence, the effects on baseline transmission were most likely mediated by a reduction in the release probability through activation of M2-type muscarinic receptors at the presynaptic terminals.

The presynaptic origin of carbachol-mediated effects on excitatory and inhibitory transmission between PV+ and pyramidal neurons is supported by previous evidence based on coefficient of variation analysis (Kimura and Baughman, 1997; Yamamoto et al., 2010), changes in paired-pulse ratios (Yamamoto et al., 2010), quantal analysis (Lawrence et al., 2015), and increased failure rates. Additionally, the increase in failure rates in this chapter of both excitatory and inhibitory transmission was consistent with carbachol exerting its effects through presynaptic modification. Moreover, changes in inhibitory short-term plasticity were also reported which, as short-term plasticity is mostly controlled presynaptically suggests presynaptic modulation. Therefore, previous evidence and presented results indicate that presynaptic muscarinic receptors mediate the reduction in basal transmission of both excitatory and inhibitory connection between PV+ and pyramidal neurons within the mPFC.

### 4.4.2 Activation of cholinergic receptors suppresses excitatory and inhibitory baseline transmission

Activation of cholinergic receptors suppressed the strength of excitatory and inhibitory transmission between connected PV+ and pyramidal neurons within deeper layers of the mPFC. The effects of carbachol reach a steady-state reduction within a few minutes. The reduction of inhibitory transmission mediated by PV+ interneurons onto pyramidal neurons is consistent with previous reports from the mPFC (Pafundo et al., 2013), CA1 (Lawrence et al., 2015) and CA3 (Szabó et al., 2010). The carbachol-mediated reduction in excitatory transmission is consistent with previously reported reductions in the mPFC (Pafundo et al., 2013), piriform cortex (Hasselmo and Bower, 1992) and somatosensory cortex (Levy et al., 2008). Therefore, the results presented in this chapter contribute to the evidence that activation of cholinergic receptors depresses baseline transmission between pairs of PV+ and pyramidal neurons.

The magnitude of the carbachol-mediated reduction of inhibitory and excitatory transmission shown was larger than has been previously reported in the mPFC (Pafundo et al., 2013). The affinity of carbachol has been shown to increase with decreasing temperature (Aronstam and Narayanan, 1988), however, the recording temperature here was maintained between 31-33°C compared to 30-32°C in the study by Pafundo et al. (2013), hence it is unlikely that this was a factor that contributed to the differences. These observations, however, raise the possibility of laminar differences in cholinergic modulation of evoked transmission between PV+ and pyramidal neurons within the mPFC. Pafundo et al. (2013) examined layer 3 neurons from the anterior cingulate, prelimbic and infralimbic areas of the mPFC. The recordings presented here were conducted in deeper layers 5 and 6 of the prelimbic area. Cholinergic modulation has been previously shown to exert differential effects on the mPFC neurons dependent on their laminar location. For instance, phasic application of acetylcholine to pyramidal neurons causes stronger inhibitory currents in pyramidal neurons within deeper layers compared to superficial layers (Gulledge et al., 2007). These direct effects have been shown to be caused by laminar differences in the expression of nicotinic receptors which have been extensively characterised (Bloem, et al., 2014). The effects of carbachol are most likely mediated by muscarinic receptors. Hence, the differences in the suppression between the results and reports in Pafundo et al. (2013) indicate that, similarly to nicotinic receptors, the muscarinic receptor expression might be layer-dependent. There is a paucity of studies examining muscarinic receptor expression within the mPFC, therefore, these observations need to be

verified with immunolabelling. The potential laminar differences in muscarinic receptor expression on pyramidal neurons are also supported by the fact that the magnitude of the reduction in excitatory transmission reported in the results is similar to carbachol-mediated suppression of excitatory transmission onto pyramidal neurons within deeper layers of the mPFC (Caruana et al., 2011). Interestingly, a study examining the connection between fast-spiking and pyramidal neuron within deeper layers of the insular cortex reported a reduction of 51% in inhibitory transmission following carbachol application compared to 53% reported in this chapter (Yamamoto et al., 2010). Therefore, this agreement might suggest that the expression of muscarinic receptors on PV+ interneurons and pyramidal neurons is higher in deeper cortical layers compared to superficial layers and this might be a pattern observable across cortical regions. The superficial and deeper layers of the mPFC differ in their efferent and afferent projections. Deeper layers are the main output layer of the mPFC that send projections to subcortical regions and contralateral cortex (Dembrow and Johnston, 2014; Lee et al., 2014). Superficial prefrontal layers are innervated by excitatory inputs from the thalamus, amygdala, hippocampus and contralateral mPFC and send projections to the amygdala, striatum as well as deeper layers within the mPFC (Little and Carter, 2012). Therefore, the superficial layers are responsible for processing of a large array of incoming information. Potential laminar differences in cholinergic modulation would result in afferent and efferent projections being differently affected by acetylcholine. Differences in reduction of recurrent connections between PV+ and pyramidal neurons will result in differences in levels of disinhibition of pyramidal cells from local inhibition. This will affect the balance of cortico-subcortical and corticocortical transmission and it might serve a role of reducing the signal-to-noise ratio of communication between the mPFC and other brain regions. Therefore, future studies should examine the laminar dependent effects of cholinergic modulation of synaptic transmission between PV+ and pyramidal neurons within the mPFC.

### 4.4.3 Activation of cholinergic receptors accelerates the decay of inhibitory transmission

The decay time constant of the inhibitory potentials was reduced by carbachol. This is consistent with a previous report from CA3 where the decay time constant was reduced in connections formed by PV+ interneurons onto granule cells (Szabó et al., 2010). Szabo et al. (2010) performed experiments at room temperature which reduces GABA uptake (Binda et al., 2002). The results presented in this chapter confirm that the acceleration of the decay time constant mediated by carbachol is also observed under physiological

temperatures of 31-33°C. Current evidence suggests that the reduction in the decay of inhibitory transmission might be due to reduction in GABA spillover (Overstreet and Westbrook, 2003).

Neurotransmitter spillover occurs when released neurotransmitter diffuses out of its synaptic cleft to activate receptors on adjacent synapses (Farrant and Nusser, 2005). Paired recordings from fast-spiking interneurons and granule cells have shown that the decay of inhibitory currents is substantially prolonged by blocking GABA neurotransmitter reuptake protein (Overstreet and Westbrook, 2003). This suggests that under basal conditions, GABA spillover may be prevented by clearance of GABA form the synaptic cleft. Importantly, without blocking the reuptake, Overstreet and Westbrook (2003) showed that decreasing the release probability with cadmium reduces the decay of inhibitory currents which suggests that a degree of spillover occurs in control conditions. This decrease in decay was also larger in synapses that are more sensitive to the block of neurotransmitter reuptake, further confirming the role of neurotransmitter clearance in controlling spillover. Therefore, given the evidence, the accelerated decay of IPSPs presented in the results might be mediated by a reduction in GABA spillover due to reduction of release probability. Future studies could verify this by testing the effects of reducing the release probability with cadmium on the decay of inhibitory potentials.

Carbachol has been shown to induce fast oscillations in acute slices (Buhl et al., 1998). Interestingly, it has been shown that prolonging the decay of inhibitory currents with benzodiazepine zolpidem decreases the frequency of oscillations induced by carbachol within the mPFC (Aerde et al., 2009). These effects were not observed when excitatory decay was increased with cyclothiazide; cyclothiazide reduces AMPA receptor desensitization and reduces the decay of AMPA mediated currents. Therefore, the reduced decay might have implications for generation of oscillations within the mPFC.

### 4.4.4 Carbachol reduces the inhibitory short-term depression

Application of carbachol decreased short-term depression at the inhibitory synapse formed by PV+ and pyramidal neurons. This effect was frequency-dependent, the short-term depression was unchanged at lower frequencies of 5 and 10Hz and was reduced at higher frequencies between 20-200Hz.

Similar effects of cholinergic activation on short-term plasticity between PV+ and pyramidal neurons have been observed before. In the mPFC, the short-term depression was reduced at 40 and 60Hz, this effect was blocked by co-application of muscarinic antagonists (Pafundo et al., 2013). In CA1 region, the activation of muscarinic receptors had no effect on the short-term dynamics of inhibitory transmission at 5Hz but reduced short-term depression at 50Hz (Lawrence et al., 2015). Additionally, in CA3, the short-term depression of inhibitory transmission mediated by PV+ interneurons onto granule cells was also reduced at higher frequency of 30Hz but not lower frequencies between 5-15Hz (Szabó et al., 2010). The reduction of short-term depression following carbachol application during 50Hz stimulation protocols was also reported at a synapse between basket cells onto granule cells in dentate gyrus (Hefft et al., 2002). These multiple reports of reduction of short-term depression at the inhibitory synapse between PV+ and pyramidal neurons show this effect is consistent across different brain regions.

### 4.4.5 Short-term plasticity model explains the reduction of short-term depression

The optimisation of the short-term plasticity model suggests that carbachol mediates the reduction in short-term depression by reducing the release probability and increasing the recovery time constant of vesicles. The model used for optimisation assumes two heterogeneous vesicle pools with different release probabilities. Parameter inference suggests that only the lower release probability release sites were affected by carbachol while the higher release probability vesicles were unaffected. As stated before (section 4.4.1), evidence shows that carbachol mediates the suppression of inhibitory transmission by acting on M2-type muscarinic receptors. The activation of presynaptic M2-type receptors blocks calcium channels which reduces release probability by reduction of calcium influx. Hence, the reduction in release probability suggested by modelling is in line with physiological evidence.

The model predicts that the lower release probability release sites are affected by carbachol but not the higher release probability release sites. This potentially indicates that the distribution of the M2-type receptors is heterogeneous and M2-type receptors are preferentially expressed on release sites with lower release probability. This observation is in supported by an earlier study examining non-uniformities at hippocampal release sites where it has been reported that $GABA_B$ receptor antagonist, baclofen, preferentially acts

on release sites with lower release probability compared to release sites with higher release probability (Rosenmund et al., 1993).

Parameter inference also suggests that the depression time constant that controls the recovery of vesicles is increased; this causes vesicles in carbachol conditions to be replenished more slowly. As discussed above, evidence suggests that the observed changes in baseline transmission and changes in short-term plasticity are mediated by presynaptic muscarinic receptors that block calcium channels. Therefore, the slowing of vesicle recovery suggests that vesicle replenishment may be a calcium dependent process. Indeed, calcium-dependent vesicle recovery has been previously reported (Wang and Kaczmarek 1998; Dittman and Regehr 1998; Stevens and Wesseling 1998). Additionally, a recent modelling study used a short-term plasticity model with calcium-dependent vesicle recovery to explain the cholinergic modulation of inhibitory transmission between PV+ and pyramidal neurons in CA1 (Lawrence et al., 2015). Parameter inference in that study showed that muscarine application reduced calcium currents by 80% which led to a reduction in release probability and a decrease in the rate of calcium-dependent recovery from depression (Lawrence et al., 2015). Future experimental studies should verify if vesicle replenishment is dependent on calcium. These experiments involve conducting recovery protocols in the presence and absence of EGTA (Luo et al., 2015). Recovery protocol experiments were previously described in section 3.4.3 in Chapter 3. These protocols involve stimulating the synapse at a relatively high frequency that induces vesicle depletion. The high frequency conditioning train is followed by a recovery pulse, at varying time intervals. The normalised amplitude of the recovery pulse to the first peak in the high frequency train is taken as a measure of vesicle recovery. EGTA is a slow calcium buffer, therefore, is reduces levels of residual calcium. Hence, comparing results of recovery protocol experiments in the presence and absence of EGTA provides a measure of the dependence of vesicle replenishment on calcium. If the recovery is larger in the absence of EGTA, it suggests that vesicles recovery is dependent on calcium. Therefore, future studies should examine calcium dependence of vesicle replenishment at the inhibitory synapse between PV+ and pyramidal neurons to verify if it contributes to short-term plasticity at this synapse.

The lack of an activity-dependent recovery of vesicles in the model used in this chapter might also be the reason why the model underestimated the short-term depression at lower frequencies in carbachol conditions (Figure 4-15). It is important to note that the study by Lawrence et al., (2015) stated that the cholinergic modulation of short-term plasticity at higher frequencies was replicated by a model with calcium dependent vesicle recovery,

however, the authors do not report on whether the model replicated the short-term dynamics at lower frequencies during carbachol conditions. Therefore, future modelling work can test if a model that is extended with calcium-dependent vesicle recovery performs better at describing the low frequency data in carbachol conditions.

It is interesting that a model without calcium-dependent recovery, the two independent pool model, performs well at capturing short-term plasticity in control conditions but fails to account for low frequency data in carbachol conditions. This might suggest that there is an additional short-term plasticity mechanisms in carbachol conditions that was not present in control conditions. Indeed, evidence exists to support that hypothesis. It has been previously shown that repetitive activity relieves a block of calcium voltage-gated channels caused by muscarine (Brody and Yue, 2000). In the study by Brody and Yue (2000), repetitive activity did not have the same effect when the release probability was simply lowered by addition of cadmium. This type of activity-dependent recovery is not implemented in the model; thus, this might provide an alternative explanation as to why the model captured the dynamics of the synapse in control conditions but not in carbachol conditions. During cholinergic modulation this activity dependent relief emerges, and it affects the short-term dynamics at this synapse, hence, as this feature was not included in the model, this might be the reason why the lower frequency data in carbachol conditions was poorly fitted. Therefore, future modelling studies of carbachol effects at this synapse should consider the activity-dependent recovery from depression during cholinergic modulation.

### 4.4.6 Functional relevance of cholinergic modulation

The results show that the activation of cholinergic receptors reduced both inhibitory and excitatory synaptic transmission between PV+ interneurons and pyramidal neurons within the deeper layers of the mPFC. Additionally, carbachol reduced the short-term depression of inhibitory transmission between PV+ and pyramidal neurons. The reduction in baseline transmission of excitatory and inhibitory synapse will affect feedback inhibition between these neurons. The reduced strength of the excitatory drive onto PV+ interneurons means that a higher number of pyramidal cells within layer 5/6 need to fire to elicit a spike in PV+ interneuron. If the PV+ interneuron fires, the magnitude of the feedback inhibition will be reduced as carbachol reduced baseline transmission. Therefore, it is possible that the reduction in the strength of the excitatory and inhibitory connections means that the feedback inhibition between layer 5/6 pyramidal and PV+ interneurons will be largely

reduced. This might contribute to the disinhibition of pyramidal neurons within the deeper layers of the mPFC.

The attenuation of the recurrent connection between PV+ and pyramidal cells can be considered in the light of a theory discussed in the introduction proposed by Hasselmo and colleagues (section 1.4.2). It was proposed that acetylcholine selectively depresses recurrent synapses compared to afferent long-range inputs. This in turn facilitates the processing of the incoming sensory inputs during attentional and mnemonic processing and it reduces the interference of previously learnt memories during encoding of new memories. As discussed in the introduction (section 1.4.2), evidence suggests that this pattern of differential cholinergic modulation of excitatory synapses exists in the mPFC. The activation of cholinergic receptors reduces the excitatory intracortical drive onto layer 5 pyramidal neurons from intracortical pyramidal neurons (Carr and Surmeier, 2007; Caruana et al., 2011; Martin et al., 2015) and facilitates the afferent thalamic drive onto pyramidal neurons within superficial and deeper layers of the mPFC (Gioanni et al., 1999; Lambe et al., 2003). Therefore, the weaker connection between the PV+ and pyramidal neurons within layer 5/6 suggest that the recurrent, intracortical communication between these cells might be suppressed in favour of afferent inputs.

It is important to note that the finding that short-term depression is reduced in carbachol conditions will affect the degree of disinhibition. The reduction in short-term depression resulted in significant attenuation of inhibitory transmission at lower frequencies of 5 and 10Hz (Figure 4-10A-C). The inhibition at frequencies above 20Hz, however, only showed differences in the initial peaks and with sustained activity, inhibition converged onto the same steady-state transmission in both control and carbachol conditions (Figure 4-10D-F). This suggests that sparse, low frequency PV+ interneurons activity will produce significantly reduced inhibition of layer 5/6 pyramidal neurons during cholinergic modulation compared to control conditions. However, if PV+ interneurons fire at higher frequencies, only the initial inhibition is reduced after which, with sustained firing, the levels of inhibition are unchanged compared to control conditions. Therefore, if PV+ interneurons fire at lower frequencies, this will contribute to the disinhibition of pyramidal cells but if PV+ interneurons fire at frequencies >20Hz, the magnitude of the inhibition will be the same compared to the control conditions. Therefore, the shift in short-term depression suggests that the degree disinhibition will be dependent on the firing frequency of PV+ interneurons. As discussed in introduction (section 1.4.1), acetylcholine does not affect the excitability of cortical PV+ interneurons (Kawaguchi and Kubota, 1997; Kruglikov and Rudy, 2008; Yi et al., 2014). This suggests that the firing of PV+

interneurons will be controlled by its excitatory and inhibitory inputs rather than the changes in its intrinsic properties. However, it is difficult to predict which excitatory inputs will be controlling firing of PV+ interneurons during cholinergic modulation due to paucity of data. PV+ interneurons are directly innervated by intracortical excitatory cells and also long-range afferents from regions such as hippocampus and thalamus (Tierney et al., 2004; Delevich et al., 2015). PV+ interneurons mediate feedforward inhibition via direct long-range connections which controls the temporal integration window of pyramidal cells. It is possible that the shift in the short-term plasticity provides dynamic means of modulating feedforward inhibition where low frequency long-range inputs would contribute to disinhibition of pyramidal neurons and this would relax the temporal integration window while stronger frequency inputs, assuming these would increase PV+ interneurons firing, would sharpen the temporal integration window. However, as stated above, these dynamics are difficult to predict as there are no studies examining the frequency or strength of long-range inputs onto the prefrontal PV+ interneurons under basal or cholinergic conditions. Nevertheless, these dynamics can be examined in small models of prefrontal circuitry. It could be tested how, under carbachol modulation, different long-range inputs of different strength and frequency affect the recurrent dynamics between intracortical pyramidal and PV+ cells, how it affects the output firing of pyramidal neurons and how it may affect the prefrontal synchrony. Activation of cholinergic receptors *in vitro* induces gamma oscillations (Buhl et al., 1998; Fisahn et al., 1998; Betterton et al., 2017). A potential future direction might be to consider the effects of the shift in short-term plasticity on oscillations within the mPFC. Activation of PV+ interneurons at gamma range is sufficient to induce gamma oscilations in the cortex (Cardin et al., 2009). Gamma power increases during succesfull allocation of atention and is reduced within the mPFC with cholinergic antagonists (Howe et al., 2017). It might be possible that tonic levels of acetylcholine induce a shift in the short-term dynamics which might contribute to enhancment of gamma power. Therefore, it would be interesting to test in network models of prefrontal circutry how the reduction in short-term depression of the inhibitory synapse contributes to the induction of oscillations and how it may contribute to the power and frequency of oscillations.

Interestingly, given the frequency dependent effects of carbachol shown in this chapter, in a study that examined the activity of prefrontal PV+ interneurons during attentional processing, it was reported that activation of PV+ at 1-10hz disrupts attentional processing while activation at higher gamma range frequencies improved attentional processing (see Chapter 1 section 1.3 for detailed description of the study) (H. Kim et al., 2016). Tonic acetylcholine levels have been shown to be elevated in attentional tasks (Paolone et al.,

2013). Therefore, computational models can test how PV+ firing at lower frequencies and higher frequencies, combined with the reduction of short-term depression affect network dynamics of the mPFC.

### 4.4.7 Chapter summary

The results in this chapter show that the activation of cholinergic receptors regulates the activity of the excitatory and inhibitory connections formed by pyramidal neurons and PV+ interneurons within layer 5/6 of the mPFC. The reduction in baseline inhibitory transmission is accompanied by a shift in short-term plasticity where the inhibitory synaptic transmission shows less short-term depression with repetitive stimulation.

These changes will impart frequency-dependent effects on the interactions between these cells. Sparse firing of PV+ cells will produce highly suppressed inhibition, while higher frequency firing of PV+ cells will mediate the same magnitude of inhibition as in basal conditions. Therefore, cholinergic receptors activation may contribute to disinhibition of the pyramidal cells within the mPFC, however, this effect will be dependent on the firing frequency of PV+ cells.

# Chapter 5. General Discussion

This thesis combined experimental and computational methods in order to understand the recurrent connections between PV+ and pyramidal neurons within the deeper layers of the mPFC. The first aim was to investigate the mechanisms of short-term plasticity between these cells using a model-based approach. The second aim was to examine how synaptic transmission between these neurons is modulated by acetylcholine.

The main findings are that short-term plasticity at excitatory synapse is controlled by release sites with homogeneous release probability while inhibitory short-term plasticity is best explained with the existence of release sites with different release probabilities. Examination of cholinergic modulation of these connections revealed that cholinergic receptor activation reduces the strength of both the inhibitory and excitatory synapse. Additionally, cholinergic modulation dynamically regulates inhibitory transmission by reducing inhibitory short-term depression. Computational modelling suggests that the changes in inhibitory short-term plasticity are mediated by a reduction in release probability and slowing of vesicle recovery.

These findings suggest that the recurrent communication between PV+ and pyramidal neurons is weakened during cholinergic modulation. However, the functional relevance of these results is challenging to predict as the data on cholinergic modulation of both afferent and recurrent connection within the mPFC is limited. Therefore, these results also highlight the need for a detailed investigation of cholinergic modulation of excitatory inputs onto PV+ interneurons within the mPFC.

## 5.1 Excitatory inputs onto prefrontal PV+ interneurons

As shown in this thesis, the reduction in short-term depression will impart frequency-dependent suppression of inhibition onto pyramidal cells. These effects will be dependent on the frequency of firing of PV+ neurons during cholinergic modulation. Therefore, there is a need to understand how the overall synaptic excitation of PV+ cells will be affected by acetylcholine. This thesis and work by Pafundo et al. (2013) provide first evidence that intralaminar excitatory drive onto PV+ cells mediated by pyramidal neurons is substantially reduced by tonic activation of cholinergic receptors. However, it is still unknown how cholinergic system modulates interlaminar excitatory inputs onto PV+ interneurons.

Additionally, as stated before, PV+ interneurons are also innervated by long-range excitatory inputs from regions such as hippocampus and thalamus (Tierney et al., 2004; Delevich et al., 2015), how cholinergic system modulates these afferent inputs is also unknown.

Furthermore, recent study reported that in carbachol conditions the excitatory drive onto PV+ cell in deeper layers of the mPFC is elevated, however, the source of this drive was not determined (Tikhonova et al., 2018). In the study by Tikhonova et al. (2018), spontaneous EPSCs in PV+ interneurons were examined during acetylcholine receptor activation. It was reported that the amplitude and frequency of spontaneous EPSCs in PV+ interneurons are elevated by activation of cholinergic receptors. This increase was induced by action potentials as it was blocked by tetrodotoxin. Tikhonova et al. (2018) suggest that the increase in EPSCs was most likely mediated by neighbouring pyramidal neurons within the deeper layers that were depolarised by acetylcholine which increased their firing rate. The results of this thesis, however, suggest that this is unlikely. Here, a robust suppression of ~60% in the amplitude of the EPSPs was reported and the amplitude of the EPSCs recorded in the study by Tikhonova et al. (2018) increased by ~50%. This raises a possibility that the cholinergic modulation heightens specific excitatory inputs onto deeper layer PV+ interneurons emerging from more superficial layers or afferent long-range inputs. Interestingly, Tikhonova et al., (2018) also show that the increase in the excitatory drive onto PV+ cells is mediated by M1 muscarinic receptors. M1 antagonists have been shown to be important for carbachol induced gamma oscillations in CA3 and the somatosensory cortex (Buhl et al., 1998; Fisahn et al., 1998; Betterton et al., 2017); and importantly, blocking M1 receptors has been shown to alter the high gamma synchrony within the mPFC during attentional tasks (Howe et al., 2017). Hence, this raises a possibility that reduction in the recurrent connections shown in this thesis concomitant with increased excitation from other source might facilitate the induction of gamma oscillations.

Therefore, to build on the work presented in this thesis and work from other labs (Pafundo et al., 2013; Tikhonova et al., 2018), it is necessary to comprehensively characterise cholinergic modulation of excitatory inputs onto PV+ interneurons within the mPFC. Optogenetic methods enable selective stimulation of long-range afferents, therefore, it provides a perfect tool for this task. Such comprehensive studies have been conducted where effects of other neuromodulators on different inputs into the mPFC was examined. For example, one study optogenetically activated a range of inputs onto pyramidal neurons within the mPFC while activating dopaminergic receptors (Burke et al., 2018). It was reported that activation of dopaminergic receptors selectively suppresses afferent inputs

from the ipsi- and contralateral mPFC and hippocampus while not affecting the inputs from thalamus and amygdala. This suggested that by suppression of some inputs, dopamine improves signal-to-noise ratio of other inputs. Conducting similar investigation within the mPFC might reveal similar patterns of selective cholinergic suppression that might enhance inputs from certain areas. Such studies will help with our understanding of the complicated activity of acetylcholine in the mPFC.

## 5.2 Conclusion

In conclusion, this thesis is a step towards understanding excitatory and inhibitory dynamics within the mPFC and how these are modulated by acetylcholine. It was demonstrated that deterministic short-term plasticity models provide a powerful method in examining the mechanisms of synaptic transmission in basal conditions but also under neuromodulatory influence. The results show how changes in short-term plasticity mean that an apparent reduction in inhibitory transmission is dynamically controlled dependent on the firing frequency. These data can inform future modelling studies to dissect the influence of short-term properties between these cells on prefrontal circuitry under basal conditions and under acetylcholine conditions.

# Chapter 6. References & Appendices

van Aerde, K. I., Mann, E. O., Canto, C. B., Heistek, T. S., Linkenkaer-Hansen, K., Mulder, A. B., van der Roest, M., Paulsen, O, Brussaard, A. B., Mansvelder, H. D. (2009) Flexible spike timing of layer 5 neurons during dynamic beta oscillation shifts in rat prefrontal cortex. Journal of Physiology, 587, 5177–5196.

Angulo, M. C., Rossier, J., Audinat, E., Rossier, J. and Audinat, E. (1999) Postsynaptic Glutamate Receptors and Integrative Properties of Fast-Spiking Interneurons in the Rat Neocortex, *Journal of Neurophysiology*, 82, 1295–1302.

Angulo, M. C., Staiger, J. F., Rossier, J. and Audinat, E. (1999) Developmental Synaptic Changes Increase the Range of Integrative Capabilities of an Identified Excitatory Neocortical Connection, *Journal of Neuroscience*, 19, 1566–1576.

Angulo, M. C., Staiger, J. F., Rossier, J. and Audinat, E. (2003) Distinct Local Circuits Between Neocortical Pyramidal Cells and Fast-Spiking Interneurons in Young Adult Rats, *Journal of Neurophysiology*, 89, 943–953.

Anwar, H., Li, X., Bucher, D. and Nadim, F. (2017) Functional roles of short-term synaptic plasticity with an emphasis on inhibition, *Current Opinion in Neurobiology*, 43, 71–78.

Aronstam, R. S. and Narayanan, T. K. (1988) Temperature effect on the detection of muscarinic receptor-G protein interactions in ligand binding assays, *Biochemical Pharmacology*, 37, 1045–1049.

Arroyo, S., Bennett, C. and Hestrin, S. (2014) Nicotinic modulation of cortical circuits, *Frontiers in Neural Circuits*, 8, 1–6.

Ascoli, G. A. et al. (2008) Petilla terminology: nomenclature of features of GABAergic interneurons of the cerebral cortex, *Nature Reviews Neuroscience*, 9, 557–568.

Ballinger, E. C., Ananth, M., Talmage, D. A. and Role, L. W. (2016) Basal Forebrain Cholinergic Circuits and Signaling in Cognition and Cognitive Decline, *Neuron*, 91, 1199–1218.

Beierlein, M. (2003) Two Dynamically Distinct Inhibitory Networks in Layer 4 of the Neocortex, *Journal of Neurophysiology*, 90, 2987–3000.

Bennett, C., Arroyo, S., Berns, D. and Hestrin, S. (2012) Mechanisms Generating Dual-Component Nicotinic EPSCs in Cortical Interneurons, *Journal of Neuroscience*, 32, 17287–17296.

Betterton, R. T., Broad, L. M., Tsaneva-atanasova, K. and Mellor, J. R. (2017) Acetylcholine modulates gamma frequency oscillations in the hippocampus by activation of muscarinic M1 receptors, *European Journal of Neuroscience*, 45, 1570–1585.

Binda, F., Bossi, E., Giovannardi, S., Forlani, G. and Peres, A. (2002) Temperature effects on the presteady-state and transport-associated currents of GABA cotransporter rGAT1, *FEBS Letters*, 512, 303–307.

Bird, A. D., Wall, M. J. and Richardson, M. J. E. (2016) Bayesian Inference of Synaptic Quantal Parameters from Correlated Vesicle Release, *Frontiers in Computational Neuroscience*, 10, 1–14.

Bloem, B., Schoppink L., Rotaru, D.C., Faiz, A., Hendriks, P., Mansvelder, H.D., van de Berg W.D., Wouterlood, F. G. (2014) Topographic mapping between basal forebrain cholinergic neurons and the medial prefrontal cortex in mice. *Journal of* Neuroscience, 34, 16234-16246.

Bloem, B., Poorthuis, R. B. and Mansvelder, H. D. (2014) Cholinergic modulation of the medial prefrontal cortex: the role of nicotinic receptors in attention and regulation of neuronal activity, *Frontiers in Neural Circuits*, 8, 1–16.

Brody, D. L. and Yue, D. T. (2000) Relief of G-Protein Inhibition of Calcium Channels and Short-Term Synaptic Facilitation in Cultured Hippocampal Neurons, *Journal of Neuroscience*, 20, 889–898.

Buhl, E. H., Tam, G. and Fisahn, A. (1998) Cholinergic activation and tonic excitation induce persistent gamma oscillations in mouse somatosensory cortex *in vitro*, *Journal of Physiology*, 11, 117–126.

Burke, K. J., Keeshen, C. M., Bender, K. J., Burke, K. J., Keeshen, C. M. and Bender, K. J. (2018) Two Forms of Synaptic Depression Produced by Differential Neuromodulation of Presynaptic Article Two Forms of Synaptic Depression Produced by Differential Neuromodulation of Presynaptic Calcium Channels, *Neuron*, 99, 969–984.e7.

Burnham, K. and Anderson, D. R. (2004) Multimodel Inference Understanding AIC and BIC in Model Selection, *Sociological Methods and Research*, 33, 261–304.

Cardin, J. A., Carlén, M., Meletis, K, Knoblich, U., Zhang, F., Deisseroth, K., Tsai, L. H., Moore, C. I. (2009) Driving fast-spiking cells induces gamma rhythm and controls sensory responses, *Nature*, 459, 663–667.

Carr, D. B. and Surmeier, D. J. (2007) M1 Muscarinic Receptor Modulation of Kir2 Channels Enhances Temporal Summation of Excitatory Synaptic Potentials in Prefrontal Cortex Pyramidal Neurons, *Journal of Neurophysiology*, 97, 3432–3438.

Caruana, D. A., Warburton, E. C. and Bashir, Z. I. (2011) Induction of Activity-Dependent LTD Requires Muscarinic Receptor Activation in Medial Prefrontal Cortex, *Journal of Neuroscience*, 31, 18464–18478.

Chaudhuri, J. D., Hiltunen, M., Soininen, H. and Miettinen, R. (2005) Localization of M2 muscarinic receptor protein in parvalbumin and calretinin containing cells of the adult rat entorhinal cortex using two complementary methods., *Neuroscience*, 131, 557–566.

Chiang, P. H., Yeh, W. C., Lee, C. T., Weng, J. Y., Huang, Y. Y. and Lien, C. C. (2010) M(1)-like muscarinic acetylcholine receptors regulate fast-spiking interneuron excitability in rat dentate gyrus., *Neuroscience*, 169, 39–51.

Cho, K. K. A., Hoch, R., Rubenstein, J. L. R. and Sohal, V. S. (2015) Gamma Rhythms Link Prefrontal Interneuron Article Gamma Rhythms Link Prefrontal Interneuron Dysfunction with Cognitive, *Neuron*, 85, 1332–1343.

Costa, R. P., Sjöström, P. J. and van Rossum, M. C. W. (2013) Probabilistic inference of short-term synaptic plasticity in neocortical microcircuits, *Frontiers in Computational Neuroscience*, 7, 1–12.

Courtin, J. Chaudun. F., Rozeske, R. R., Karalis, N., Gonzalez-Campo, C., Wurtz, H., Abdi, A., Baufreton, J., Bienvenu. T. C., Herry, C. (2014) Prefrontal parvalbumin interneurons shape neuronal activity to drive fear expression, *Nature*, 505, 92–96.

Dalley, J. W., Mcgaughy, J., Connell, M. T. O., Cardinal, R. N., Levita, L. and Robbins, T. W. (2001) Distinct Changes in Cortical Acetylcholine and Noradrenaline Efflux during Contingent and Noncontingent Performance of a Visual Attentional Task, *Journal of Neuroscience*, 21, 4908–4914.

Dasari, S. and Gulledge, A. T. (2011) M1 and M4 Receptors Modulate Hippocampal Pyramidal Neurons, *Journal of Neurophysiology*, 105, 779–792.

Delevich, K., Tucciarone, J., Huang, Z. J. and Li, X. B. (2015) The Mediodorsal Thalamus Drives Feedforward Inhibition in the Anterior Cingulate Cortex via Parvalbumin Interneurons, *Journal of Neuroscience*, 35, 5743–5753.

Dembrow, N. C., Chitwood, R. A. and Johnston, D. (2010) Projection-Specific Neuromodulation of Medial Prefrontal Cortex Neurons, *Journal of Neuroscience*, 30, 16922–16937.

Dembrow, N. and Johnston, D. (2014) Subcircuit-specific neuromodulation in the prefrontal cortex, *Frontiers in Neural Circuits*, 8, 1–9.

Descarries, L., Gisiger, V. and Steriade, M. (1997) Diffuse Transmission by Acetylcholine in the CNS, *Progress in Neurobiology*, 53.

Dobrunz, L. E. and Stevens, C. F. (1997) Heterogeneity of Release Probability, Facilitation, and Depletion at Central Synapses, *Neuron*, 18, 995–1008.

van Eden, C. G. and Uylings, B. M. (1985) Cytoarchitectonic Development of the Prefrontal Cortex in the Rat, *Journal of Comparative Neurology*, 241.

Farrant, M. and Nusser, Z. (2005) Variations on an inhibitory theme: Phasic and tonic activation of GABA A receptors, *Nature Reviews Neuroscience*, 6, 215–229.

Ferguson, B. R. and Gao, W. (2018) PV Interneurons : Critical Regulators of E / I Balance for Prefrontal Cortex-Dependent Behavior and Psychiatric Disorders, *Frontiers in Neural Circuits*, 12, 1–13.

Fisahn, A., Pike, F. G., Buhl, E. H. and Paulsen, O. (1998) Cholinergic induction of network oscillations at 40 Hz in the hippocampus, *Nature*, 394, 3–6.

Forsythe, I. D., Tsujimoto, T., Barnes-Davies, M., Cuttle, M. F. and Takahashi, T. (1998) Inactivation of presynaptic calcium current contributes to synaptic depression at a fast central synapse, *Neuron*, 20, 797–807.

Fuhrmann, G., Cowan, A., Segev, I., Tsodyks, M. and Stricker, C. (2004) Multiple mechanisms govern the dynamics of depression at neocortical synapses of young rats, *Journal of Physiology*, 557, 415–438.

Fuhrmann, G., Segev, I., Markram, H. and Tsodyks, M. (2002) Coding of Temporal Information by Activity-Dependent Synapses, *Journal of Neurophysiology*, 87, 140–148.

Gabbott, P., Headlam, A. and Busby, S. (2002) Morphological evidence that CA1 hippocampal afferents monosynaptically innervate PV-containing neurons and NADPH-diaphorase reactive cells in the medial prefrontal cortex ( Areas 25 / 32 ) of the rat, *Brain Research*, 946, 314–322.

Galarreta, M. and Hestrin, S. (1998) Frequency-dependent synaptic depression and the balance of excitation and inhibition in the neocortex., *Nature Neuroscience*, 1, 587–594.

Geiger, R. P., Jonas, P. and Universita, P. I. Der (2000) Dynamic control of presynaptic Ca(2+) inflow by fast-inactivating K(+) channels in hippocampal mossy fiber boutons, *neuron*, 28, 927–939.

Gil, Z., Connors, B. W. and Amitai, Y. (1997) Differential Regulation of Neocortical Synapses by Neuromodulators and Activity, *Neuron*, 19, 679–686.

Gioanni, Y., Rougeot, C., Clarke, P. B. S. and Lepouse, C. (1999) Nicotinic receptors in the rat prefrontal cortex : increase in glutamate release and facilitation of mediodorsal thalamo-cortical transmission, *European Journal of Neuroscience*, 11, 18–30.

Gittis, A. H., Nelson, A. B., Thwin, M. T., Palop, J. J. and Kreitzer, A. C. (2010) Distinct Roles of GABAergic Interneurons in the Regulation of Striatal Output Pathways, *Journal of Neuroscience*, 30, 2223–2234.

Gonzalez-Burgos, G. (2005) Dopaminergic Modulation of Short-Term Synaptic Plasticity in Fast-Spiking Interneurons of Primate Dorsolateral Prefrontal Cortex, *Journal of Neurophysiology*, 94, 4168–4177.

Gritton, H. J., Howe, W. M., Mallory, C. S., Hetrick, V. L., Berke, J. D. and Sarter, M. (2016) Cortical Cholinergic Signaling Controls the Detection of Cues, *Proceedings of the National Academy of Sciences*, 113, 1089–1097.

Gulledge, A. T., Park, S. B., Kawaguchi, Y. and Stuart, G. J. (2007) Heterogeneity of Phasic Cholinergic Signaling in Neocortical Neurons, *Journal of Neurophysiology*, 97, 2215–2229.

Gupta, A. (2000) Organizing Principles for a Diversity of GABAergic Interneurons and Synapses in the Neocortex, *Science*, 287, 273–278.

Hajos, N., Papp, E. C., Acsady, L., Levey, A. I. and Freund, T. F. (1998) Distinct Interneuron Types Express M2 Muscarinic Receptor Immunoreactivity on Their dendrites or Axon Terminals in the Hippocampus., *Neuroscience*, 82, 355–76.

Hallermann, S., Fejtova, A., Schmidt, H., Weyhersmu, A., Silver, R. A., Gundelfinger, E. D. and Eilers, J. (2010) Bassoon Speeds Vesicle Reloading at a Central Excitatory Synapse, *Neuron*, 68.

Hallermann, S. and Silver, R. A. (2013) Sustaining rapid vesicular release at active zones : potential roles for vesicle tethering, *Trends in Neurosciences*, 36, 185–194.

Hangya, B., Ranade, S. P., Lorenc, M. and Kepecs, A. (2015) Central Cholinergic Neurons Are Rapidly Recruited by Reinforcement Feedback, *Cell*, 162, 1155–1168.

Hasselmo, M. E. and Bower, J. M. (1992) Cholinergic suppression specific to intrinsic not afferent fiber synapses in rat piriform (olfactory) cortex, *Journal of Neurophysiology*, 67, 1222–1229.

Hasselmo, M. E. and Cekic, M. (1996) Suppression of synaptic transmission may allow combination of associative feedback and self-organizing feedforward connections in the neocortex, *Behavioural Brain Research*, 79, 153–161.

Hasselmo, M. E. and McGaughy, J. (2004) High acetylcholine levels set circuit dynamics for attention and encoding and low acetylcholine levels set dynamics for consolidation, *Progress in Brain Research*, 145, 207–31.

Hasselmo, M. E. and Sarter, M. (2010) Modes and Models of Forebrain Cholinergic Neuromodulation of Cognition, *Neuropsychopharmacology*. Nature Publishing Group, 36, 52–73.

Hasselmo, M. and Schnell, E. (1994) Laminar Selectivity of the Cholinergic Suppression of Synaptic Transmission in Rat Hippocampal Region CA 1 : Computational Modeling and Brain Slice Physiology Piriform cortex, *Journal of Neuroscience*, 14, 3898–914.

Hay, Y. A., Lambolez, B. and Tricoire, L. (2016) Nicotinic Transmission onto Layer 6 Cortical Neurons Relies on Synaptic Activation of Non-α7 Receptors, *Cerebral Cortex*, 26, 2549–2562.

Hedrick, T. and Waters, J. (2015) Acetylcholine excites neocortical pyramidal neurons via nicotinic receptors, *Journal of Neurophysiology*, 113, 2195–2209.

Hefft, S., Kraushaar, U., Geiger, J. R. P. and Jonas, P. (2002) Presynaptic short-term depression is maintained during regulation of transmitter release at a GABAergic synapse in rat hippocampus, *Journal of Physiology*, 539, 201–208.

Heidbreder, C. A. and Groenewegen, H. J. (2003) The medial prefrontal cortex in the rat : evidence for a dorso-ventral distinction based upon functional and anatomical characteristics, *Neuroscience & Biobehavioral Reviews*, 27, 555–579.

Hennig, M. H. (2013) Theoretical models of synaptic short term plasticity, *Frontiers in Computational Neuroscience*, 7, 1–10.

Hessler, N. A., Shirke, A. M. and Malinow, R. (1993) The probability of transmitter release at a mammalian central synapse, *Nature*, 366, 569–572.

Hironaka, N., Tanaka, K., Izaki, Y., Hori, K. and Nomura, M. (2001) Memory-related acetylcholine efflux from rat prefrontal cortex and hippocampus : a microdialysis study, *Brain Research*, 901, 143–150.

Hoover, W. B. and Vertes, Æ. R. P. (2007) Anatomical analysis of afferent projections to the medial prefrontal cortex in the rat, *Brain Structure and Function*, 212, 149–179.

Howe, W. M., Gritton, H. J., Lusk, N. A., Roberts, E. A., Hetrick, V. L., Berke, J. D. and Sarter, M. (2017) Acetylcholine Release in Prefrontal Cortex Promotes Gamma Oscillations and Theta–Gamma Coupling during Cue Detection, *The Journal of Neuroscience*, 37, 3215–3230.

Isaac, J. T. R., Ashby, M. C. and Mcbain, C. J. (2007) The Role of the GluR2 Subunit in AMPA Receptor Function and Synaptic Plasticity, *Neuron*, 54, 859–871.

Ishiyama, S., Schmidt, H., Cooper, X. B. H., Brose, N. and Eilers, X. J. (2014) Munc13-3 Superprimes Synaptic Vesicles at Granule Cell-to- Basket Cell Synapses in the Mouse Cerebellum, *Journal of Neuroscience*, 34, 14687–14696.

Jackman, S. L., Turecek, J., Belinsky, J. E. and Regehr, W. G. (2016) The calcium sensor synaptotagmin 7 is required for synaptic facilitation, *Nature*. Nature Publishing Group, 529, 88–91.

Jia, X. and Kohn, A. (2011) Gamma Rhythms in the Brain, *PLOS Biology*, 9, 2–5.

Jones, M. V, Jonas, P., Sahara, Y. and Westbrook, G. L. (2001) Microscopic Kinetics and Energetics Distinguish GABA A Receptor Agonists from Antagonists, *Biophysical Journal*, 81, 2660–2670.

Kabbani, N., Nordman, J. C., Corgiat, B. A., Veltri, D. P., Shehu, A., Seymour, V. A. and Adams, D. J. (2013) Are nicotinic acetylcholine receptors coupled to G proteins?, *BioEssays*, 35, 1025–1034.

Kawaguchi, S. and Sakaba, T. (2015) Control of Inhibitory Synaptic Outputs by Low Excitability of Axon Terminals Revealed by Direct Article Control of Inhibitory Synaptic Outputs by Low Excitability of Axon Terminals Revealed by Direct Recording, *Neuron*, 85, 1273–1288.

Kawaguchi, Y. and Kubota, Y. (1997) GABAergic cell subtypes and their synaptic connections in rat frontal cortex, *Cerebral Cortex*, 7, 476–486.

Kim, D., Jeong, H., Lee, J., Ghim, J. W., Her, E. S., Lee, S. H., Jung, M. W. (2016) Distinct Roles of Parvalbumin- and Somatostatin- Expressing Interneurons in Working Memory Article Distinct Roles of Parvalbumin- and Somatostatin-Expressing Interneurons in Working Memory, *Neuron*, 92, 902–915.

Kim, H., Ährlund-Richter, S., Wang, X., Deisseroth, K. and Carlén, M. (2016) Prefrontal Parvalbumin Neurons in Control of Attention, *Cell*, 164, 208–218.

Kimura, F. and Baughman, R. (1997) Distinct Muscarinic Receptor Subtypes Suppress Excitatory and Inhibitory Synaptic Responses in Cortical Neurons, *Journal of Neurophysiology*, 77, 709–716.

Kirischuk, S., Clements, J. D. and Grantyn, R. (2002) Presynaptic and postsynaptic mechanisms underlie paired pulse depression at single GABAergic boutons in rat collicular cultures, *Journal of Physiology*, 543, 99–116.

Koike-tani, M., Kanda, T., Saitoh, N., Yamashita, T. and Takahashi, T. (2008) Involvement of AMPA receptor desensitization in short-term synaptic depression at the calyx of Held in developing rats, *Journal of Physiology*, 9, 2263–2275.

Kraushaar, U. and Jonas, P. (2000) Efficacy and stability of quantal GABA release at a hippocampal interneuron-principal neuron synapse, *The Journal of neuroscience*, 20, 5594–607.

Kruglikov, I. and Rudy, B. (2008) Perisomatic GABA Release and Thalamocortical Integration onto Neocortical Excitatory Cells Are Regulated by Neuromodulators, *Neuron*, 58, 911–924.

Lambe, E. K., Picciotto, M. R. and Aghajanian, G. K. (2003) Nicotine Induces Glutamate Release from Thalamocortical Terminals in Prefrontal Cortex, *Neuropsychopharmacology*, 28, 216–225.

Lawrence, J. J., Haario, H. and Stone, E. F. (2015) Presynaptic cholinergic neuromodulation alters the temporal dynamics of short-term depression at parvalbumin-positive basket cell synapses from juvenile CA1 mouse hippocampus, *Journal of Neurophysiology*, 113, 2408–2419.

Lee, A. T., Gee, S. M., Vogt, D., Patel, T., Rubenstein, J. L. and Sohal, V. S. (2014) Pyramidal neurons in prefrontal cortex receive subtype-specific forms of excitation and inhibition, *Neuron*, 81, 61–68.

Lee, J. S., Ho, W.-K., Neher, E. and Lee, S.-H. (2013) Superpriming of synaptic vesicles after their recruitment to the readily releasable pool, *Proceedings of the National Academy of Sciences*, 110, 15079–15084.

Levey, A., Kitt, C., Simonds, W., Price, D. and Brann, M. (1991) Identification and localization of muscarinic acetylcholine receptor proteins in brain with subtype-specific antibodies, *The Journal of Neuroscience*, 11, 3218–3226.

Levy, R. B., Reyes, A. D. and Aoki, C. (2008) Cholinergic modulation of local pyramid-interneuron synapses exhibiting divergent short-term dynamics in rat sensory cortex, *Brain Research*, 1215, 97–104.

Little, J. P. and Carter, A. G. (2012) Subcellular Synaptic Connectivity of Layer 2 Pyramidal Neurons in the Medial Prefrontal Cortex, 32, 12808–12819.

Luo, F., Bacaj, T. and Sudhof, T. C. (2015) Synaptotagmin-7 Is Essential for Ca 2 ∂ -Triggered Delayed Asynchronous Release But Not for Ca 2 ∂ -Dependent Vesicle Priming in Retinal Ribbon Synapses, *Journal of Neuroscience*, 35, 11024–11033.

Ma, Y., Hu, H. and Agmon, A. (2012) Short-Term Plasticity of Unitary Inhibitory-to-Inhibitory Synapses Depends on the Presynaptic Interneuron Subtype, *Journal of Neuroscience*, 32, 983–988.

Maccaferri, G., Roberts, J. D. B., Szucs, P. and Cottingham, C. A. (2000) Cell surface domain specific postsynaptic currents evoked by identified GABAergic neurones in rat hippocampus *in vitro*, *Journal of Physiology*, 524, 91–116.

Mahfooz, K., Singh, M., Renden, R. and Wesseling, J. F. (2016) A Well-Defined Readily Releasable Pool with Fixed Capacity for Storing Vesicles at Calyx of Held, *PLoS Computational Biology*, 12, 1–38.

Marín, O. (2012) Interneuron dysfunction in psychiatric disorders, *Nature Reviews Neuroscience*, 13, 107–120.

Markram, H., Wang, Y. and Tsodyks, M. (1998) Differential signaling via the same axon of neocortical pyramidal neurons, *Proceedings of the National Academy of Sciences*, 95, 5323–5328.

Marrosu, F., Portas, C., Mascia, M. S., Casu. M. A., Fa, M., Giagheddu, M., Imperato, A. and Gessa, G. L.(1995) Microdialysis measurement of cortical and hippocampal acetylcholine release during sleep-wake cycle in freely moving cats, *Brain Research*, 671, 329–332.

Martin, H. G. S., Bernabeu, A., Lassalle, O., Bouille, C. and Martina, M. (2015) Endocannabinoids Mediate Muscarinic Acetylcholine Depression in the Adult Medial Prefrontal Cortex, *Frontiers in Cellular Neuroscience*, 9, 1–11.

McDonnell, M. D., Mohan, A., Stricker, C. and Ward, L. M. (2012) Input-rate modulation of gamma oscillations is sensitive to network topology, delays and short-term plasticity, *Brain Research*,1434, 162–177.

Mesulam, M., Mufson, E. J., Levey, A. I. and Wainer, B. H. (1983) Cholinergic Innervation of Cortex by the Basal Forebrain: Cytochemistry and Cortical Connections of the Septa1 Area, Diagonal Band Nuclei, Nucleus Basalis (Substantia Innominata), and Hypothalamus in the Rhesus Monkey, *Neuroscience*, 197, 457–74.

Mrzljak, L. (1993) Association of ml and m2 muscarinic receptor proteins with asymmetric synapses in the primate cerebral cortex : Morphological evidence for cholinergic modulation of excitatory neurotransmission, *Proceedings of the National Academy of Sciences*, 90, 5194–5198.

Murthy, V. N., Sejnowski, T. J. and Stevens, C. F. (1997) of Visualized Individual Hippocampal Synapses, 18, 599–612.

Nandi, P. and Lunte, S. M. (2009) Analytica Chimica Acta Recent trends in microdialysis sampling integrated with conventional and microanalytical systems for monitoring biological events : A review, 651, 1–14.

Naundorf, B., Wolf, F. and Volgushev, M. (2006) Unique features of action potential initiation in cortical neurons, *Nature*, 440, 1060–1063.

Oline, S. N. and Burger, R. M. (2014) Short-Term Synaptic Depression Is Topographically Distributed in the Cochlear Nucleus of the Chicken, 34, 1314–1324.

Oswald, A. M. and Reyes, A. D. (2010) Development of Inhibitory Timescales in Auditory Cortex, *Cerebral Cortex*, 21, 1351–61.

Overstreet, L. S. and Westbrook, G. L. (2003) Synapse density regulates independence at unitary inhibitory synapses., *The Journal of neuroscience*, 23, 2618–2626.

Pafundo, D. E., Miyamae, T., Lewis, D. A. and Gonzalez-Burgos, G. (2013) Cholinergic modulation of neuronal excitability and recurrent excitation-inhibition in prefrontal cortex circuits: Implications for gamma oscillations, *Journal of Physiology*, 591, 4725–4748.

Paolone, G., Angelakos, C. C., Meyer, P. J., Robinson, T. E. and Sarter, M. (2013) Cholinergic Control over Attention in Rats Prone to Attribute Incentive Salience to Reward Cues, *Journal of Neuroscience*, 33, 8321–8335.

Parikh, V., Kozak, R., Martinez, V. and Sarter, M. (2007) Prefrontal Acetylcholine Release Controls Cue Detection on Multiple Timescales, *Neuron*, 56, 141–154.

Patil, P. G., Brody, D. L. and Yue, D. T. (1998) Preferential Closed-State Inactivation of Neuronal Calcium Channels, *Neuron*, 20, 1027–1038.

Pinto, L. and Dan, Y. (2015) Cell-Type-Specific Activity in Prefrontal Cortex Article Cell-Type-Specific Activity in Prefrontal Cortex during Goal-Directed Behavior, *Neuron*, 87, 437–450.

Reyes, A., Lujan, R., Rozov, A., Burnashev, N., Somogyi, P. and Sakmann, B. (1998) Target-cell-specific facilitation and depression in neocortical circuits, *Nature Neuroscience*, 1, 279–285.

Riga, D., Matos, M. R., Glas, A., Smit, A. B., Spijker, S. and Van den Oever, M. C. (2014) Optogenetic dissection of medial prefrontal cortex circuitry, *Frontiers in Systems Neuroscience*, 8, 1–19.

Rosenmund, C., Clementst, J. D. and Westbrookt, G. L. (1993) Nonuniform Probability of Glutamate Release at a Hippocampal Synapse, *Science*, 262, 754–7.

Rotaru, D. C., Barrionuevo, G. and Sesack, S. R. (2005) Mediodorsal Thalamic Afferents to Layer III of the Rat Prefrontal Cortex : Synaptic Relationships to Subclasses of, *Journal of Comparative Neurology*, 238, 220–238.

Rudy, B., Fishell, G., Lee, S. and Hjerling-leffler, J. (2010) Three Groups of Interneurons Account for Nearly 100% of Neocortical GABAergic Neurons, *Developmental Neurobiology*, 71, 45–61.

Sarter, M., Gehring, W. J. and Kozak, R. (2006) More attention must be paid : The neurobiology of attentional effort, *Brain Research Reviews*, 51, 145–60.

Sarter, M. and Kim, Y. (2015) Interpreting Chemical Neurotransmission in Vivo: Techniques, Time Scales, and Theories, 2014–2016.

Sarter, M., Lustig, C., Howe, W. M., Gritton, H. and Berry, A. S. (2014) Deterministic functions of cortical acetylcholine, *European Journal of Neuroscience*, 39, 1912–1920.

Schluter, O. M., Basu, J., Su, T. C. and Rosenmund, C. (2006) Rab3 Superprimes Synaptic Vesicles for Release : Implications for Short-Term Synaptic Plasticity, *Journal of Neuroscience*, 26, 1239–1246.

Scott, P., Cowan, A. I. and Stricker, C. (2012) Quantifying impacts of short-term plasticity on neuronal information transfer.

Silver, R. A. (2010) Neuronal arithmetic, *Nature Reviews Neuroscience*, 11, 474–89.

Sohal, V. S., Zhang, F., Yizhar, O. and Deisseroth, K. (2009) Parvalbumin neurons and gamma rhythms enhance cortical circuit performance, *Nature*, 459, 698–702.

Sparta, D. R., Hovelso, N., Mason, A. O., Kantak, P. A., Ung, R. L., Decot, H. K. and Stuber, G. D. (2014) Activation of Prefrontal Cortical Parvalbumin Interneurons Facilitates Extinction of Reward-Seeking Behavior, *Journal of Neuroscience*, 34, 3699–3705.

Stevens, C. F. and Wesseling, J. F. (1998) Activity-dependent modulation of the rate at which synaptic vesicles become available to undergo exocytosis, *Neuron*, 21, 415–424.

Stone, E., Haario, H. and Lawrence, J. J. (2014) A kinetic model for the frequency dependence of cholinergic modulation at hippocampal GABAergic synapses, *Mathematical Biosciences*, 258, 162–175.

Sudhof, T. (2004) The synaptic vesicle cycle, *Annual Review of Neuroscience*, 27, 509–47.

Szabó, G. G., Holderith, N., Gulyás, A. I., Freund, T. F. and Hájos, N. (2010) Distinct synaptic properties of perisomatic inhibitory cell types and their different modulation by cholinergic receptor activation in the CA3 region of the mouse hippocampus, *European Journal of Neuroscience*, 31, 2234–2246.

Taschenberger, H., Woehler, A. and Neher, E. (2016) Superpriming of synaptic vesicles as a common basis for intersynapse variability and modulation of synaptic strength, *Proceedings of the National Academy of Sciences*, 113, E4548–E4557.

Teles-Grilo Ruivo, L. M., Baker, K. L., Conway, M. W., Kinsley, P. J., Gilmour, G., Phillips, K. G., Isaac, J. T. R., Lowry, J. P. and Mellor, J. R. (2017) Coordinated Acetylcholine Release in Prefrontal Cortex and Hippocampus Is Associated with Arousal and Reward on Distinct Timescales, *Cell Reports*, 18, 905–917.

Thiele, A. (2013) Muscarinic Signaling in the Brain, *Annual Review of Neuroscience*, 36, 271–294.

Thomson, A., Deuchars, J. and West, D. (1993) Large , Deep Layer Pyramid-Pyramid Single Axon EPSPs in Slices of Rat Motor Cortex Display Paired Pulse and Frequency-Dependent Depression , Mediated Presynaptically and Self-Facilitation , Mediated Postsynaptically, *Journal of Neurophysiology*, 70, 2354–69.

Thomson, A. M. and Bannister, A. P. (1999) Release-independent depression at pyramidal inputs onto specific cell targets : dual recordings in slices of rat cortex, *Journal of Physiology*, 15, 57–70.

Tierney, P. L., Degenetais, E., Thierry, A., Glowinski, J. and Gioanni, Y. (2004) Influence of the hippocampus on interneurons of the rat prefrontal cortex, *European Journal of Neuroscience*, 20, 514–524.

Tikhonova, T. B., Miyamae, T., Gulchina, Y., Lewis, D. A. and Gonzalez Burgos, G. (2018) Cell type- and layer-specific muscarinic potentiation of excitatory synaptic drive onto parvalbumin neurons in mouse prefrontal cortex, *Eneuro*, 5, e0208-18.2018 1–21.

Trommershäuser, J., Schneggenburger, R., Zippelius, A. and Neher, E. (2003) Heterogeneous presynaptic release probabilities: Functional relevance for short-term plasticity, *Biophysical Journal*, 84, 1563–1579.

Tsodyks, M. and Markram, H. (1998) Neural Networks with Dynamic Synapses, *Neural Computation*, 835, 821–835.

Tsodyks, M. and Markram, H. (1997) The neural code between neocortical pyramidal neurons depends, *Proceedings of the National Academy of Sciences of the United States of America*, 94, 719–723.

Turecek, J., Jackman, S. L., Regehr, G., Turecek, J., Jackman, S. L. and Regehr, W. G. (2016) Synaptic Specializations Support Frequency- Independent Purkinje Cell Output from the Cerebellar Cortex Article Synaptic Specializations Support Frequency-Independent Purkinje Cell Output from the Cerebellar Cortex, *Cell Reports*, 17, 3256–3268.

Unal, C. T., Jorge, P., Zaborszky, L. and Eggermann, E. (2012) Adult mouse basal forebrain harbors two distinct cholinergic populations defined by their electrophysiology, *Frontiers in Behavioural Neuroscience*, 6, 1–14.

Uylings, H. B. M., Groenewegen, H. J. and Kolb, B. (2003) Do rats have a prefrontal cortex?, *Behavioural Brain Research*, 146, 3–17.

Varela, J., Song, S., Turrigiano, G. G. and Nelson, S. B. (1999) Differential depression at excitatory and inhibitory synapses in visual cortex., *Journal of Neuroscience*, 19, 4293–304.

Verhoog, M. B., Obermayer, J., Kortleven, C. A., Wilbers, R., Wester, J., Baayen, J. C., De Kock, C. P. J., Meredith, R. M. and Mansvelder, H. D. (2016) Layer-specific cholinergic control of human and mouse cortical synaptic plasticity, *Nature Communications*, 7, 1–13.

Voinova, O., Valiullina, F., Zakharova, Y., Mukhtarov, M. and Draguhn, A. (2016) Layer Specific Development of Neocortical Pyramidal to Fast Spiking Cell Synapses, *Frontiers in Cellular Neuroscience*, 9, 1–12.

Wadel, K., Neher, E. and Sakaba, T. (2007) The Coupling between Synaptic Vesicles and Ca2+Channels Determines Fast Neurotransmitter Release, *Neuron*, 53, 563–575.

Wadiche, J. I., Jahr, C. E., Jackson, S. W. S. and Road, P. (2001) Multivesicular Release at Climbing Fiber-Purkinje Cell Synapses, *Neuron*, 32, 301–313.

Wagenmakers, E. and Farrell, S. (2004) AIC model selection using Akaike weights, *Psychonomic Bulletin & Review*, 11, 192–196.

Wang, H. X. and Gao, W. J. (2010) Development of calcium-permeable AMPA receptors and their correlation with NMDA receptors in fast-spiking interneurons of rat prefrontal cortex, *Journal of Physiology*, 588, 2823–2838.

Wang, L. Y. and Kaczmarek, L. K. (1998) High-frequency firing helps replenish the readily releasable pool of synaptic vesicles, *Nature*, 394, 384–388.

Wen, H., Mcginley, M. J., Mandel, G. and Brehm, P. (2015) Nonequivalent release sites govern synaptic depression, *Proceedings of the National Academy of Sciences*, 113, 373–86.

Wolfel, M., Lou, X. and Schneggenburger, R. (2007) A Mechanism Intrinsic to the Vesicle Fusion Machinery Determines Fast and Slow Transmitter Release at a Large CNS Synapse, *Journal of Neuroscience*, 27, 3198–3210.

Wu, L. G. and Borst, J. G. G. (1999) The reduced release probability of releasable vesicles during recovery from short-term synaptic depression, *Neuron*, 23, 821–832.

Xu, J. and Wu, L. (2005) The Decrease in the Presynaptic Calcium Current Is a Major Cause of Short-Term Depression at a Calyx-Type Synapse, *Neuron*, 46, 633–645.

Yamamoto, K., Koyanagi, Y., Koshikawa, N. and Kobayashi, M. (2010) Postsynaptic Cell Type-Dependent Cholinergic Regulation of GABAergic Synaptic Transmission in Rat Insular Cortex, *Journal of Neurophysiology*, 104, 1933–1945.

Yi, F., Ball, J., Stoll, K. E., Satpute, V. C., Mitchell S. M., Pauli J. L., Holloway B. B., Johnston A. D., Nathanson N. M., Deisseroth K., Gerber D. J., Tonegawa S. and Lawrence J. J. (2014) Direct excitation of parvalbumin-positive interneurons by M1 muscarinic acetylcholine receptors: roles in cellular excitability, inhibitory transmission and cognition, *Journal of Physiology*, 592, 3463-3494.

Zhang, Z. W., Burke M. W., Calakos N., Beaulieu J. M. and Vaucher E. (2010) Confocal analysis of cholinergic and dopaminergic inputs onto pyramidal cells in the prefrontal cortex of rodents, *Frontiers in Neuroanatomy*, 4, 1–14.

Zucker, R. and Regehr, W. (2002) Short-term synaptic plasticity, *Annual Review in Physiology*, 64, 355–405.

# Appendix I

This appendix contains analytical solutions to the differential equations of the short-term plasticity models presented in Chapter 3.

Solutions to the Tsodyks-Markram models:

The solution to replenishment of variable representing available synaptic resources, $R_{n+1}$:

$$R_{n+1} = 1 + (R_n - 1)e^{-\Delta t/D}$$

The solution to release probability, $p_{n+1}$:

$$p_{n+1} = p_0 + (p_n - p_0)e^{-\Delta t/F}$$

Solutions to the release-independent depression models:

The solution to release probability, $p_{n+1}$, in the release-independent depression model with no frequency-dependent recovery:

$$p_{n+1} = p_0 + (p_n - p_0)e^{-\Delta t/\tau_{RID}}$$

The release-independent depression model that also includes an activity-dependent recovery of release probability mediated through decreases in $\tau_{RID}$. The solution to the equation for $p_{n+1}$ is based on a solution to a similar equation in Scott et al., (2012). The solutions for $p_{n+1}$ and $\tau_{RID}$

$$p_{n+1} = p_0 + (p_n - p_0)\left(\frac{\tau_{RID_n}}{\tau_{RID_{n+1}}}\right)^{\tau_{FDR}/\tau_0} e^{-\Delta t/\tau_0}$$

$$\tau_{RID} = \tau_0 + \left(\tau_{RID_n} - \tau_0\right)e^{-\Delta t/\tau_{FDR}}$$

Solutions to the sequential models:

The solutions for low release probability pool, $R_{1_{n+1}}$, and high release probability pool $R_{2_{n+1}}$:

$$R_{1_{n+1}} = 1 - \frac{k_2}{k_2 + k_3} + \beta\left(\frac{R_{1_n} + R_{2_n}}{1+\beta} - \frac{\alpha}{k_1}\right)e^{-\Delta k_1} + \left(\frac{R_{1_n} + R_{2_n}}{1+\beta} - R_{2_n} - \frac{\alpha}{\rho}\right)e^{-\Delta t\rho}$$

$$R_{2_{n+1}} = \frac{k_2}{k_2 + k_3} + \left(\frac{R_{1_n} + R_{2_n}}{1+\beta} - \frac{\alpha}{k_1}\right)e^{-\Delta k_1} - \left(\frac{R_{1_n} + R_{2_n}}{1+\beta} - R_{2_n} - \frac{\alpha}{\rho}\right)e^{-\Delta t\rho}$$

where $k_1 = D_1^{-1}$, $k_2 = D_2^{-1}$, $k_3 = D_3^{-1}$, $\rho = k_2 + k_3$, $\alpha = \frac{k_1 k_2}{\rho - k_1}$, $\beta = \frac{\rho - k_1 - k_2}{k_2}$.

# Appendix II

This appendix contains the results of statistical analysis of results presented in Chapter 3.

| | Dependent variable | | | | | | | | |
|---|---|---|---|---|---|---|---|---|---|
| **Stimulation Frequency** | Peak 2 | Peak 3 | Peak 4 | Peak 5 | Peak 6 | Peak 7 | Peak 8 | Peak 9 | Peak 10 |
| 5 Hz | 0.0089 | 0.0059 | 0.0161 | 0.0109 | 0.0485 | 0.0109 | 0.0195 | 0.0283 | 0.0072 |
| 10 Hz | 0.0340 | 0.0132 | 0.0161 | 0.0485 | 0.0235 | 0.0235 | 0.0195 | 0.0195 | 0.0109 |
| 20 Hz | 0.0809 | 1.0000 | 0.2408 | 0.0485 | 0.1789 | 0.0235 | 0.2408 | 0.0485 | 0.0161 |
| 50 Hz | 0.0137 | 0.0469 | 1.0000 | 1.0000 | 0.7586 | 0.8658 | 0.4319 | 0.9848 | 1.0000 |
| 100 Hz | 0.1352 | 1.0000 | 1.0000 | 1.0000 | 1.0000 | 1.0000 | 1.0000 | 1.0000 | 1.0000 |
| 200 Hz | 0.0456 | 0.3299 | 1.0000 | 1.0000 | 1.0000 | 1.0000 | 1.0000 | 1.0000 | 1.0000 |

**Table 1. Wilcoxon signed-rank test with post-hoc Bonferroni correction for multiple comparisons results of IPSPs amplitudes, peak 2-10.** p-values for the data presented in Figure 4-10 in section 4.3.2.2.

| | Dependent variable | | | | | | | | |
|---|---|---|---|---|---|---|---|---|---|
| **Stimulation Frequency** | Peak 2 | Peak 3 | Peak 4 | Peak 5 | Peak 6 | Peak 7 | Peak 8 | Peak 9 | Peak 10 |
| 5 Hz | 0.0089 | 0.0072 | 0.0195 | 0.0089 | 0.0340 | 0.0109 | 0.0161 | 0.0235 | 0.0072 |
| 10 Hz | 0.0161 | 0.0109 | 0.0132 | 0.0195 | 0.0235 | 0.0195 | 0.0235 | 0.0235 | 0.0089 |
| 20 Hz | 0.2408 | 1.0000 | 0.2782 | 0.0809 | 0.3680 | 0.0340 | 0.2079 | 0.0809 | 0.0340 |
| 50 Hz | 0.0386 | 0.1671 | 1.0000 | 1.0000 | 1.0000 | 1.0000 | 1.0000 | 1.0000 | 1.0000 |
| 100 Hz | 0.2062 | 1.0000 | 1.0000 | 1.0000 | 1.0000 | 1.0000 | 1.0000 | 1.0000 | 1.0000 |
| 200 Hz | 0.0456 | 0.2558 | 1.0000 | 1.0000 | 1.0000 | 1.0000 | 1.0000 | 1.0000 | 1.0000 |

**Table 2. Wilcoxon signed-rank test with post-hoc Bonferroni correction for multiple comparisons results of IPSPs amplitudes, peak 2-10.** p-values for the data presented in Figure 4-11 in section 4.3.2.2.